

CIVIL ENGINEERING STUDIES
Illinois Center for Transportation Series No. 17-022
UIIU-ENG-2017-2022
ISSN: 0197-9191

Integral Abutment Bridges under Thermal Loading: Field Monitoring and Analysis

Prepared By

James M. LaFave

Larry A. Fahnestock

Gabriela Brambila

Joseph K. Riddle

Matthew W. Jarrett

Jeffrey S. Svatora

Beth A. Wright

Huayu An

University of Illinois at Urbana–Champaign

Research Report No. FHWA-ICT-17-017

A report of the findings of

ICT PROJECT R27-115

Analysis of Superstructures of Integral Abutment Bridges

**ILLINOIS CENTER FOR
TRANSPORTATION**



Illinois Center for Transportation

August 2017

TECHNICAL REPORT DOCUMENTATION PAGE

1. Report No. FHWA-ICT-17-017		2. Government Accession No. N/A		3. Recipient's Catalog No. N/A	
4. Title and Subtitle Integral Abutment Bridges under Thermal Loading: Field Monitoring and Analysis				5. Report Date August 2017	
				6. Performing Organization Code N/A	
7. Author(s) James M. LaFave, Larry A. Fahnestock, Gabriela Brambila, Joseph K. Riddle, Matthew W. Jarrett, Jeffrey S. Svatora, Beth A. Wright, and Huayu An				8. Performing Organization Report No. ICT-17-022 UIUL 2017-2022	
9. Performing Organization Name and Address Illinois Center for Transportation Department of Civil and Environmental Engineering University of Illinois at Urbana-Champaign 205 North Mathews Avenue, MC-250 Urbana, IL 61801				10. Work Unit No. N/A	
				11. Contract or Grant No. R27-115	
12. Sponsoring Agency Name and Address Illinois Department of Transportation (SPR) Bureau of Material and Physical Research 126 East Ash Street Springfield, IL 62704				13. Type of Report and Period Covered Final Report: 3/1/12 – 8/15/17	
				14. Sponsoring Agency Code FHWA	
15. Supplementary Notes Conducted in cooperation with the U.S. Department of Transportation, Federal Highway Administration, and the Illinois State Toll Highway Authority.					
16. Abstract Integral abutment bridges (IABs) have gained popularity throughout the United States due to their low construction and maintenance costs. Previous research on IABs has been heavily focused on substructure performance, leaving a need for better understanding of IAB superstructure behavior and interdependent effects. This report presents findings of a field monitoring program for two Illinois IABs (which supplements findings from a parametric study portion of the overall project that are summarized in a previous volume). The field monitoring program included collecting data about (i) global bridge movements; (ii) pile, deck, girder, and approach-slab strains; and (iii) rotations at different abutment interfaces. Field results have been compared to finite-element models of each bridge in order to provide further insight into IAB behavior. Field monitoring results corroborated that IAB longitudinal expansion and contraction is somewhat less than theoretical free expansion and contraction, and is influenced by bridge skew as well. Significant girder stresses were observed, particularly at the girder bottom flange, which should be considered in design. Pile strain values indicate there is likely some reserve pile-deformation capacity typically available.					
17. Key Words Integral Abutment Bridge; Field Monitoring; Skewed Bridges; Thermal Loading; Pile Strain; Girder Stress; Global Movement; Girder Fixity.			18. Distribution Statement No restrictions. This document is available through the National Technical Information Service, Springfield, VA 22161.		
19. Security Classif. (of this report) Unclassified.		20. Security Classif. (of this page) Unclassified		21. No. of Pages 75 pp	22. Price N/A

ACKNOWLEDGMENT, DISCLAIMER, MANUFACTURERS' NAMES

This publication is based on the results of **ICT-R27-115, Analysis of Superstructures of Integral Abutment Bridges**. ICT-R27-115 was conducted in cooperation with the Illinois Center for Transportation; the Illinois Department of Transportation (IDOT), Division of Highways; the U.S. Department of Transportation, Federal Highway Administration (FHWA); and the Illinois State Toll Highway Authority (ISTHA).

Members of the Technical Review panel were the following:

- Mark Shaffer, TRP chair, IDOT
- Nick Barnett, IDOT
- Bill Flannigan, AECOM
- Steven Gillen, ISTHA
- Chad Hodel, WHKS & Co.
- Micah Loesch, FHWA
- Matt Pregmon, AECOM
- Kevin Riechers, IDOT
- Bob Tessiatore, AECOM
- Dan Tobias, IDOT

The contents of this report reflect the view of the authors, who are responsible for the facts and the accuracy of the data presented herein. The contents do not necessarily reflect the official views or policies of the Illinois Center for Transportation, the Illinois Department of Transportation, or the Federal Highway Administration. This report does not constitute a standard, specification, or regulation.

EXECUTIVE SUMMARY

The use of integral abutment bridges (IABs) has become quite popular with departments of transportation throughout the United States due to their lower maintenance and construction costs and longer service life. Yet IAB design varies widely across the country, and not all aspects of their behavior are fully understood. Research has previously been conducted on IABs but primarily with a focus on substructure demand and behavior. However, recent studies have shown that IAB superstructures may develop significant forces, which should likely be considered in their design. Most previous Illinois Department of Transportation (IDOT) IAB design limits have been based mainly on substructure behavior and demands, and thus there was a need to investigate the effect of integral connections on superstructures. This project has sought to address the need to understand further not only IAB substructure behavior but also superstructure behavior, with the goal of improving design and construction provisions for IDOT IABs. To do so, a parametric study of different bridge parameters was conducted, along with implementation of a field monitoring program, the latter of which is discussed in this report. The field monitoring program was implemented in order to validate various modeling assumptions and to gain further insight into overall IAB behavior.

Two Illinois IABs, the Kishwaukee River Bridge and the Union Pacific Railroad (UPRR) Bridge along I-90, were instrumented for long-term monitoring. Vibrating-wire strain gages were installed on the girders and piles and embedded in the bridge deck at both bridges. Additionally, a limited number of strain gages were embedded in an approach slab at Kishwaukee. Tiltmeters were installed on an abutment of each bridge to measure the absolute and differential rotation at different abutment interfaces. Displacement transducers (or “crackmeters”) were also placed at different joints at Kishwaukee to monitor global movement. Data collection for both bridges began in May 2014 and continued for 16 months and 24 months for UPRR and Kishwaukee, respectively. The data were initialized utilizing the first data point, taken in the summer, so the majority of the field data corresponds to a net negative change in temperature, corresponding to bridge contraction.

To supplement the field monitoring results, numerical models of the two instrumented IABs were developed in SAP2000. These models utilized the same modeling assumptions from the parametric study (provided in a previous volume of the final project report), including rigid connections at the abutment cold joint and girder–abutment connections, as well as exclusion of approach slabs and cross-frames, among others. The models were run using nonlinear analysis for combinations of dead, thermal, and live loading.

The field monitoring results from all of the gages exhibited clear trends with respect to change in temperature. Results from the crackmeters indicated that bridge expansion and contraction are less than the theoretical free expansion/contraction, as was found in the parametric study. The crackmeter results, along with approach-slab strains, were then utilized to calculate the longitudinal abutment displacement at Kishwaukee. The resulting abutment displacements demonstrated clear trends with change in temperature and larger-magnitude displacements near the bridge’s acute corner. Further analysis of the approach-slab strains showed a decrease

in approach-slab stress after every year, which is likely indicative of reduced soil friction due to settlement.

Pile-strain results from both bridges also demonstrated clear linear relationships with change in temperature. The acute piles typically exhibited the highest-magnitude strains, yet peak strains still remained below yield strain, demonstrating some remaining available deformation capacity. The most variable data resulted from the girder gages, especially at their bottom flanges. The top-flange, web, and deck gage data displayed clear seasonal trends with temperature. As was seen in the parametric study, the bottom-flange gages had the highest magnitude of stress. The bottom-flange data typically followed a clear linear trend with change in temperature for the first 6–12 months but then deviated into further tension or compression. This behavior was especially apparent near the supports, including at the abutments and piers. No single distinct reason for this behavior was found; possible causes include cyclic / time-dependent effects related to abutment fixity, live loading, and/or deck cracking, or perhaps even localized yielding due to out-of-plane bending of the bottom flange.

Analysis of the tiltmeter-rotation data provided insight into the modeling assumptions made regarding different abutment interfaces. Tiltmeter rotations from above and below the abutment cold joint showed essentially zero differential rotation, thus validating the assumption of a rigid cold joint. By contrast, comparison of the abutment-to-girder rotations showed a small amount of differential rotation. The maximum relative rotation was 0.1° and 0.33° at UPRR and Kishwaukee, respectively. This small differential rotation demonstrated that in reality the girder–abutment connection is not entirely rigid; however, the differential rotation is of a magnitude small enough that the assumption of a rigid connection is still valid.

The models of the instrumented bridges were also utilized to analyze further the collected field data. Field and model abutment-displacement data showed good correlation, including larger displacement of the north (acute) side. The models slightly overestimated pile strains, more so at UPRR; however, both the field and model data exhibited similar trends with respect to change in temperature. It was also found that the pile field data exhibited more weak-axis flexure than combined flexure. The model data showed consistent correlation with girder top-flange field data in terms of both stress magnitudes and trends with change in temperature. The bottom-flange field data also correlated well with the model, but only for the first few months of data collection before beginning to deviate. The magnitudes of the top- and bottom-flange stresses (even before deviating) are significant enough that they should be considered during IAB design. Overall, the field data and corresponding bridge numerical models provided valuable insight into different aspects of IAB behavior and validated key modeling assumptions, indicating the potential for further application of the parametric study and field monitoring results in future IAB design.

CONTENTS

LIST OF FIGURES	VI
LIST OF TABLES	IX
CHAPTER 1: INTRODUCTION	1
CHAPTER 2: LITERATURE REVIEW	3
2.1 IAB FIELD MONITORING	3
2.2 SITE CONDITIONS	5
CHAPTER 3: MONITORING OF TWO ILLINOIS INTEGRAL ABUTMENT BRIDGES.....	7
3.1 BRIDGE SITE DESCRIPTIONS.....	7
3.2 SUMMARY OF INSTRUMENTATION GOALS	8
3.3 DETAILED INSTRUMENTATION AND MONITORING SCHEME.....	9
3.3.1 Strain Gages	10
3.3.2 Tiltmeters.....	14
3.3.3 Displacement Transducers (Crackmeters).....	15
3.3.4 Surveying	16
3.3.5 Data Acquisition	16
CHAPTER 4: FIELD RESULTS.....	18
4.1 DATA INITIALIZATION.....	18
4.2 AVERAGE SUPERSTRUCTURE TEMPERATURE	18
4.3 GLOBAL BRIDGE MOVEMENT	19
4.3.1 Crackmeter Results.....	19
4.3.2 Approach Slab Results	21
4.3.3 Calculated Abutment Displacements.....	25
4.4 ABUTMENT ROTATION.....	27
4.5 PILE DEMANDS.....	31
4.6 GIRDER DEMANDS	40
CHAPTER 5: FINITE-ELEMENT MODELING OF SITE BRIDGES	50
5.1 MODELING ASSUMPTIONS AND PROCEDURE	50
5.2 LOAD CASES AND ANALYSIS	53
CHAPTER 6: FE MODEL RESULTS VS. IAB FIELD DATA	55

6.1 GLOBAL BRIDGE MOVEMENT	55
6.2 ROTATIONS.....	57
6.3 PILE DEMANDS.....	59
6.4 GIRDER DEMANDS	65
CHAPTER 7: CONCLUSIONS	70
7.1 BEST PRACTICES FOR FIELD MONITORING IMPLEMENTATION.....	70
7.2 CONCLUSIONS FROM FIELD DATA.....	70
7.3 MODELING CONCLUSIONS AND RECOMMENDATIONS.....	71
REFERENCES	73

LIST OF FIGURES

FIGURE 1. TYPICAL IDOT IAB DETAIL (IDOT ABD 12.3).....	1
FIGURE 2. THERMALLY INDUCED FORCES (1 kN = 0.225 k) AS A FUNCTION OF CONCRETE IAB LENGTH (1 M = 3.28 FT): (A) AXIAL FORCE AND (B) MOMENT (PAUL ET AL. 2005, FIGURE 8).....	4
FIGURE 3. P-MULTIPLIER CURVES (HAN 2014, FIGURE 6.8).....	6
FIGURE 4. SCHEMATIC OF INSTRUMENTATION GOALS.	8
FIGURE 5. PILE-INSTRUMENTATION SCHEMATICS.	11
FIGURE 6. ARC-WELDED PILE STRAIN-GAGE INSTALLATION.	12
FIGURE 7. PLAN VIEW OF INSTRUMENTATION SCHEME FOR KISHWAUKEE (TOP) AND UPRR (BOTTOM).	13
FIGURE 8. INSTRUMENTATION SCHEMATIC FOR SUPERSTRUCTURE CROSS SECTIONS.	13
FIGURE 9. SPOT-WELDED GIRDER STRAIN GAGE WITHOUT AND WITH ITS COVER PLATE.	14
FIGURE 10. APPROACH-SLAB-EMBEDDED STRAIN GAGE.	14
FIGURE 11. ELEVATION OF EAST ABUTMENT AT KISHWAUKEE.....	15
FIGURE 12. ELEVATION OF WEST ABUTMENT AT UPRR.	15
FIGURE 13. TILTMETER INSTALLATION AT KISHWAUKEE ON THE NORTH SIDE (LEFT) AND MIDDLE (RIGHT) OF ABUTMENT.....	15
FIGURE 14. CRACKMETER INSTALLED AT APPROACH SLAB–TRANSITION SLAB INTERFACE.	16
FIGURE 15. KISHWAUKEE SURVEY LOCATIONS.	16
FIGURE 16: KISHWAUKEE TEMPERATURE COMPARISON FROM 8/10/2014 TO 8/12/2014.	19
FIGURE 17. KISHWAUKEE CRACKMETER DISPLACEMENTS.....	20
FIGURE 18. APPROACH–TRANSITION SLAB JOINT DISPLACEMENTS (KISHWAUKEE) FOR THE NORTH (LEFT) AND SOUTH (RIGHT) ENDS.	20
FIGURE 19. COMPARISON OF AVERAGE SUPERSTRUCTURE TEMPERATURE AND AVERAGE APPROACH-SLAB TEMPERATURE OVER TIME (KISHWAUKEE).	21
FIGURE 20. APPROACH-SLAB 8-2 GAGE STRAIN AND AVERAGE APPROACH-SLAB TEMPERATURE VS. TIME (KISHWAUKEE).	22
FIGURE 21. APPROACH-SLAB CHANGE IN LENGTH (KISHWAUKEE).	23
FIGURE 22. APPROACH-SLAB STRESS (KISHWAUKEE).....	24
FIGURE 23. AVERAGE APPROACH-SLAB STRESS VS. CHANGE IN TEMPERATURE (KISHWAUKEE).	25
FIGURE 24. ABUTMENT DISPLACEMENTS OF THE NORTH AND SOUTH EDGES OF THE KISHWAUKEE EAST ABUTMENT.	26
FIGURE 25. NORTH AND SOUTH KISHWAUKEE CALCULATED ABUTMENT DISPLACEMENTS AND ABUTMENT SURVEY DATA.	27
FIGURE 26. TILTMETER LABELING CONVENTION AT AN ABUTMENT.	28
FIGURE 27. KISHWAUKEE SOUTH SIDE TOP TILTMETER ROTATIONS VS. CHANGE IN TEMPERATURE AND TIME.	28
FIGURE 28. SOUTH TOP TILTMETER ROTATION VS. CHANGE IN TEMPERATURE FOR KISHWAUKEE AND UPRR.	29
FIGURE 29. KISHWAUKEE AND UPRR ABUTMENT ROTATIONS ALONG THE ABUTMENT.	29
FIGURE 30. COLD-JOINT DIFFERENTIAL ROTATIONS FOR THE SOUTH SIDE OF THE KISHWAUKEE AND UPRR ABUTMENTS.	30
FIGURE 31. DIFFERENTIAL ROTATION BETWEEN THE ABUTMENT AND GIRDERS AT THE NORTH SIDE OF THE KISHWAUKEE AND UPRR ABUTMENTS.	31

FIGURE 32. SCHEMATIC OF PILE STRAIN GAGE LOCATIONS.	32
FIGURE 33. KISHWAUKEE ACUTE PILE STRAINS OVER TIME.	32
FIGURE 34. KISHWAUKEE ACUTE PILE STRAINS FROM 10:00 A.M. ON 5/28/2014 TO 4:00 A.M. ON 6/1/2014. 33	33
FIGURE 35. KISHWAUKEE ACUTE (NORTH) PILE HEAD STRAINS.	34
FIGURE 36. KISHWAUKEE MIDDLE-PILE HEAD STRAINS.	34
FIGURE 37. KISHWAUKEE OBTUSE (SOUTH) PILE HEAD STRAINS.	35
FIGURE 38. KISHWAUKEE ACUTE (NORTH) AND MIDDLE-PILE STRAINS BELOW THE PILE-CAP BOUNDARY.....	35
FIGURE 39. UPRR ACUTE (NORTH) PILE HEAD STRAINS.....	36
FIGURE 40. UPRR MIDDLE-PILE HEAD STRAINS.	36
FIGURE 41. UPRR OBTUSE (SOUTH) PILE HEAD STRAINS.	37
FIGURE 42. UPRR ACUTE (NORTH) AND OBTUSE (SOUTH) PILE STRAINS BELOW PILE-CAP BOUNDARY.	37
FIGURE 43. KISHWAUKEE (LEFT) AND UPRR (RIGHT) ACUTE PILE FLANGE-TIP STRAINS.....	38
FIGURE 44. PILE STRESS DUE TO AXIAL FORCE IN THE PILES AT KISHWAUKEE (LEFT) AND UPRR (RIGHT).....	38
FIGURE 45. PILE STRESS DUE TO STRONG-AXIS MOMENT IN THE PILES AT KISHWAUKEE (LEFT) AND UPRR (RIGHT). 39	39
FIGURE 46. PILE STRESS DUE TO WEAK-AXIS MOMENT IN THE PILES AT KISHWAUKEE (LEFT) AND UPRR (RIGHT). ..	39
FIGURE 47. GIRDER CROSS-SECTION LABELING SCHEME FOR KISHWAUKEE (TOP) AND UPRR (BOTTOM).	40
FIGURE 48. ORIGINAL DATA (LEFT) AND DAILY RUNNING AVERAGE DATA (RIGHT) FOR KISHWAUKEE GIRDER 8 STRESSES AT THE MID-SPAN OF THE INTERIOR SPAN.	41
FIGURE 49. KISHWAUKEE GIRDER 8 STRESSES AT THE MID-SPAN OF THE INTERIOR SPAN (LEFT) AND UPRR GIRDER 10 STRESSES AT THE EAST QUARTER-SPAN (RIGHT).	42
FIGURE 50. KISHWAUKEE GIRDER 8 STRESSES AT INTERIOR MID-SPAN VERSUS CHANGE IN TEMPERATURE.....	43
FIGURE 51. UPRR GIRDER 10 STRESSES AT THE EAST QUARTER-SPAN VS. CHANGE IN TEMPERATURE.	43
FIGURE 52. KISHWAUKEE TOP-FLANGE STRESSES ALONG GIRDER 2 ON “HOT” DAYS.....	44
FIGURE 53. KISHWAUKEE TOP-FLANGE STRESSES ALONG GIRDER 2 ON “COLD” DAYS.	45
FIGURE 54. UPRR TOP-FLANGE STRESSES ALONG GIRDER 10 ON “HOT” DAYS.....	45
FIGURE 55. UPRR TOP-FLANGE STRESSES ALONG GIRDER 10 ON A “COLD” DAY.	46
FIGURE 56. KISHWAUKEE BOTTOM-FLANGE STRESSES ALONG GIRDER 2 ON “HOT” DAYS.	47
FIGURE 57. KISHWAUKEE BOTTOM-FLANGE STRESSES ALONG GIRDER 2 ON “COLD” DAYS.	47
FIGURE 58. UPRR BOTTOM-FLANGE STRESSES ALONG GIRDER 10 ON “HOT” DAYS.	48
FIGURE 59. UPRR BOTTOM-FLANGE STRESSES ALONG GIRDER 10 ON A “COLD” DAY.....	48
FIGURE 60. TYPICAL FINITE-ELEMENT MODEL OF AN INTEGRAL ABUTMENT BRIDGE (IAB).	50
FIGURE 61. COMPOSITE SECTION MODELING AND GIRDER-END OFFSET (ADAPTED FROM CSI TECHNICAL KNOWLEDGE BASE “COMPOSITE SECTION TUTORIAL”).....	51
FIGURE 62. KISHWAUKEE P-Y CURVE FOR SOIL SPRING IN THE LONGITUDINAL BRIDGE DIRECTION AT 10-FT DEPTH. 52	52
FIGURE 63. UPRR P-Y CURVE FOR SOIL SPRING IN THE LONGITUDINAL BRIDGE DIRECTION AT 10-FT DEPTH.....	53
FIGURE 64. UPRR FE MODEL GLOBAL BRIDGE MOVEMENTS DUE TO CHANGE IN TEMPERATURE (125X SCALE; NORTH IS UP).....	55
FIGURE 65. KISHWAUKEE FE MODEL GLOBAL BRIDGE MOVEMENTS DUE TO CHANGE IN TEMPERATURE (125X SCALE; NORTH IS UP).....	56
FIGURE 66. COMPARISON OF KISHWAUKEE EAST-ABUTMENT NORTH SIDE LONGITUDINAL DISPLACEMENT.....	57
FIGURE 67. COMPARISON OF KISHWAUKEE EAST-ABUTMENT SOUTH SIDE LONGITUDINAL DISPLACEMENT.	57
FIGURE 68. KISHWAUKEE FIELD AND FE MODEL ABUTMENT-ROTATION MEASUREMENTS.....	58
FIGURE 69. UPRR FIELD AND FE MODEL ABUTMENT-ROTATION MEASUREMENTS.	58

FIGURE 70. COMPARISON OF KISHWAUKEE FIELD-MEASURED AND FE-MODEL ACUTE PILE STRAINS AT THE PILE-CAP BOUNDARY.....	60
FIGURE 71. COMPARISON OF KISHWAUKEE FIELD-MEASURED AND FE-MODEL OBTUSE PILE STRAINS AT THE PILE CAP BOUNDARY.....	60
FIGURE 72. COMPARISON OF UPRR FIELD-MEASURED AND FE-MODEL ACUTE PILE STRAINS AT GAGE LOCATIONS AT THE PILE-CAP BOUNDARY.	61
FIGURE 73. COMPARISON OF UPRR FIELD-MEASURED AND FE-MODEL OBTUSE PILE STRAINS AT GAGE LOCATIONS AT THE PILE-CAP BOUNDARY.	61
FIGURE 74. KISHWAUKEE FE-MODEL PILE STRAINS DUE TO WEAK-AXIS BENDING.	62
FIGURE 75. KISHWAUKEE FE-MODEL PILE STRAINS DUE TO STRONG-AXIS BENDING.	63
FIGURE 76. KISHWAUKEE FE-MODEL PILE STRAINS DUE TO AXIAL FORCE.	63
FIGURE 77. KISHWAUKEE FE MODEL (PURE THERMAL LOADING) VS. FIELD-ESTIMATED PILE STRAINS AT ACUTE PILE FLANGE TIPS.	64
FIGURE 78. UPRR FE MODEL (PURE THERMAL LOADING) VS. FIELD-ESTIMATED PILE STRAINS AT ACUTE PILE FLANGE TIPS.	64
FIGURE 79. TOP-FLANGE STRESS COMPARISON OF FIELD DATA TO FE-MODEL PREDICTION FOR GIRDER 8 INTERIOR MID-SPAN AT KISHWAUKEE AND GIRDER 10 EAST QUARTER-SPAN AT UPRR.	65
FIGURE 80. BOTTOM-FLANGE STRESS COMPARISON OF FIELD DATA TO FE-MODEL PREDICTION FOR GIRDER 8 INTERIOR MID-SPAN AT KISHWAUKEE AND GIRDER 10 EAST QUARTER-SPAN AT UPRR.	66
FIGURE 81. GIRDER STRESSES OVER TIME AT KISHWAUKEE AND UPRR.	66
FIGURE 82. BOTTOM-FLANGE GIRDER STRESS FOR KISHWAUKEE 8-3 (MAY 2014–MAY 2015) AND UPRR 10-2.3 (MAY 2014–DEC 2014).	67
FIGURE 83. HOT- AND COLD-DAYS FIELD DATA AND FE-MODEL COMPARISON OF KISHWAUKEE GIRDER 2 STRESSES.	68
FIGURE 84. HOT- AND COLD-DAYS FIELD DATA AND FE-MODEL COMPARISON OF UPRR GIRDER 10 STRESSES.	69

LIST OF TABLES

TABLE 1. KISHWAUKEE AND UPRR BRIDGE-GEOMETRY INFORMATION 7
TABLE 2. INSTRUMENTS USED AT THE MONITORED BRIDGES..... 10
TABLE 3. LOAD CASES 54

CHAPTER 1: INTRODUCTION

Integral abutment bridges (IABs) are becoming more widely used amongst departments of transportations in the United States due to their long service life and lower maintenance and construction costs (Arsoy et al. 1999; Hassiotis et al. 2006). In an IAB, the abutment and deck are cast to be monolithic; and the girders and piles are embedded into the abutment, as shown in Figure 1. Therefore, unlike in conventional bridges, the superstructure and substructure of an IAB act as one continuous unit under thermal loads.

The behavior of IABs is more difficult to analyze due to the continuous structural form, and thus design practices across the country vary greatly. As the behavior of these bridges, especially that of their superstructures, is still not completely understood, several states (including Illinois) have pursued research projects regarding IABs. Two previous projects were even conducted by the University of Illinois about IABs; however, they focused on substructure behavior. Many uncertainties still remain regarding IAB superstructure behavior and design, which provides some of the motivation for this research project on overall IAB behavior, with an emphasis on thermal loads and superstructures.

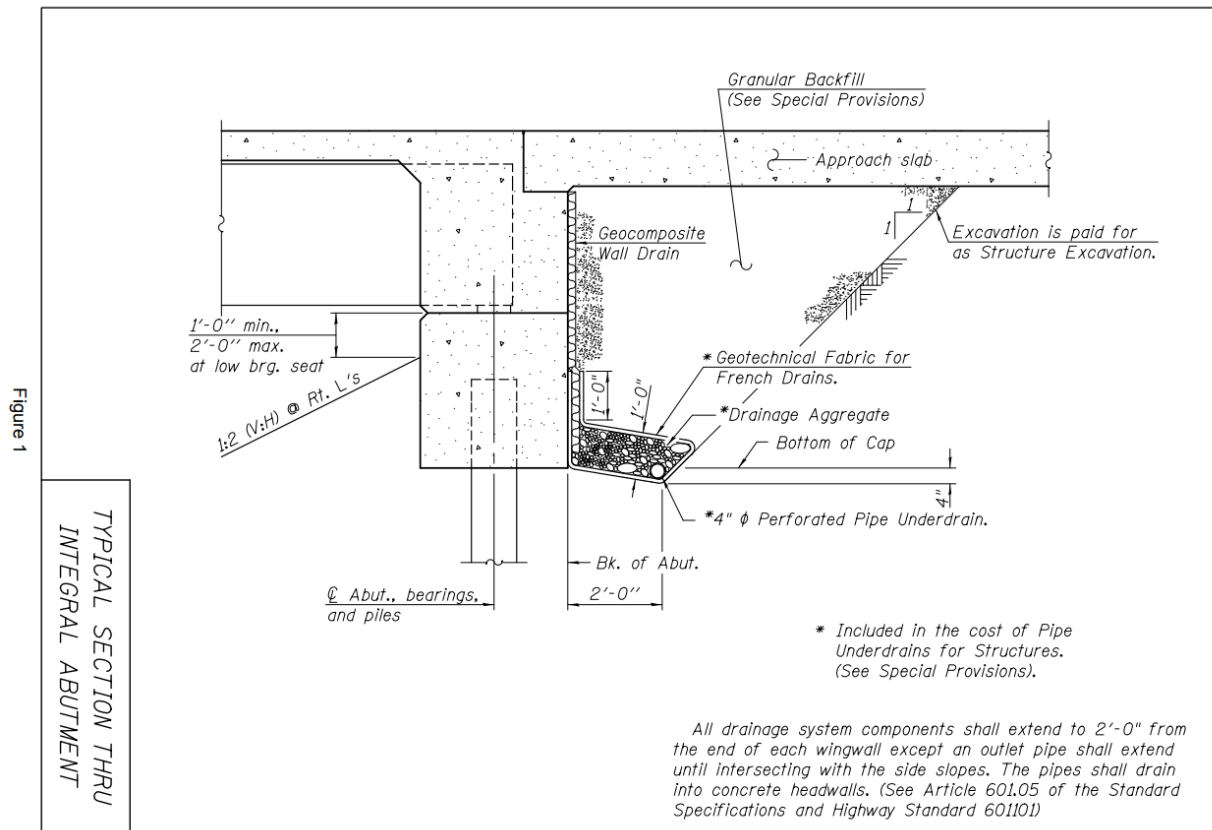


Figure 1. Typical IDOT IAB detail (IDOT ABD 12.3).

The objective of the research has been to explore IAB thermal behavior, particularly on superstructures, and to provide improved design and construction provisions for IABs. This overall research project includes a comprehensive parametric study utilizing finite-element (FE) bridge models and field monitoring of two IABs in Illinois. The superstructure and substructure of the Union Pacific Railroad (UPRR) and Kishwaukee River bridges, both of which are I-90 mainline (Illinois Tollway) bridges, were instrumented as part of the field monitoring program. The goals of the field monitoring program have been to validate previous modeling assumptions and more accurately capture different aspects of IAB behavior in the field.

This report summarizes field monitoring results from both instrumented bridges and compares the field data to results from FE models of each site's bridge. The report also includes a brief literature review and a description of the site bridge model assumptions and modeling procedures. Findings from the parametric study component of this project can be found in the preceding volume of this report (LaFave et al. 2016a).

CHAPTER 2: LITERATURE REVIEW

Chapter 2 summarizes previous field monitoring research work regarding IAB substructures and superstructures, as well as work regarding specific site conditions pertinent to the current study.

2.1 IAB FIELD MONITORING

Overall, the majority of previous IAB research, including prior research conducted at the University of Illinois, has been primarily focused on substructure behavior. Prior research conducted at Illinois on IAB substructures is summarized in the preceding volume of this report (LaFave et al. 2016a). The primary focus on IAB substructures has been influenced by the significant increase in substructure demands due to integral construction. Dicleli (2004), Ingram et al. (2004), and Paul et al. (2005) all found a bridge's effective expansion length (EEL) to have significant influence on IAB behavior, with global bridge superstructure movement and pile-displacement demand both being directly related to EEL. Other primary factors affecting IAB pile behavior and overall bridge response to thermal loading include backfill soil stiffness, pile-soil stiffness, and the superstructure itself (Dicleli 2005). The relationship and mutual effects between IAB superstructure and substructure behavior are also mentioned by Burdette et al. (2004), Kim and Laman (2010), and Olson et al. (2012). Research efforts implementing field monitoring of IABs have provided some insights to complement previous analytical findings regarding IABs, as briefly outlined below.

In New Jersey, a two-span, high-performance, steel-girder IAB was monitored to investigate abutment displacements and the effect of relevant design parameters on pile forces and pile-soil interaction (Khodair and Hassiotis 2013). The field results indicated that increases in abutment rotation due to temperature change resulted in an increase in pile axial forces. An increase in soil pressure near the bridge's obtuse side was also observed, due to larger transverse movement of the bridge at this location, thus resulting in higher axial stresses in the piles near the obtuse side.

Pennsylvania State University (Paul et al. 2005) explored IAB superstructure behavior due to thermal loading through instrumentation and monitoring of the top and bottom of a prestressed concrete slab-on-beam bridge. Additionally, a 2-D parametric analysis was conducted, which confirmed that substantial superstructure forces can be induced by thermal loading. In the field, several different possible factors that are difficult to isolate affect girder forces. However, the numerical and field data indicated that creep and shrinkage may have a significant effect on girder forces, and that thermally induced stresses may lead to cracking in concrete IABs. Figure 2 shows how these thermally induced girder forces become more pronounced with increasing EEL.

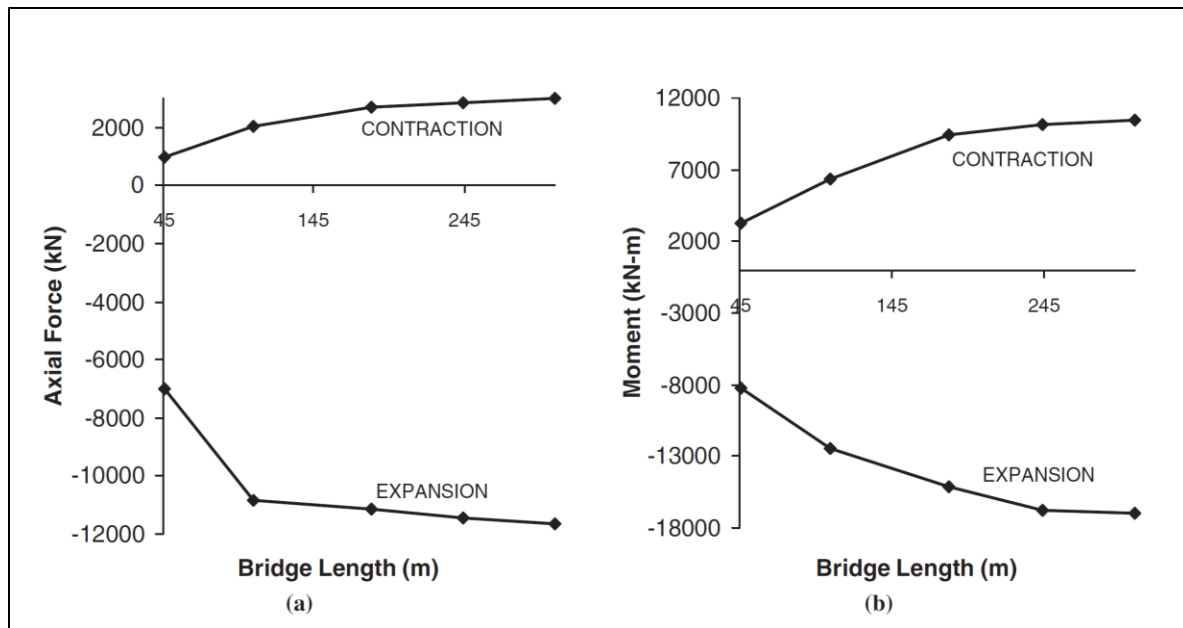


Figure 2. Thermally induced forces (1 kN = 0.225 k) as a function of concrete IAB length (1 m = 3.28 ft): (a) axial force and (b) moment (Paul et al. 2005, Figure 8).

Additional longer-term monitoring was conducted in Pennsylvania as part of a study regarding four short to medium-long, concrete-girder IABs, which were monitored for 7 years to track long-term trends for abutment displacement, backfill pressure, abutment rotation, girder rotation, girder forces, pile forces, and approach-slab strains (Kim and Laman 2012). The monitoring results demonstrated that the abutment displacements exhibited an increase in unrecoverable total abutment movement for all four bridges. In analyzing the girder-to-abutment connection, differential rotation was observed between the girders and abutment, indicating that the connection was not completely rigid. Kim and Laman also concluded that girder moments and axial forces induced by thermal loading should be considered in design. Further comparison to FE models of the four IABs revealed that girder axial forces are primarily influenced by end-span length, as opposed to overall bridge length (Kim and Laman 2010).

In West Virginia, field monitoring of a three-span, steel-girder IAB was conducted to observe abutment movement and its corresponding effect on superstructure stresses due to thermal loading (Shoukry et al. 2008). Strain results from the girder top and bottom flanges indicate they are primarily caused by temperature changes and the weight of the bridge deck, thus demonstrating clear seasonal trends over time. Analysis of calculated girder bending moments showed close agreement with theoretical bending-moment values. The calculated axial forces in the girders due to passive backfill pressure were significant, and thus it was recommended to account for this when designing the bridge superstructure. William et al. (2012) found that these forces are induced: due to restraint of the abutment by the backfill, and supporting piles are not explicitly considered in typical bridge-design procedures.

Minnesota (Huang et al. 2004) has also conducted field monitoring of an IAB with prestressed concrete girders, by instrumenting various cross sections of the superstructure. The field results

showed that, due to creep and shrinkage, girder strains kept decreasing over the years. Girder-strain variations across the cross section at different bridge locations were explained; however, no recommendation was provided regarding modifications of IAB superstructure design. Another long-term field monitoring program, implemented on three different IABs in Indiana, observed “ratcheting” of contraction displacements due to deck shrinkage; and the amount of shrinkage contraction controlled over thermal contraction (Frosch and Lovell 2011). Due to uncertainty regarding modeling of these time-dependent demands, such effects have not been incorporated into the numerical models for the parametric study of this current Illinois work nor in the field models described later in this report.

2.2 SITE CONDITIONS

More limited IAB research has been conducted on specific bridge and site conditions that vary from bridge to bridge, including some debated topics such as pile orientation, pile-head fixity, and pile relief. All of these conditions affect one or both of the instrumented bridges in this study and are factors that were only partially assessed in the project’s previous parametric study (if implemented at all). Pile orientation was explored on a limited basis as part of the so-called secondary parameter analysis in the parametric study (LaFave et al. 2016a). Results indicated that weak-axis pile orientation imposes less built-up forces on the superstructure because it maximizes bridge expansion and contraction, as compared to strong-axis-oriented piles. However, this allows for larger pile deformations, which are more likely to lead to plastification at the pile head. The strong-axis-oriented piles provided increased foundation stiffness, which reduced peak pile strains but resulted in larger girder internal forces. Therefore, it is important to consider effects on both the substructure and superstructure when determining an appropriate pile orientation.

Quinn and Civjan (2017) also conducted a parametric study to investigate pile orientation and found no single optimal orientation, but rather the optimal orientation for any particular IAB is dependent on several factors. The parametric study looked at configurations of single-span bridges for three different lengths at four different degrees of skew for both strong-axis and weak-axis pile orientations under thermal loading. Results showed that the construction temperature (as well as minimum and maximum design temperatures) is important to consider in determining the appropriate pile orientation, as these factors play a role in determining whether transverse movement is greater in contraction or expansion. Therefore it was recommended that these factors, along with backfill conditions, bridge length, and skew, be considered in the selection of pile orientation.

Direct or indirect pile relief also plays a significant role in IAB substructure and superstructure behavior because it allows for more pile flexibility. At the Kishwaukee Bridge, pile top relief was employed by encasing 10 ft of the pile directly below the pile-head location in a soft bentonite slurry. This method of pile relief was explored as part of the parametric study portion of this project (LaFave et al. 2016a), which showed reduced pile strains for the bridges employing pile relief with bentonite. Even though pile relief increases pile deflections, the longer unrestrained length leads to a reduction in pile bending moments. Modeling of the bentonite slurry was

included in the Kishwaukee site model and resulted in better correlation of pile results between the FE model and field data.

The UPRR Bridge has mechanically stabilized earth (MSE) walls at each abutment, which most likely results in an indirect pile “relief.” Han (2014) conducted full-scale testing of pipe piles located at different distances behind an MSE wall, to analyze the effects on pile behavior. These results, combined with those from previous work by Nelson (2013) and Price (2012), showed that the lateral resistance of piles decreases as the distance from the pile to the MSE wall decreases. The decreased amount of soil surrounding the pile due to the addition of an MSE wall decreases the foundation stiffness in the contraction direction. To account for the effect of the MSE wall, “p-multipliers” can be back-calculated to account for the reduced soil capacities. Combined with the previous results from Nelson (2013) and Price (2012), the data were utilized to create p-multiplier curves demonstrating the relationship between p-multipliers and the spacing between a pile and an MSE wall, as shown in Figure 3. These p-multipliers allow for modifications to load-deflection curves in order to consider MSE wall effects. To account for the MSE wall at the UPRR Bridge, the corresponding p-multiplier was implemented in its FE model, as further explained in section 5.1. However, it should be noted that these other studies were conducted on steel pipe piles. Parametric study results from LaFave et al. (2016a) show that pipe piles and H-piles have similar behaviors until pipe piles reach yielding. Therefore, application of Han’s findings (2014) may become less reliable upon reaching pile yielding.

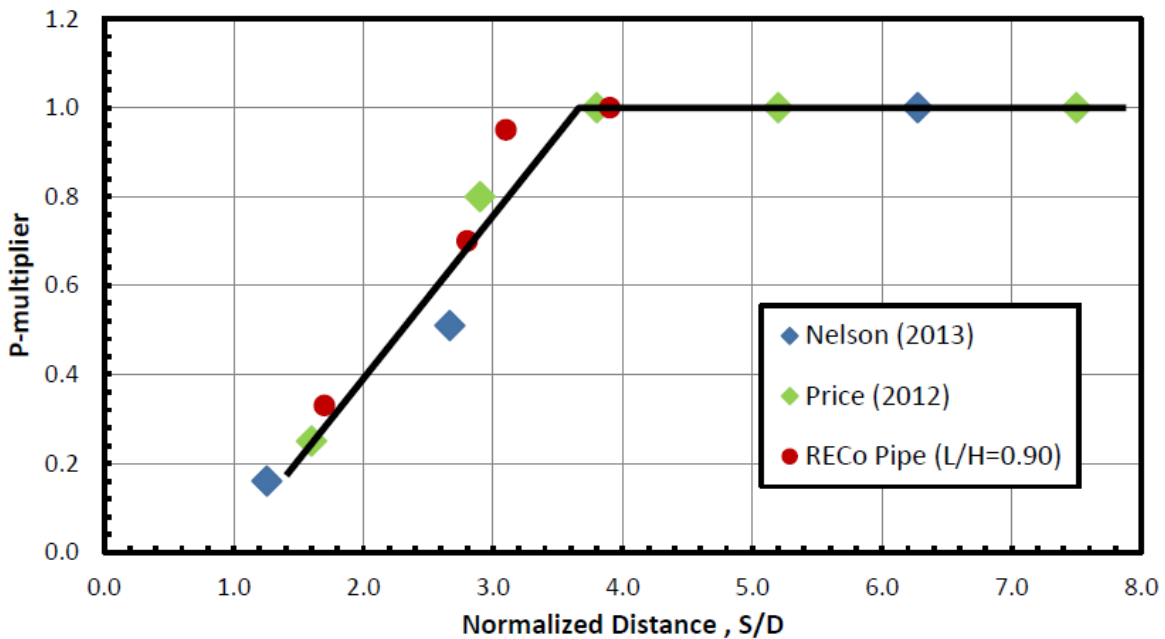


Figure 3. P-multiplier curves (Han 2014, Figure 6.8).

CHAPTER 3: MONITORING OF TWO ILLINOIS INTEGRAL ABUTMENT BRIDGES

Chapter 3 provides site descriptions, instrumentation goals, and the field instrumentation and monitoring schemes used for two Illinois IABs that have been instrumented and monitored as part of this project. Some related details about this part of the work may also be found elsewhere (Wright et al. 2015 and Brambila 2017).

3.1 BRIDGE SITE DESCRIPTIONS

Two different I-90 mainline (Illinois Tollway) IABs in northern Illinois were chosen for instrumentation and field monitoring. Their bridge-geometry information is summarized in Table 1. The eastbound Kishwaukee River Bridge is a four-span, continuous bridge with span lengths of 125 ft, 152 ft, 152 ft, and 120 ft from east to west. With a total length of 549 ft, it is a mere 1 ft short of the maximum permissible IDOT IAB length of 550 ft for multi-span bridges at the time of construction. The maximum permissible length for IDOT IABs is now in the process of being increased to 610 ft, based in part on results from the prior parametric study (LaFave et al. 2016a). The Kishwaukee Bridge is also of interest because it employs HP14x117 piles, the largest pile size currently in service for IDOT IABs. Aside from these characteristics, the bridge is fairly standard, with a 30° abutment skew, approximately a 1.25 ratio of end-span to intermediate-span, a 69-ft width, and a typical girder design. All deck, abutment, and approach-slab dimensions conform to standard IDOT details. Construction of the Kishwaukee Bridge concluded in October 2013.

Table 1. Kishwaukee and UPRR Bridge-Geometry Information

Bridge	Kishwaukee	UPRR
Spans	125', 152', 152', 120' (west to east)	184.5'
Overall length	549'	184.5'
Width	69'1/4"	69'1"
Abutment skew	30°	42.5°
Number of girders	8	10
Girder size	Plate girder: 60" web	Plate girder: 72" web
Abutment piles	30 (15 each end)	38 (19 on each end)
Pile designation	HP14x117	HP14x89

The eastbound UPRR Bridge is a single-span structure with a length of 184.5 ft, which actually exceeds the current IDOT limit for a single-span IAB. The bridge is also of interest because its skew of 42.5° is near the skew limit, which is currently set at 45°. Another unique aspect is the use of MSE walls at each abutment, which is no longer permitted, according to the latest IDOT memo regarding design and construction of IABs (IDOT ABD Memo 12.3). All other facets of this

particular bridge’s design are relatively modest and/or are based on standard IDOT details. The eastbound UPRR Bridge was built in stages: Stage 1 included approximately the southern one-third of the bridge, and stage 1A included the remaining two-thirds of the eastbound portion of the bridge. Construction of the bridge was delayed due to extreme winter weather and was therefore not completed until April 2014.

3.2 SUMMARY OF INSTRUMENTATION GOALS

The project’s instrumentation goals stem from specific requests of various parties at IDOT and the Illinois Tollway, as well as from the need to validate modeling assumptions made in the earlier parametric study phase of this project (LaFave et al. 2016a) and for the analytical IAB models associated with the instrumented bridges. With the project’s main focus being on the behavior of IAB superstructures, that is where most of the instrumentation effort was directed, with limited additional instrumentation on the substructure, as summarized in Figure 4.

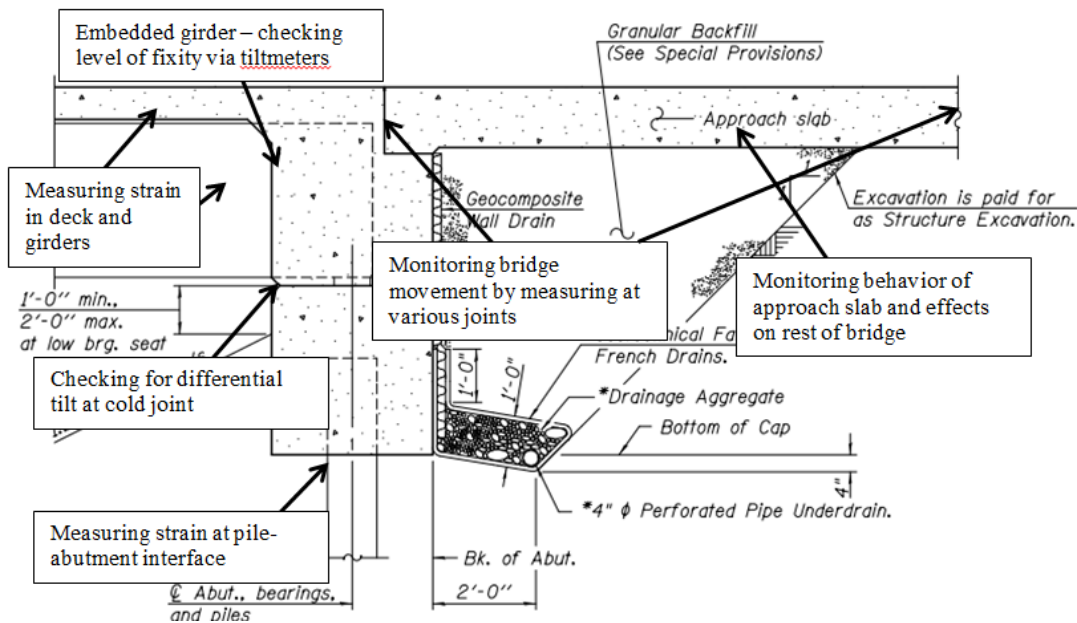


Figure 4. Schematic of instrumentation goals.

A concern for IAB superstructure behavior, and something that has scarcely been investigated to date, is the additional buildup of thermal stresses in the superstructure due to the integral abutment construction. To better understand this, strain gages were installed throughout the superstructure of each bridge, including longitudinal gages affixed to the girder at different depths and embedded in the deck. Another important aspect of IAB behavior is the overall displacement at the deck level caused by volumetric changes in the structure itself due to thermal and other loading effects. Displacement transducers, or “crackmeters,” were therefore placed at the approach slab–transition slab, approach slab–abutment, and pier–girder interfaces (of the Kishwaukee Bridge) to measure these movements. Standard surveying of the abutment was also done on a limited basis to capture its movement during extreme cold and extreme heat.

Another important aspect to evaluate was the rigidity at the abutment cold joint and girder–abutment interface. Integral abutments consist of the lower-footing (pile cap) portion and the upper-diaphragm portion, between which there is a cold joint. This joint is heavily reinforced with the objective that it behaves in a continuous, moment-resisting fashion. Therefore, tiltmeters were installed above and below the joint to measure any differential rotation that might occur. The less differential rotation there is, the closer the joint is to being completely rigid. Additionally, rotation at the two ends of the abutment can be compared to check for any twisting occurring over the abutment width. Tiltmeters were also installed at the girder end to measure any differential rotation versus the abutment. This measurement of differential rotation directly corresponds to the level of fixity at this connection. For analytical modeling, fixed connections were assumed for the abutment cold joint and girder–abutment connections, which can be further validated with the rotation measurements from the tiltmeters.

Monitoring for possible buildup of stresses in the approach slab was also deemed important, especially as approach slabs were assumed to have minimal impact on IAB behavior and were therefore neglected in the parametric study. A limited number of embedded strain gages were placed in the approach slab (at Kishwaukee) to capture any buildup of stresses or major axial force applied to the IAB superstructure. The concern is that frictional forces can occur due to soil–concrete interaction on the bottom of the approach slab, causing additional axial restraint to be imposed on the bridge. Finally, limited focus was also placed on substructure behavior, with an emphasis on confirming pile behavior previously investigated by other research projects. Strain gages were therefore installed on the H-pile abutment foundations to gather strain data at the pile–abutment interface, which is where the maximum strain is known to occur.

3.3 DETAILED INSTRUMENTATION AND MONITORING SCHEME

To minimize costs and simplify the instrumentation scheme, the symmetry of the two bridges was utilized. Instruments were placed only on the east half of the Kishwaukee River Bridge, with an assumption that the west half would behave similarly. Likewise, abutment and pile behavior was monitored only on the west end of the UPRR Bridge. Tiltmeters, displacement transducers (“crackmeters”), strain gages, and multiplexers (to act as junction boxes) were installed throughout each of the instrumented bridges. All necessary instruments and data acquisition equipment were procured from GEOKON, Inc., and are outlined in Table 2. Each instrument, except for the multiplexers (junction boxes), is equipped with a temperature sensor.

Table 2. Instruments Used at the Monitored Bridges.

Instrument Name	Model Number	Range	Resolution	Accuracy
Arc-welded strain gage	4000	3000 $\mu\epsilon$	1.0 $\mu\epsilon$	+/- 0.5%
Spot-welded strain gage	4150	3000 $\mu\epsilon$	0.4 $\mu\epsilon$	+/- 0.5%
Embedded strain gage	4200	3000 $\mu\epsilon$	1.0 $\mu\epsilon$	+/- 0.5%
Tiltmeter	6350	+/- 10°	8 arc seconds	+/- 0.1%
Displacement transducer (“crackmeter”)	4420	+/- 6”	0.025%	+/- 0.1%
Multiplexer (junction box)	8032	Can connect up to 16 instruments (1 per channel)		
Datalogger	8021	Can connect up to 8 multiplexers		

3.3.1 Strain Gages

Strain gages were placed on piles and girders and in the deck of both bridges, as well as in the approach slab of the Kishwaukee Bridge. Arc-welded strain gages were used to instrument three abutment piles of each bridge prior to their being shipped to the site. Two exterior piles—the pile nearest the obtuse corner and the pile second-nearest to the acute corner—and a middle pile were chosen so as to represent the south, middle, and north portions of each bridge, located at the east abutment of the Kishwaukee Bridge and at the west abutment of the UPRR Bridge. This permitted the measurement of pile strain at or near both acute and obtuse corners of the bridge. Two different instrumentation configurations were planned—configuration A, with a total of 8 gages; and configuration B, with a total of 4 gages; as shown in Figure 5. Configuration A has two sets of 4 gages—one set at the pile-cap boundary and the other 14 in. below that. Configuration B has only one set of 4 gages located at the pile-cap boundary. The gages are located at the quarter points of each pile flange. It was originally planned for exterior piles at both bridges to have configuration A; however, during construction the south exterior pile and the interior pile at Kishwaukee were switched. Therefore, the north exterior and interior pile at Kishwaukee have configuration A of pile strain gages.

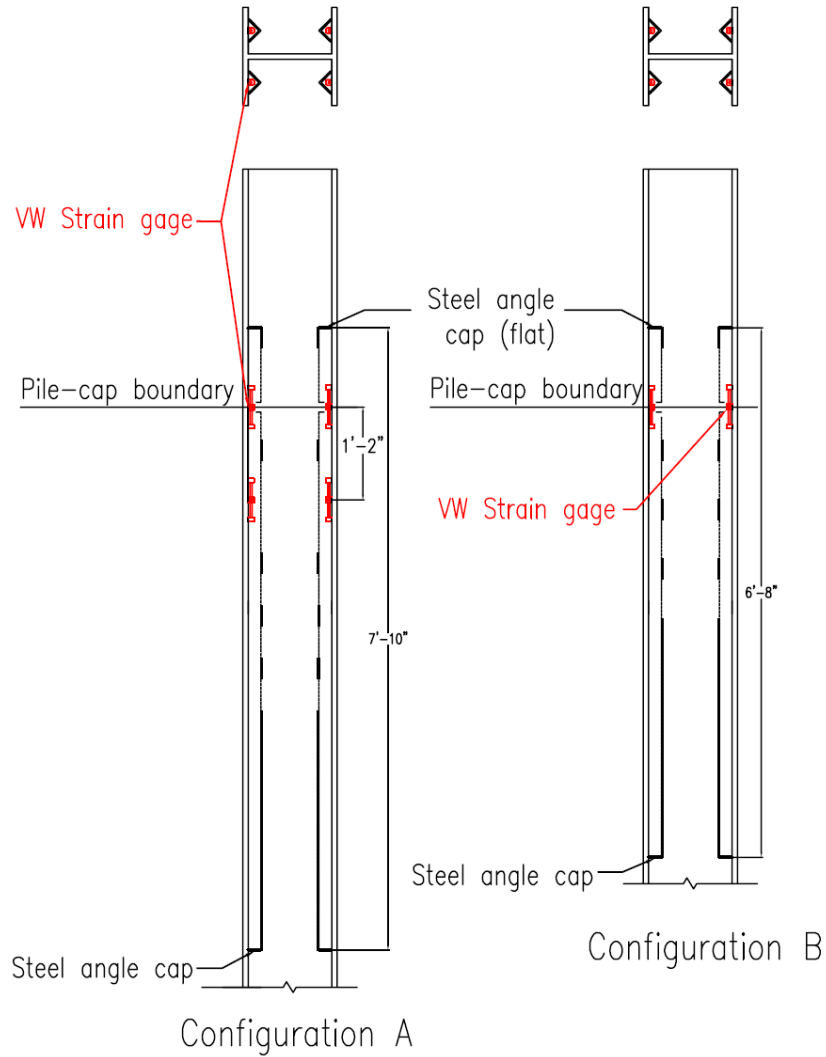


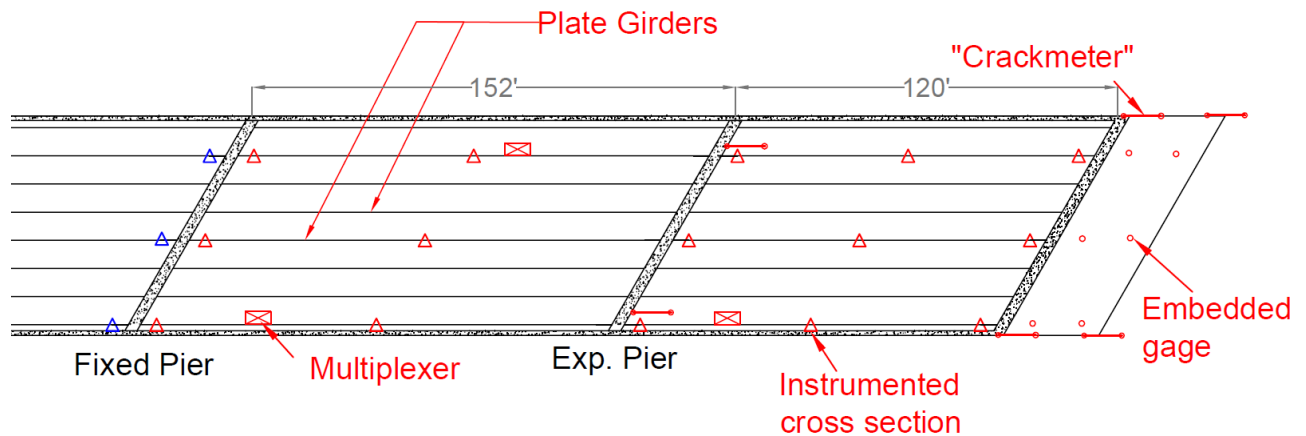
Figure 5. Pile-instrumentation schematics.

The piles were instrumented before being placed, so a steel angle cap was used to protect the pile gages on both bridges; and the Kishwaukee piles also had an additional tapered end-cap to protect the angles from being dislodged during the driving process. (The steel angle caps are not anticipated to increase the pile stiffness.) The arc-welded gages were attached using two steel mounting blocks and set screws, as shown in Figure 6. The coil housing was secured to the gage using a hose clamp; and the wires exited the protective steel angle through a notch, which was later sealed with spray-foam insulation.



Figure 6. Arc-welded pile strain-gage installation.

The three girders corresponding to the instrumented piles on each bridge were also instrumented, with spot-welded strain gages. These gages were placed at various cross sections along the length of each bridge and at different depths on the girder, as shown in Figure 7 (north is up) and Figure 8. The gages were typically installed on the top flange, the bottom flange, and at mid-height of the girder web. Additionally, embedded strain gages were placed within the concrete deck at the same cross-section locations along each bridge. (Note that the Kishwaukee Bridge also has six more embedded strain gages placed in the approach slab.)



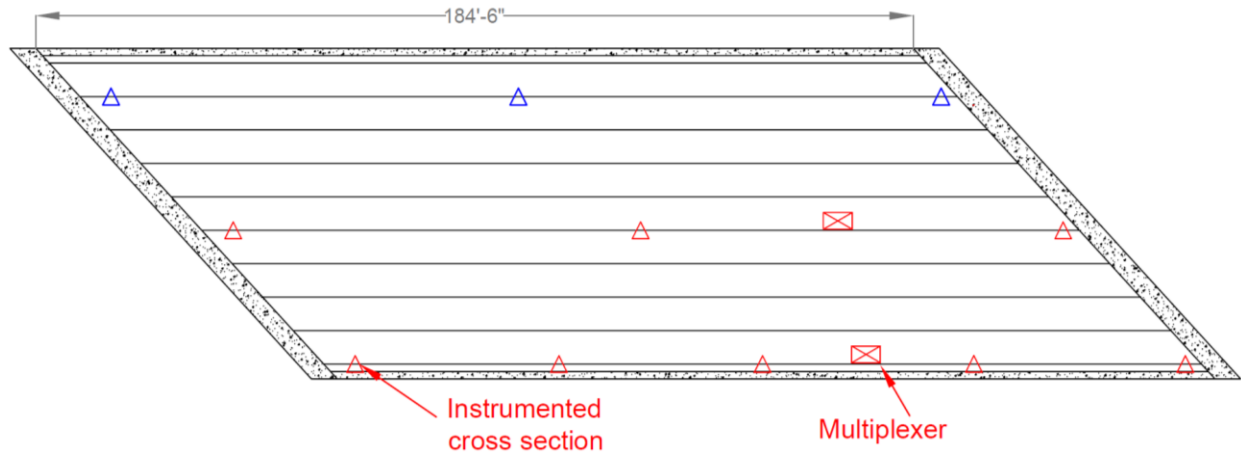


Figure 7. Plan view of instrumentation scheme for Kishwaukee (top) and UPRR (bottom).

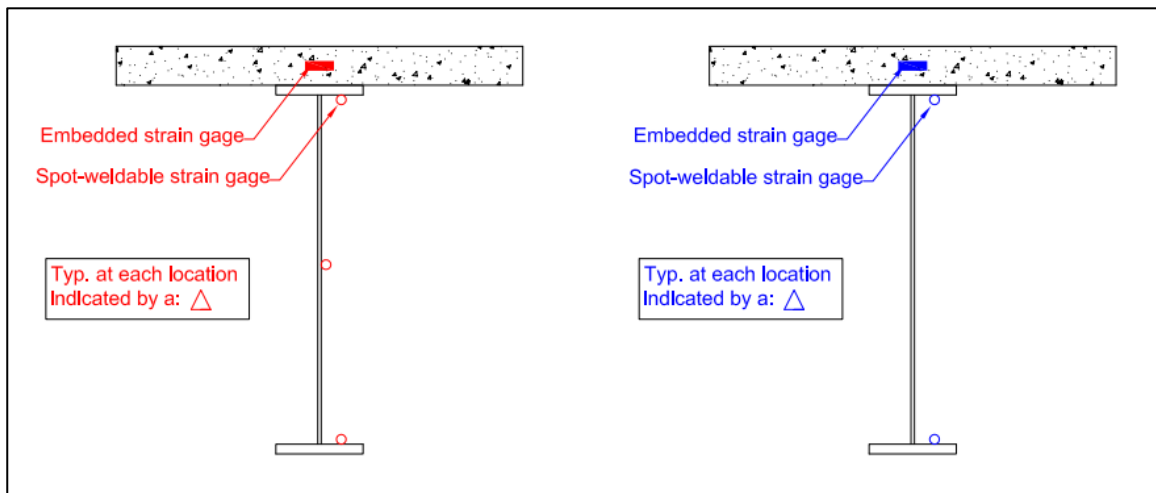


Figure 8. Instrumentation schematic for superstructure cross sections.

The spot-welded girder gages were attached at the steel fabricators, after preparing the surface with a power sander and wire brush, before then being shipped to the site. The spot-welding process uses very low energy and is specifically for use with strain gages and in other electronic applications. Therefore, these spot-welded connections had negligible effect on the steel used for the plate girders, and the process was consequently easier to get approved by the bridge designers and fabricators. The girder strain gages are protected by a cover plate, as shown in Figure 9, to prevent damage during construction and general elemental exposure. The embedded strain gages in the deck and approach slab were tied off to the steel reinforcement with wooden blocks so as to measure only the concrete strain, as shown in Figure 10. Coil housing was connected to the gage, with the wiring running along rebar and through the forms down to multiplexers attached to the girders.

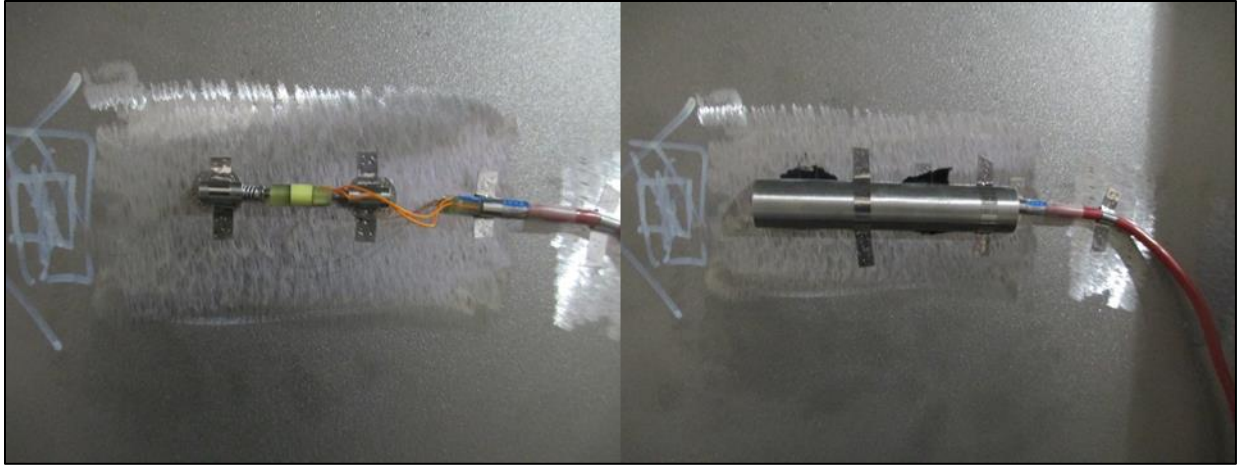


Figure 9. Spot-welded girder strain gage without and with its cover plate.



Figure 10. Approach-slab-embedded strain gage.

3.3.2 Tiltmeters

To evaluate the rigidity of the cold joint and girder–abutment interface, one abutment and a number of corresponding girder ends on both bridges were instrumented using tiltmeters. These gages can measure only rotation about one axis, and thus they were oriented to measure rotation in the longitudinal direction. Tiltmeters were placed at the north, middle, and south portions of the abutment, corresponding to the instrumented girder lines, as shown in Figure 11 and Figure 12. At the north and south ends, tiltmeters were placed on the abutment above and below the cold joint and on the girder. In the middle of the abutment (at Kishwaukee), tiltmeters were placed only on the abutment above the cold joint and on the girder; at UPRR, a tiltmeter was placed only above the cold joint of the abutment. The tiltmeters were attached with brackets to the steel girders and anchored to the concrete abutment, as shown in Figure 13. The tiltmeters are flush with the abutment face, and thus an offset equal to the abutment skew is used when analyzing the field data, to account for the fact that the abutment and girder-rotation measurements are not parallel to one another.

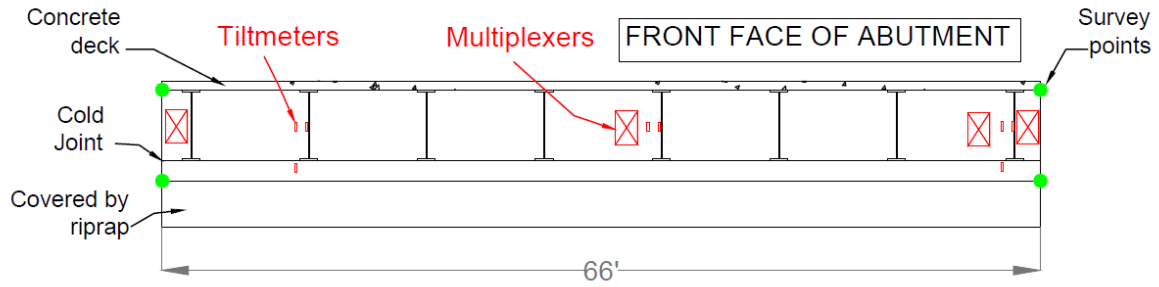


Figure 11. Elevation of east abutment at Kishwaukee.

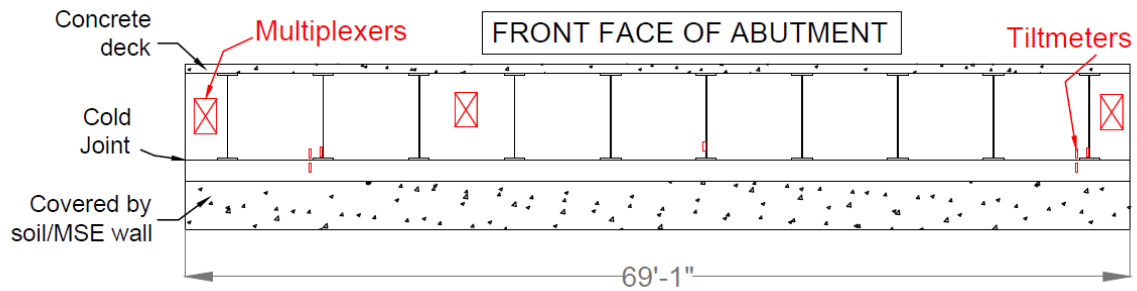


Figure 12. Elevation of west abutment at UPRR.

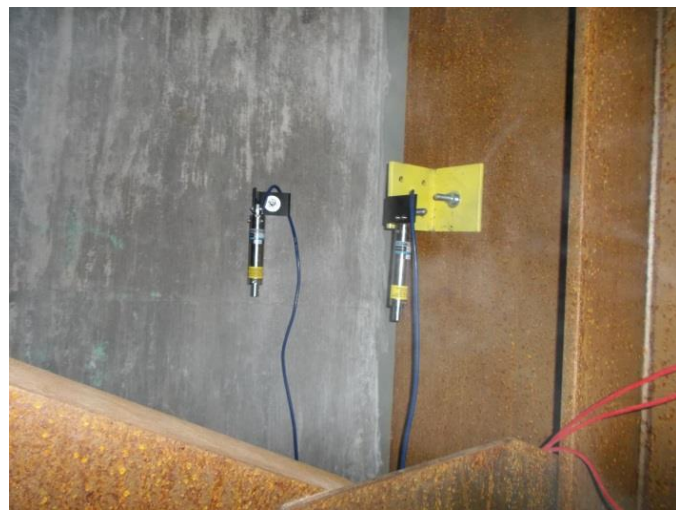


Figure 13. Tiltmeter installation at Kishwaukee on the north side (left) and middle (right) of abutment.

3.3.3 Displacement Transducers (Crackmeters)

To monitor overall bridge movement, the girder–pier, abutment – approach slab, and approach slab–transition slab interfaces at the north and south ends of the east side of the Kishwaukee Bridge were instrumented with displacement transducers (crackmeters). The largest available

crackmeters, which have a range of +/- 6 in., were used to ensure an ability to measure “expansion joint” displacements at the approach slab–transition slab interface. The crackmeters were installed by anchoring each end into the concrete, with a small spacer, as shown in Figure 14. At the girder–pier interface, the crackmeter was installed using various brackets in order to bolt one end to the cross-frame connection plate and then anchor the other end to the concrete pier.



Figure 14. Crackmeter installed at approach slab–transition slab interface.

3.3.4 Surveying

For the Kishwaukee east abutment, surveying was conducted in September 2014 and February 2015 at two points on both the north and south ends of the abutment. These survey points were determined to align roughly with the top and bottom of the girders, as indicated in Figure 11 and Figure 15. The surveying data provides points of comparison for the crackmeter joint-displacement data.



Figure 15. Kishwaukee survey locations.

3.3.5 Data Acquisition

A GEOKON Micro-1000 Datalogger was used to collect the data from both sites. A cellular modem was placed at each site to allow data to be collected remotely. A null modem adapter was also installed to remove the need for a computer at each site and to allow the modem to

communicate directly with the datalogger. A 130W solar panel and two 110Ah batteries in parallel were installed at each site as a power source for the modem and datalogger.

Several multiplexers were placed throughout each bridge site to be used as junction boxes. A maximum of 16 instruments can connect to each multiplexer, which then in turn connects to the central datalogger at each site. The multiplexers were mounted to the steel girders or the face of the concrete abutment. A daisy-chain was utilized to connect the multiple multiplexers to each other before connecting to the datalogger, as a way to reduce the amount of necessary wiring.

Data collection from the Kishwaukee Bridge began on May 24, 2014, and ended on May 26, 2016. At UPRR, data collection began on June 18, 2014, and ended on September 10, 2015. (Data collection at both bridges eventually ended due to issues preventing the download of data from the datalogger.) For the Kishwaukee Bridge, the sensors were sampled every 15 minutes until March 2015. From then on, the sampling rate was increased to collect data every 5 minutes. For the UPRR Bridge, sensors were always sampled every 15 minutes. A smaller collection interval on the order of seconds was not feasible because it takes approximately 2 seconds to read a vibrating-wire gage, which means it requires several minutes for all the data to be collected. However, the intervals utilized are adequate for analyzing thermal load effects; and they can help to give at least some insight about live-load effects as well. For data processing, a macro was created to save all the data to a field data Excel workbook, after which MATLAB was then used for data analysis and processing.

CHAPTER 4: FIELD RESULTS

4.1 DATA INITIALIZATION

Initial readings were taken for the spot-welded strain gages on the girders, at the steel fabricator right after being installed (and thus are not indicative of their condition upon completion of bridge construction). Therefore to be consistent with all the other instruments, initialization was made using the first field-collected data point for each gage, which is most indicative of the bridge condition after it became integral (and thus it is assumed that this already incorporates the dead-load contribution). The reported measurements are then due only to thermal changes, perhaps also with some modest live-load and/or other time-dependent effects. The first data points were taken at relatively warm temperatures, so most of the field results represent net thermal contraction.

4.2 AVERAGE SUPERSTRUCTURE TEMPERATURE

To analyze the IAB thermal effects represented by the sensor measurements, a definition of the average bridge-superstructure temperature had to be established. After observing temperature trends from all the different sensors, it was felt that the exposed girder strain gages best represented the air temperature. Focusing on only the girder gages, an average was then taken of the strain values at a specific girder depth (e.g., top flange, web, bottom flange) along each instrumented girder. These averages displayed very little temperature variation along the girder length; however, the exterior girders had larger temperature ranges through the depth of the girder. From these observations, the average superstructure temperature was defined as the mean value of the temperature readings from all the spot-welded strain gages on the middle girder.

This definition was validated with data from a weather station at the nearest airports, which were Rockford International Airport (10 miles from the Kishwaukee Bridge) and DuPage Airport (15 miles from the UPRR Bridge). The calculated average superstructure temperature tracks closely with the temperature from the weather station throughout the year, as seen in Figure 16, with the best correlation during warmer seasons. Average superstructure temperature lags slightly behind the weather station temperature and typically does not quite reach as extreme magnitudes of temperature as those reported by the weather station. The same average superstructure temperature definition has been utilized for both bridges; however, for the UPRR Bridge, readings from the gages closest to the west abutment on the middle girder were not included because their temperature trends were inconsistent with the trends for the rest of the bridge. The average superstructure temperature at the onset of monitoring was 75 °F and 73 °F for Kishwaukee and UPRR, respectively. Thus, the majority of the subsequently reported field data represents net thermal contraction.

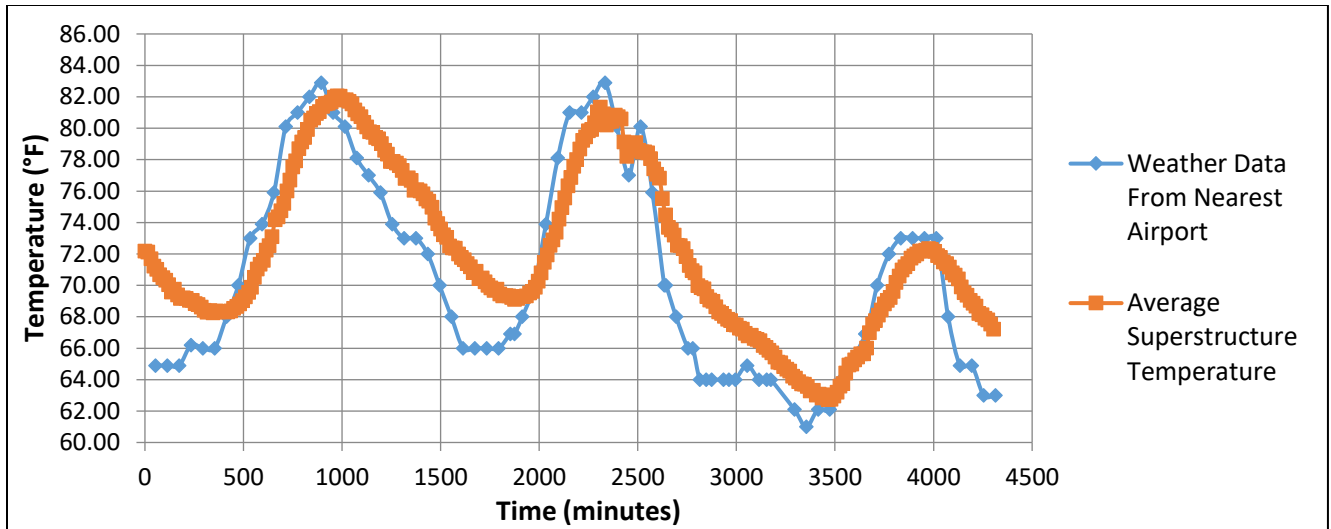


Figure 16: Kishwaukee temperature comparison from 8/10/2014 to 8/12/2014.

4.3 GLOBAL BRIDGE MOVEMENT

4.3.1 Crackmeter Results

An important aspect of this project was to gain a better understanding of the IAB deck displacement and overall bridge movement. Because the gages (crackmeters) used to monitor this movement were installed only at the Kishwaukee Bridge, this section focuses only on that bridge. As expected, the instrument readings show that global bridge movement is directly affected by change in temperature. Crackmeter readings fall within a relatively wide band, in part due to any influence of live-load and/or other time-dependent effects. The crackmeter data show a linear trend when plotted against the average superstructure temperature, as can be seen in Figure 17. The approach slab–transition slab interface displays the largest magnitude of displacement with change in temperature. This finding is as expected because it is the location of the expansion joint. At both the north and south ends, data for this interface show two distinct lines. Figure 18 indicates that this shift happened after a full year of data collection, when the bridge appears to have overcome some resistance and the joint closed to even beyond its original gap width, setting up a new “permanent” displacement. However, the overall trend is consistent thereafter, as the slope remained the same. This shift could in part be attributable to possible backfill compaction from the previous expansion cycle, thus allowing the bridge to expand even more and the expansion joint to close even further than in the previous year.

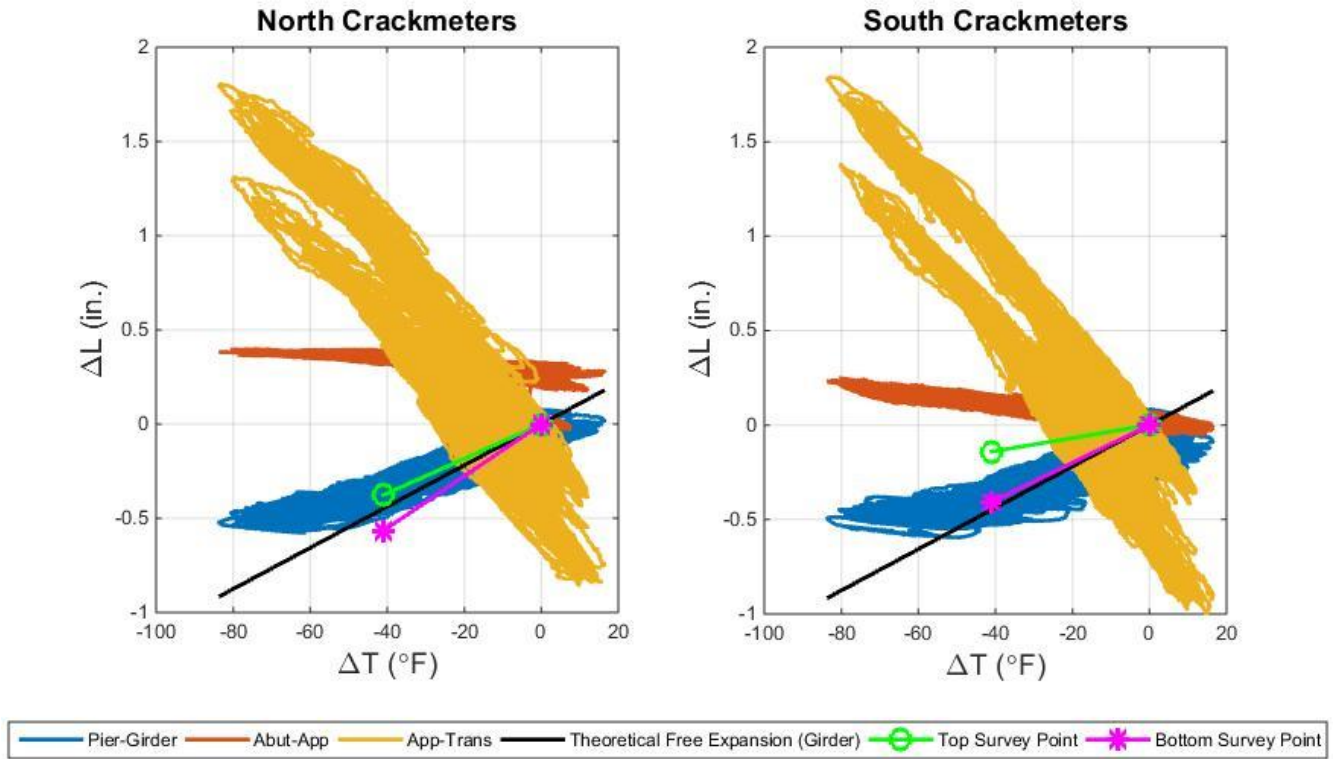


Figure 17. Kishwaukee crackmeter displacements.

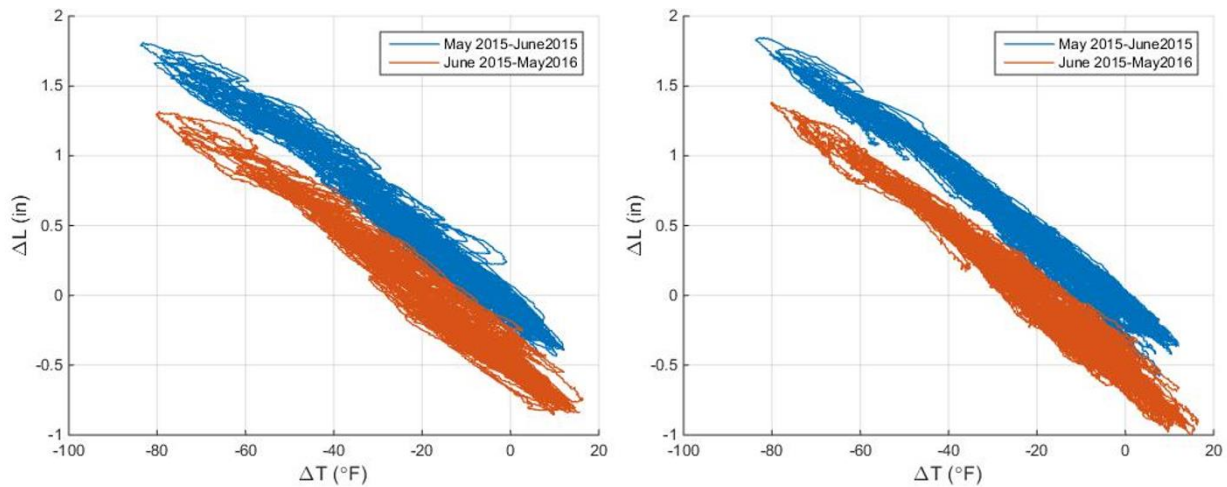


Figure 18. Approach-transition slab joint displacements (Kishwaukee) for the north (left) and south (right) ends.

As compared to the approach slab-transition slab interface, the approach slab-abutment interface data has a very shallow slope, as expected due to reinforcing steel continuity across this construction joint. The slight jump seen in the north approach slab-abutment curve is likely due to the removal of construction equipment. Figure 17 also shows that the pier-girder displacements are lower than what is calculated from theoretical free expansion/contraction (using a coefficient of thermal expansion of 6×10^{-6} in./in./ $^{\circ}F$ for the 152-ft span of composite

plate girder and concrete deck from the middle of the bridge out to this pier). These lower displacements measured in the field support a general finding from the parametric study that longitudinal movement at the deck level does not reach the displacement magnitude of total free thermal expansion/contraction (LaFave et al. 2016a). Both the north and south pier–girder curves shallow out at temperature reductions greater than 50°F from the ambient at the onset of monitoring, which is likely due to interaction with the expansion bearing at such cold temperatures.

4.3.2 Approach Slab Results

The Kishwaukee approach-slab strains were analyzed to better understand approach slab behavior and to help calculate bridge–abutment movement. Upon analysis of the embedded approach-slab gage temperature readings, it was noted that the average temperature of the approach slab differed from the calculated average bridge superstructure temperature by an average of ± 5 °F, and sometimes up to 22 °F, as seen in Figure 19. Therefore, the average temperature from the approach-slab gages was utilized as the temperature for subsequent analysis of the approach-slab data (i.e., for gage-temperature correction). Readings from each approach-slab strain gage trend well over time with the average approach-slab temperature, as shown in Figure 20.

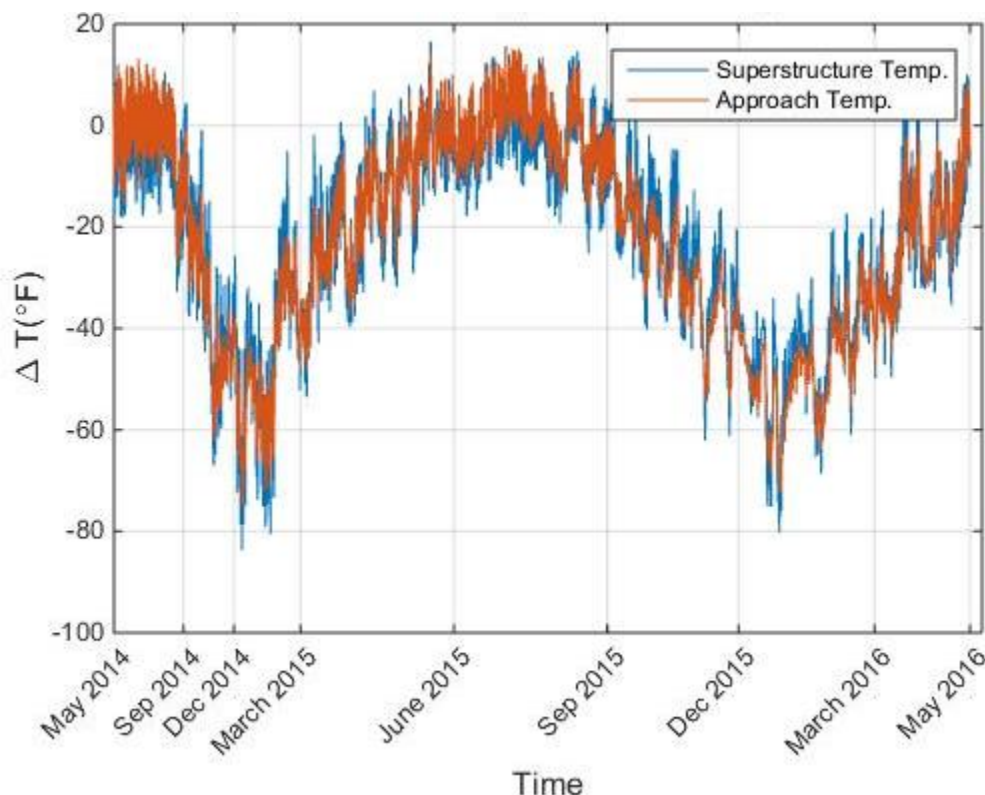


Figure 19. Comparison of average superstructure temperature and average approach-slab temperature over time (Kishwaukee).

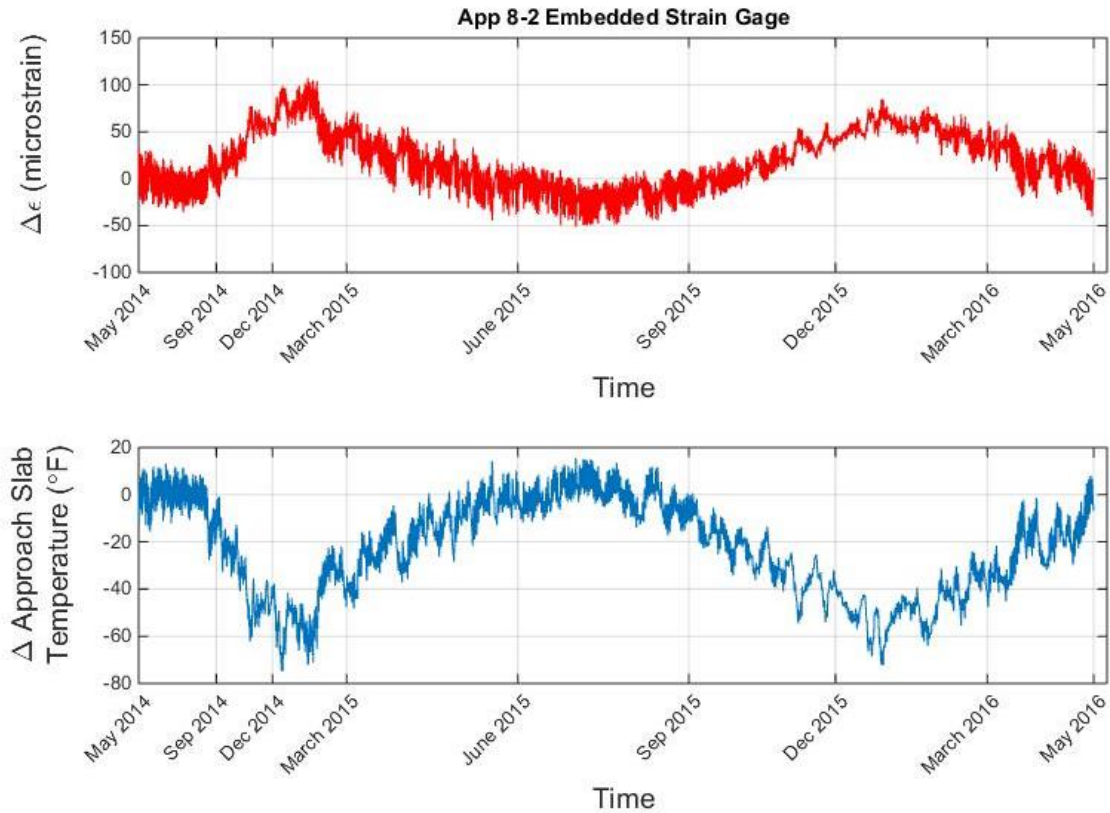


Figure 20. Approach-slab 8-2 gage strain and average approach-slab temperature vs. time (Kishwaukee).

With an assumption of elastic behavior, the strain measurements were used to estimate the approach-slab displacement. To do so, the average strain of the two gages along each instrumented girder line was taken and then corrected for temperature effects on the gage due to the difference in coefficient of thermal expansion of the steel vibrating wire of the gage and of the concrete the gage is embedded in. Accounting for this correction then gives the actual strain of the concrete member (i.e., the change in unit length that a dial gage attached to the surface would measure), which is given by

$$\Delta\varepsilon_{actual} = \Delta\varepsilon_{measured} + \Delta T_{Approach\ Slab} \times \alpha_{gage\ steel}$$

where $\Delta\varepsilon_{measured}$ is the change in strain directly reported from readout/datalogger in microstrain and $\alpha_{gage\ steel}$ is the coefficient of thermal expansion of steel (6.78 microstrain/°F for a model 4200 embedded strain gage).

The actual strain results were then multiplied by the approach slab's total length (30 ft) to obtain a change in length along each instrumented line. Results show that the north and south ends have very similar displacements and follow a linear trend with change in temperature, as seen in Figure 21. The results show that, during negative changes in temperature, the approach slab contracts, which is designated by a negative change in length. This finding indicates that even though the bridge pushes and pulls the approach slab, it is still able to go through its own

cycles of thermal expansion and contraction due to the relative freedom of movement provided by the expansion joint. This approach-slab change in length was then also used as one component to calculate the overall abutment displacement in the field, as discussed later in section 4.3.3.

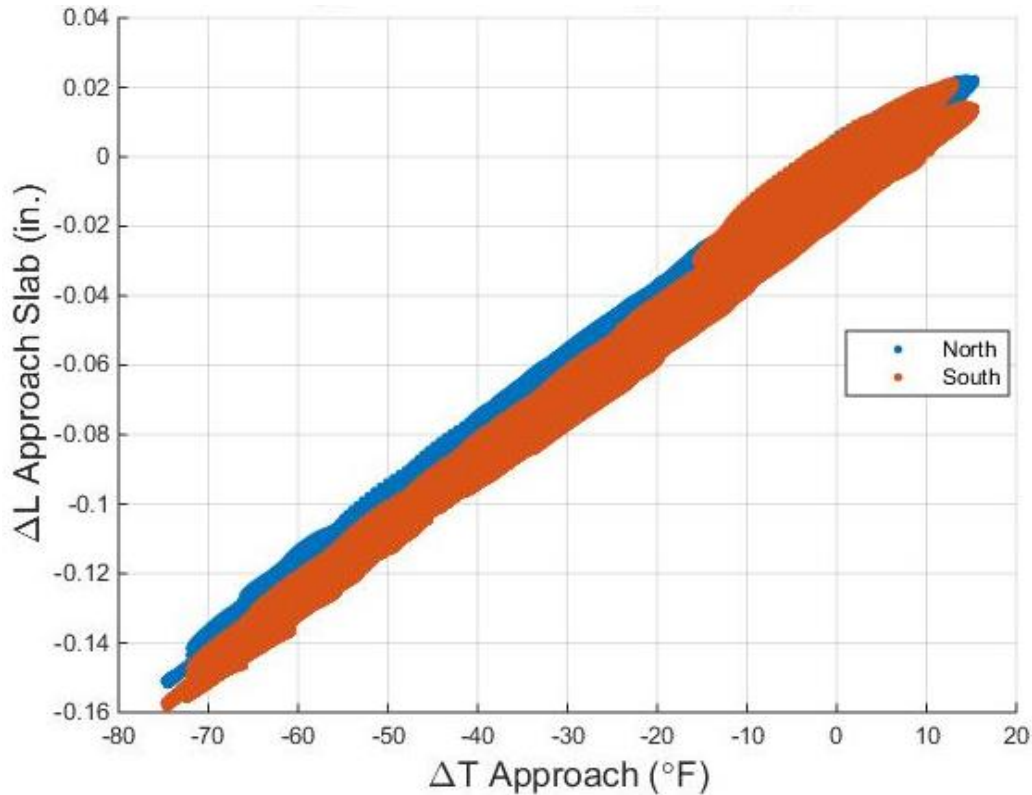


Figure 21. Approach-slab change in length (Kishwaukee).

To gain an overall sense of the *stress* imparted on the approach slab, another correction was applied to the original strain measurement to obtain the load-related strain. An average strain from all of the approach-slab gages was taken and then corrected for both the thermal effects on the gage itself and the strain related to thermal expansion and contraction of the slab, as given by

$$\Delta\varepsilon_{load} = \Delta\varepsilon_{measured} + \Delta T_{Approach\ Slab} \times (\alpha_{gage\ steel} - \alpha_{concrete})$$

where $\alpha_{concrete}$ is the coefficient of thermal expansion of the approach slab (assumed to be 5.5 microstrain/°F).

The load-related strain calculated from the expression above represents the strain in the approach slab due to external forces or restraint, which would lead to stress in the slab. Using Young’s modulus of the slab to convert strain to stress, Figure 22 shows the calculated stress in the approach slab over the entire period of data collection. The results show seasonal trends over time. Figure 23 plots this same data versus change in temperature and indicates a shift (decrease in slope) in the stress after every year of data collection. It should also be noted that

there is a shift in the data after the first 4 months of data collection (shown in blue), which may be related to construction activity (as mentioned previously). After this shift, the data clearly follows a linear trend with change in temperature, however the slope decreases after each summer. As the slope decreases, the approach slab stress becomes more constant and appears to be less constrained and able to displace more easily. This could likely be attributed to soil settlement beneath the approach slab, which would reduce the friction on the bottom surface of the approach slab after each annual cycle. This behavior is similar (and could also be related) to the shift seen in the approach – transition slab displacements in Figure 18, where the bridge overcomes some resistance and the expansion joint closes further than in the previous year.

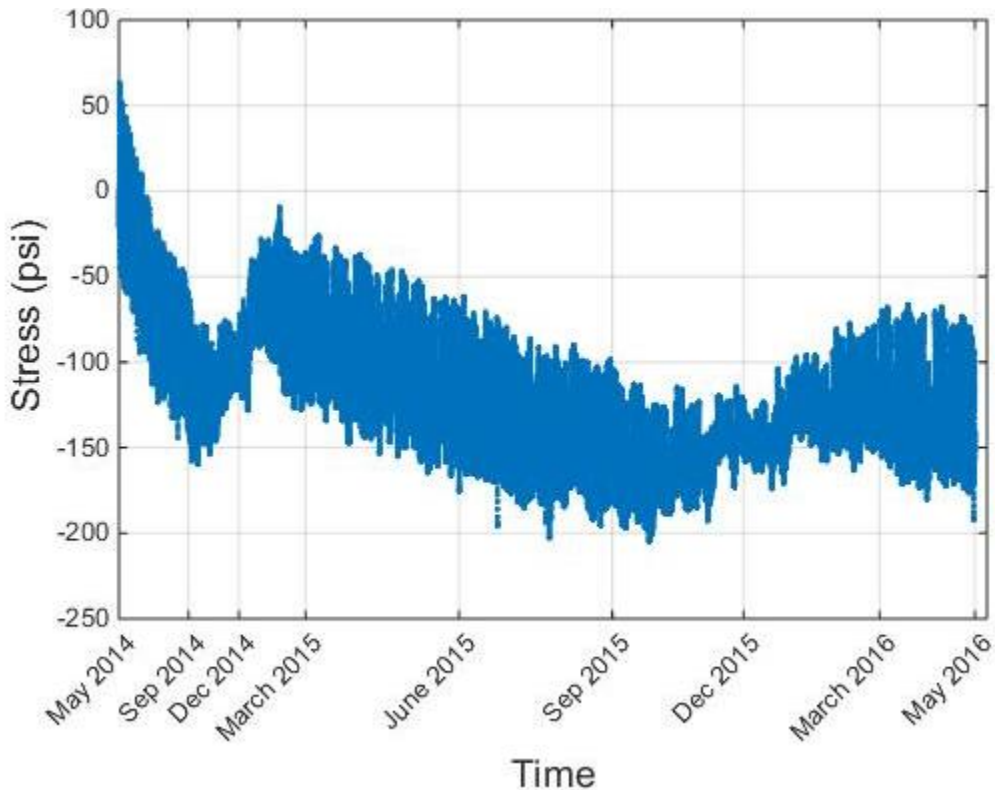


Figure 22. Approach-slab stress (Kishwaukee).

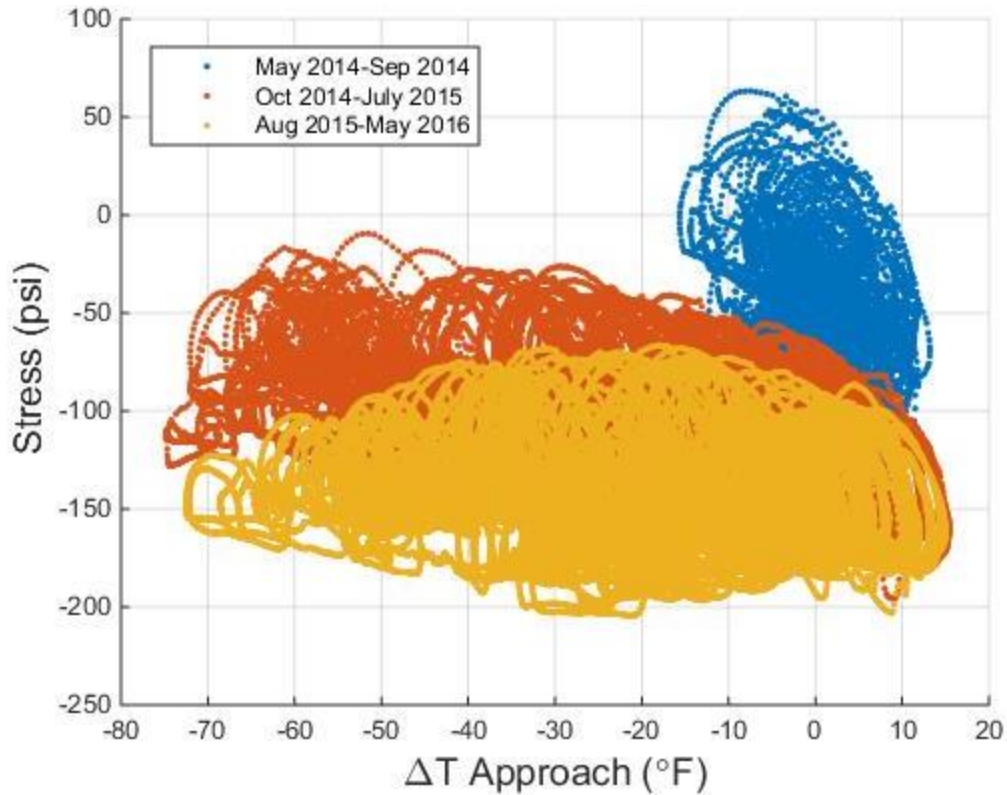


Figure 23. Average approach-slab stress vs. change in temperature (Kishwaukee).

4.3.3 Calculated Abutment Displacements

As stated earlier, a major point of interest for IABs is the longitudinal bridge displacement at the deck level, which can be taken from the abutment movement. At Kishwaukee, this abutment movement was calculated using the crackmeter and approach-slab strain gage measurements, along with other certain necessary assumptions. The crackmeters measure relative displacement, so there is no set reference point, making it difficult to distinguish which component is actually moving in an absolute sense (e.g., the abutment moving versus the approach slab moving). Therefore, the strategy used to calculate abutment displacement assumes the transition slab as the fixed point. Then the calculated approach-slab change in length was summed with the negative (to account for direction) total of the approach slab–transition slab and approach slab–abutment crackmeter displacements, to calculate the abutment displacement. Due to the previously mentioned shift in approach slab–transition slab measurements, the resulting abutment-displacement plots also show a shift, as seen in Figure 24. As the east abutment and approach slab were instrumented, a negative displacement indicates that the movement is toward the east, signifying bridge contraction.

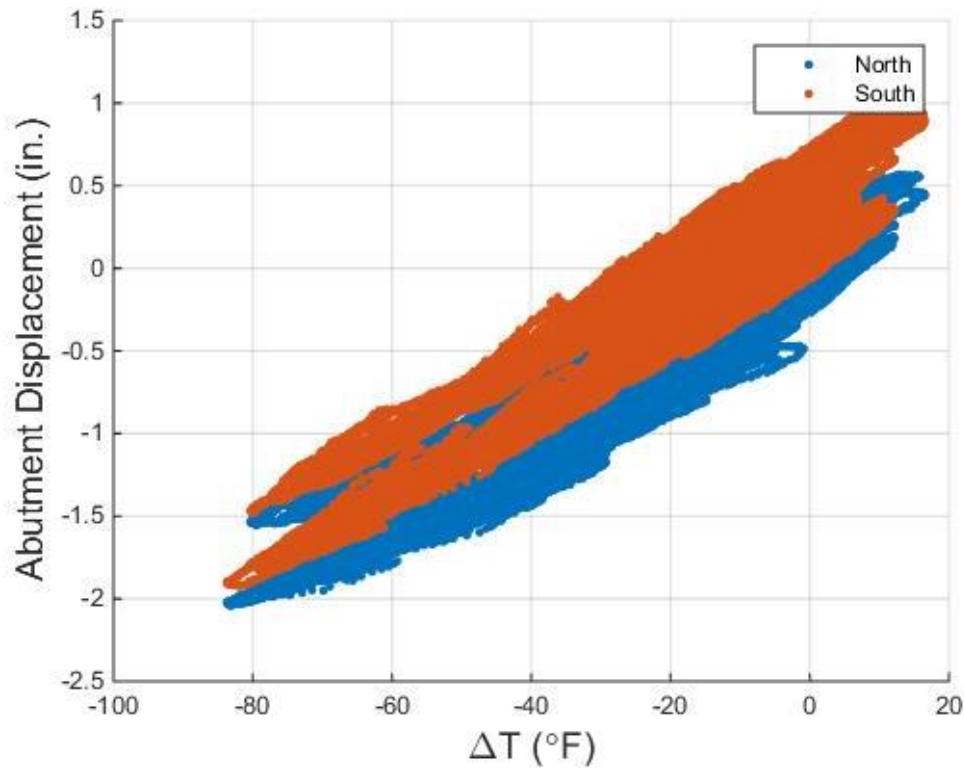


Figure 24. Abutment displacements of the north and south edges of the Kishwaukee east abutment.

As can be seen in Figure 25, the calculated abutment displacements are greater than the displacements measured by surveying. This finding could be due to several factors, including the fact that the abutment-displacement calculations are based on relative displacements and the fact that the surveying data was initialized in the fall, whereas the bridge sensors were initialized with data from the spring. However, the overall linear trend with temperature is fairly similar; and both the field data and surveying data show that the north abutment side (near the acute corner) has a greater magnitude of longitudinal displacement in contraction. This displacement pattern is in agreement with the parametric study findings, which indicate greater longitudinal abutment displacement near the acute corner for bridges with mild to high skew (LaFave et al. 2016a). It should also be noted that the survey data points have been shifted to align with the middle of the field abutment displacements, corresponding to the actual change in temperature at the time of surveying.

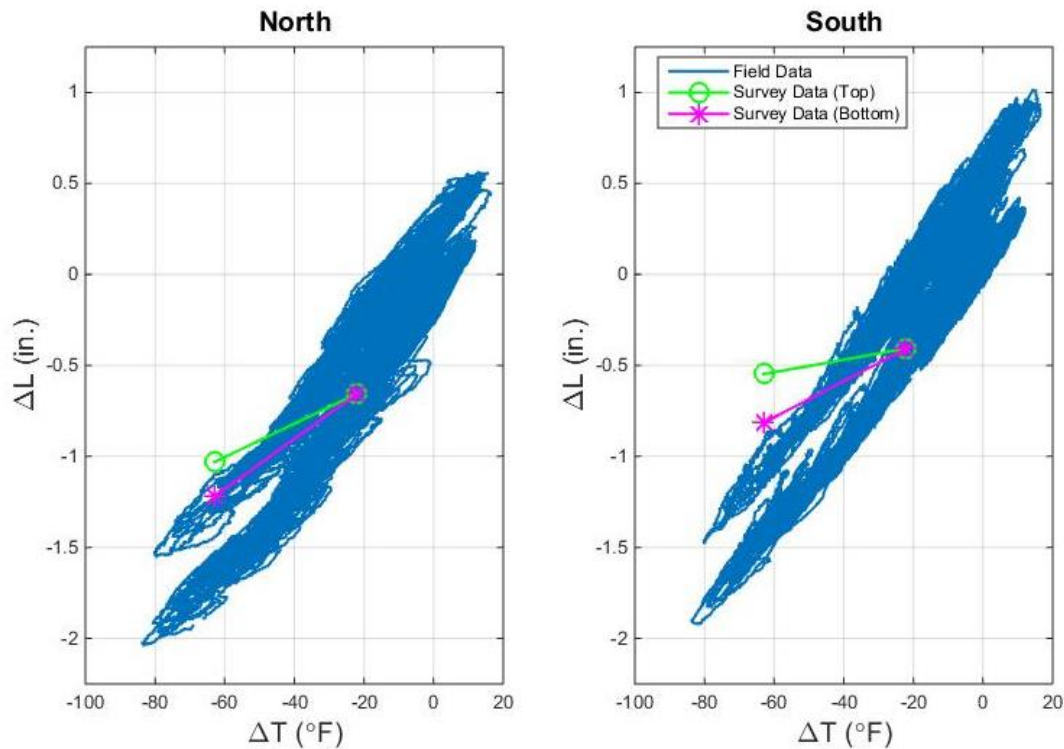


Figure 25. North and south Kishwaukee calculated abutment displacements and abutment survey data.

4.4 ABUTMENT ROTATION

A main goal of the field instrumentation was to evaluate the level of fixity at several interfaces of the abutment, in order to validate previous modeling assumptions. To do this, both individual tiltmeter measurements and calculated relative rotations were analyzed. For reference, Figure 26 depicts the labeling convention used for the girder and top/bottom abutment tiltmeter gages at a typical abutment location. For both bridges, overall rotation measurements from the individual tiltmeters show a linear trend throughout the entire data collection period when plotted versus change in temperature, cycling back and forth along the same path every season. However, as can be seen in Figure 27, the rotations in the plots appear in bands, regardless of whether they are plotted against temperature or time. The distinct bands are most likely due to different live-load scenarios in the span (possibly along with some abutment cracking, allowing for different levels of rotation). Figure 28 highlights the central band, which contains the majority of the data points and tends to validate the previous assumptions. This central band of data can thus be taken as indicative of the effects due solely to thermal changes.

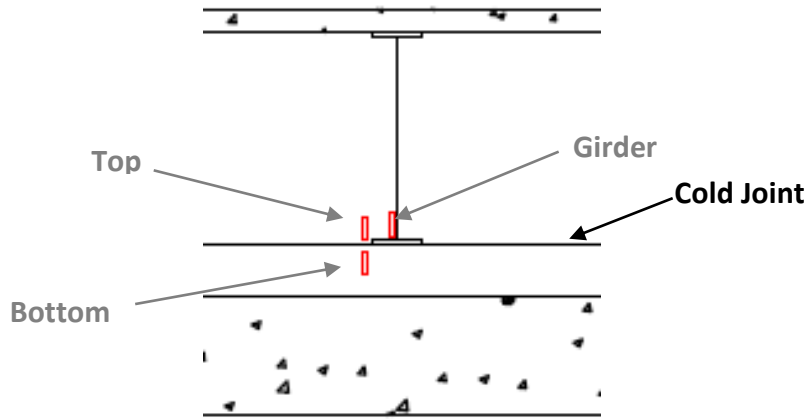


Figure 26. Tiltmeter labeling convention at an abutment.

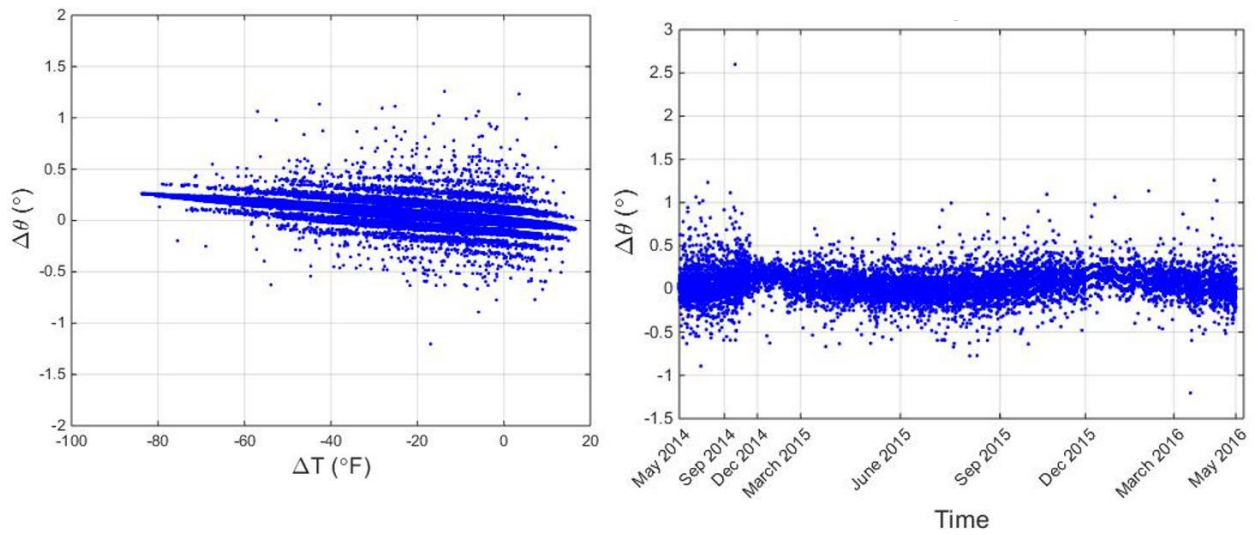
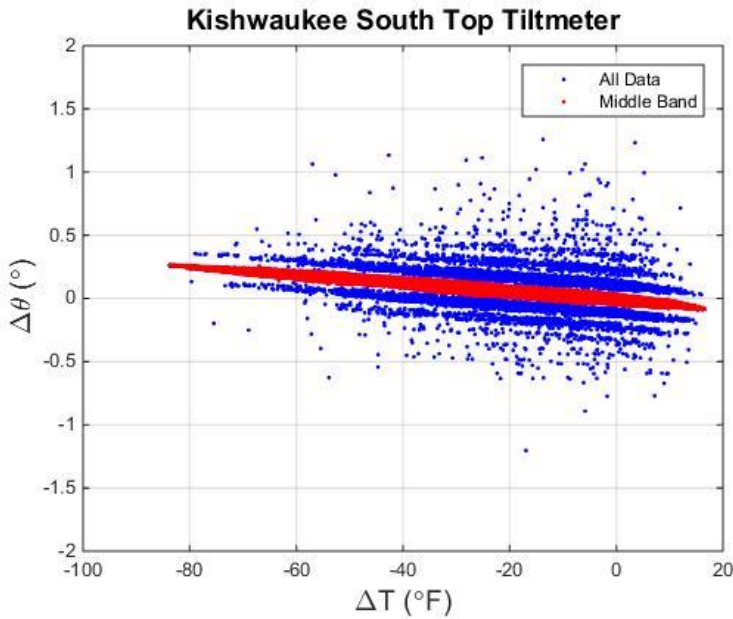
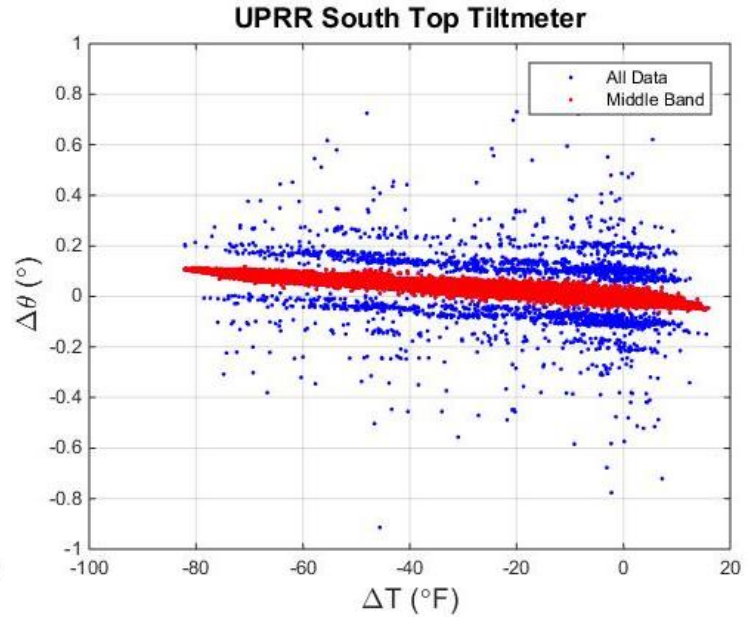


Figure 27. Kishwaukee south side top tiltmeter rotations vs. change in temperature and time.



Middle band = 93% of total data



Middle band = 94% of total data

Figure 28. South top tiltmeter rotation vs. change in temperature for Kishwaukee and UPRR.

The tiltmeter data can be utilized to analyze what is happening to the abutment itself. Looking at the top tiltmeter rotation measurements provides a representation of the amount of rotation the abutment undergoes along its length. Figure 29 shows a comparison of the three top tiltmeters along the abutment at Kishwaukee and UPRR. An overall higher abutment rotation is observed at Kishwaukee. Upon further trend line analysis, abutment rotations slightly increase from north to south, or from acute to obtuse corner, at UPRR. Similarly, at Kishwaukee, the south abutment rotations are greater than at the middle, however the trends in regards to the north of the abutment are unclear due to the noise in the data.

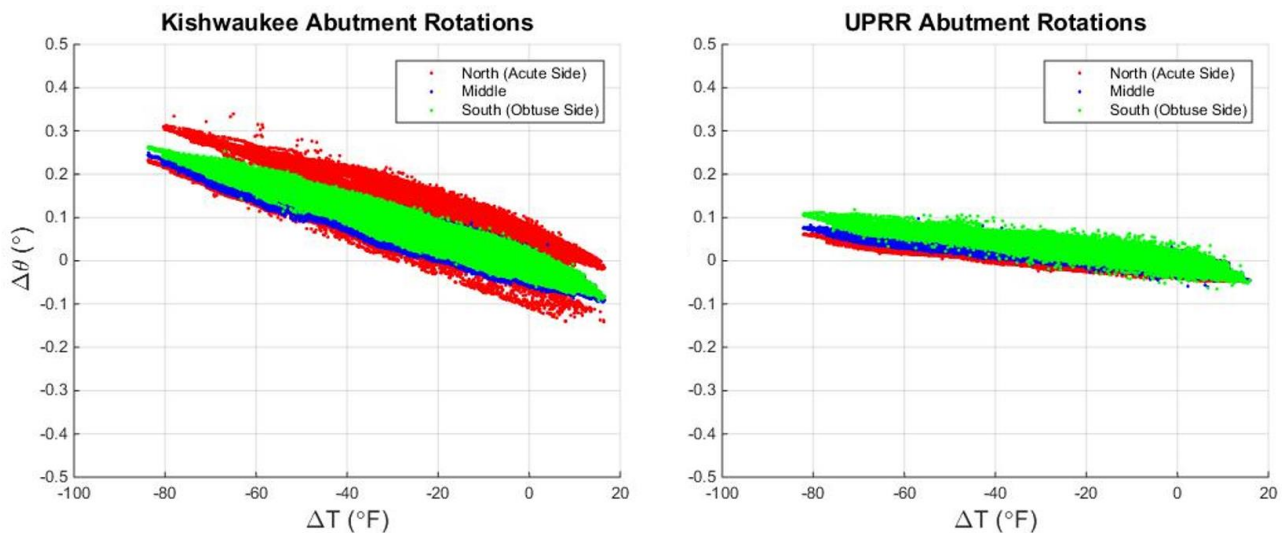


Figure 29. Kishwaukee and UPRR abutment rotations along the abutment.

One of the goals of monitoring the tiltmeter measurements was to determine the rigidity of the abutment cold-joint connection. To do this, the differential rotation between the upper-diaphragm (top tiltmeter) and pile cap/lower-footing (bottom tiltmeter) regions of the abutment was assessed. Focusing on the central band of data, the observed differential rotation at both the north and south sides of the approach slab appears to be essentially zero at all temperatures for both bridges, as can be seen in Figure 30 for the south side. This validates the fully continuous (and uncracked), moment-resisting connection assumption that was used in the modeling for the site bridges and as part of the previous parametric study models.

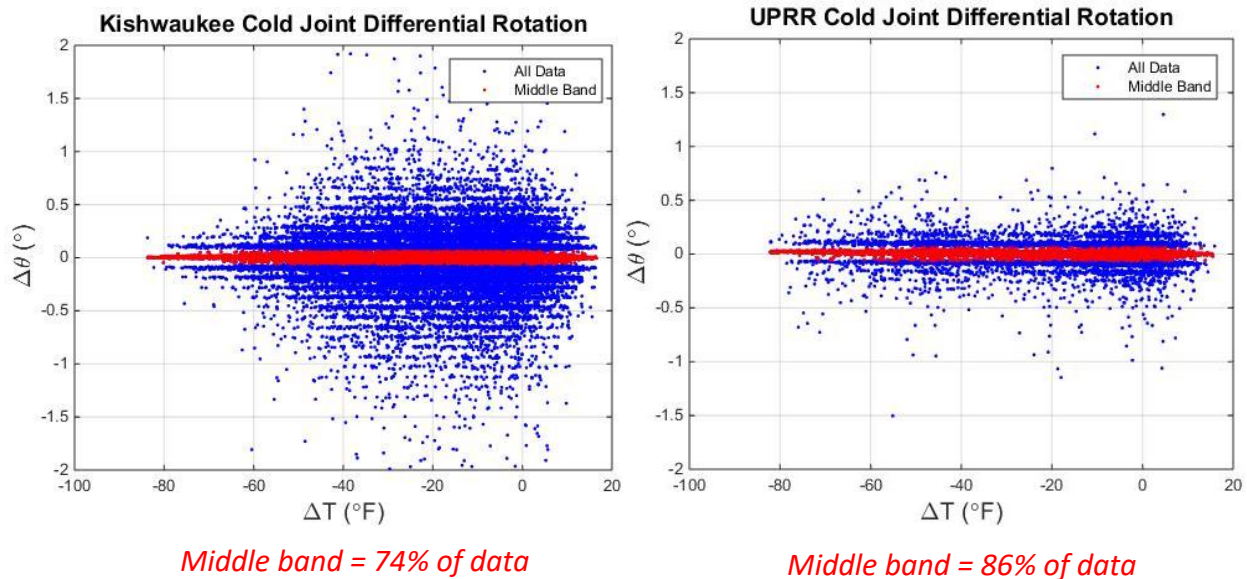


Figure 30. Cold-joint differential rotations for the south side of the Kishwaukee and UPRR abutments.

The connections between the abutment and the girders were another area of concern. For modeling purposes, this connection was assumed as rigid because the girders are embedded into the abutment. To assess the actual fixity level of this connection, the differential rotations between the girder and the top abutment tiltmeters were calculated. Unlike at the cold joint, some differential rotation was observed between the abutment and girders at both bridges. At Kishwaukee, a greater differential rotation was seen at the north and south ends of the abutment, as compared to that at the center. Upon further evaluation, it was determined that the three top abutment tiltmeters (north, middle, and south) all displayed roughly the same amount of rotation. However, the north and south girder tiltmeters exhibited almost no rotation, resulting in a larger differential rotation, whereas the middle girder tiltmeter exhibited a rotation of almost the same magnitude as the middle top abutment tiltmeter, causing a lower magnitude of differential rotation at this location. At UPRR, there are not sufficient tiltmeters at the center of the abutment to fully assess joint rigidity; however, both the south and north abutment locations showed similar girder-to-abutment differential rotations.

By looking at the central band of data, one can see the maximum differential rotations measured 0.33° and 0.29° at Kishwaukee, and 0.1° and 0.08° at UPRR, for the north and south

sides, respectively. The absolute maximum girder–abutment differential rotation occurred at the north side of both bridges, as presented in Figure 31. As UPRR is a single-span bridge, it was possible to conduct a simple hand-calculation to determine the expected end rotation for a pinned-pinned case. For this pinned scenario, the differential rotation at the yield moment is approximately 1.06° for a fully composite section and 1.92° for a noncomposite section. Comparing these results to the observed field differential rotation of 0.1°, the connection appears to be much closer to a continuous, rigid connection than a pinned one. Similarly, extrapolating this data to the field results at Kishwaukee, the girder-to-abutment connection seems to behave more as continuous/rigid than pinned. Even though both bridges displayed a slight level of differential rotation, assuming these connections as being essentially rigid for modeling seems to be valid.

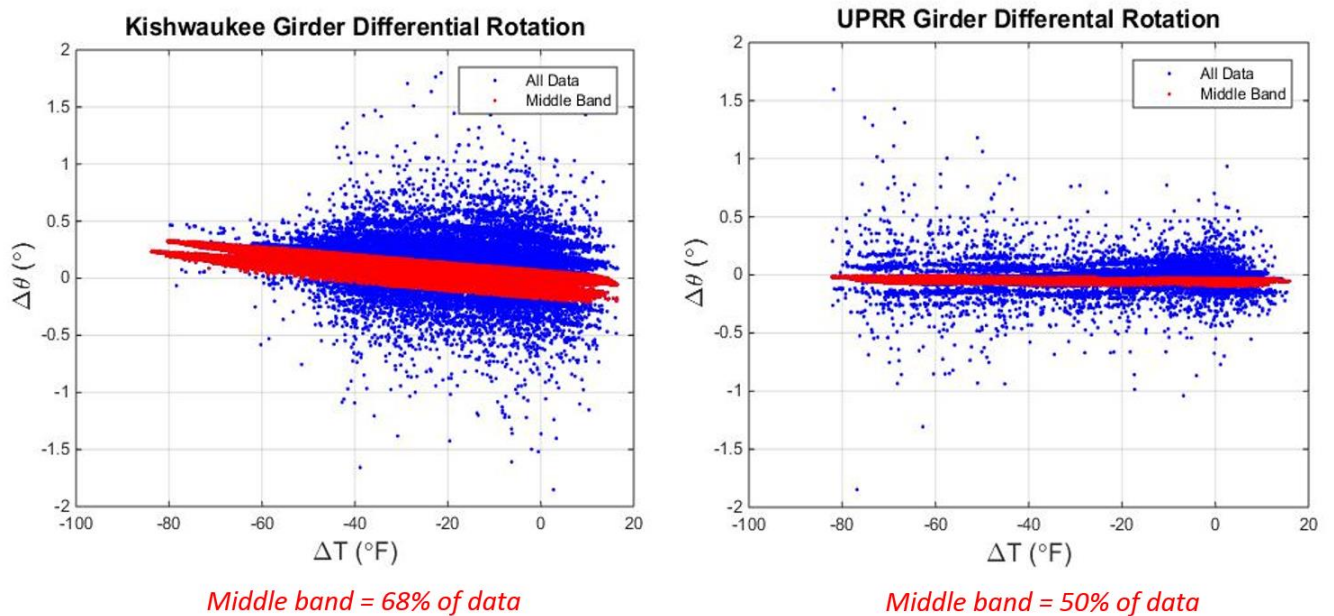


Figure 31. Differential rotation between the abutment and girders at the north side of the Kishwaukee and UPRR abutments.

4.5 PILE DEMANDS

Analyzing the pile strain data can provide a comprehensive representation of overall IAB substructure behavior and thermal demand. The pile gages (see Figure 32 for location schematics) generally exhibit clear trends over time due to the change in temperature, as can be seen for the Kishwaukee acute pile in Figure 33 for the entire term of monitoring. Additionally, when looking at a short period of time, each gage goes through a daily cycle of differential compressive/tensile strain corresponding to daily variations in temperature, as shown in Figure 34. Due to the location of the gages and bridge geometry, gage locations 1 and 4 exhibit the largest differential compressive (positive) and tensile (negative) strain magnitudes during negative changes in temperature.

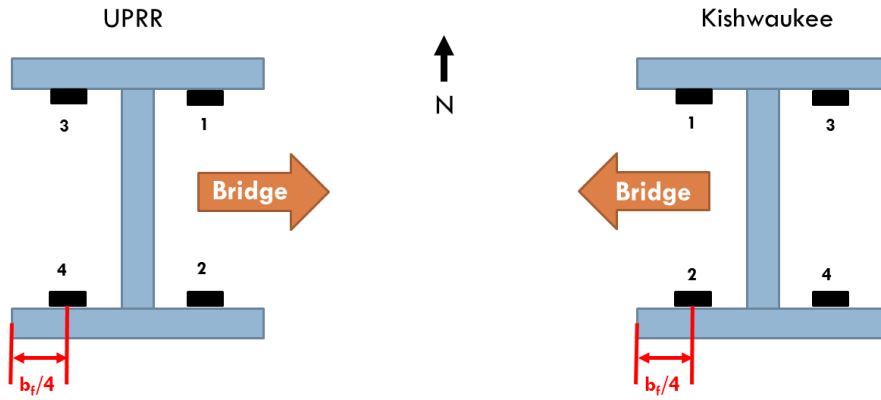


Figure 32. Schematic of pile strain gage locations.

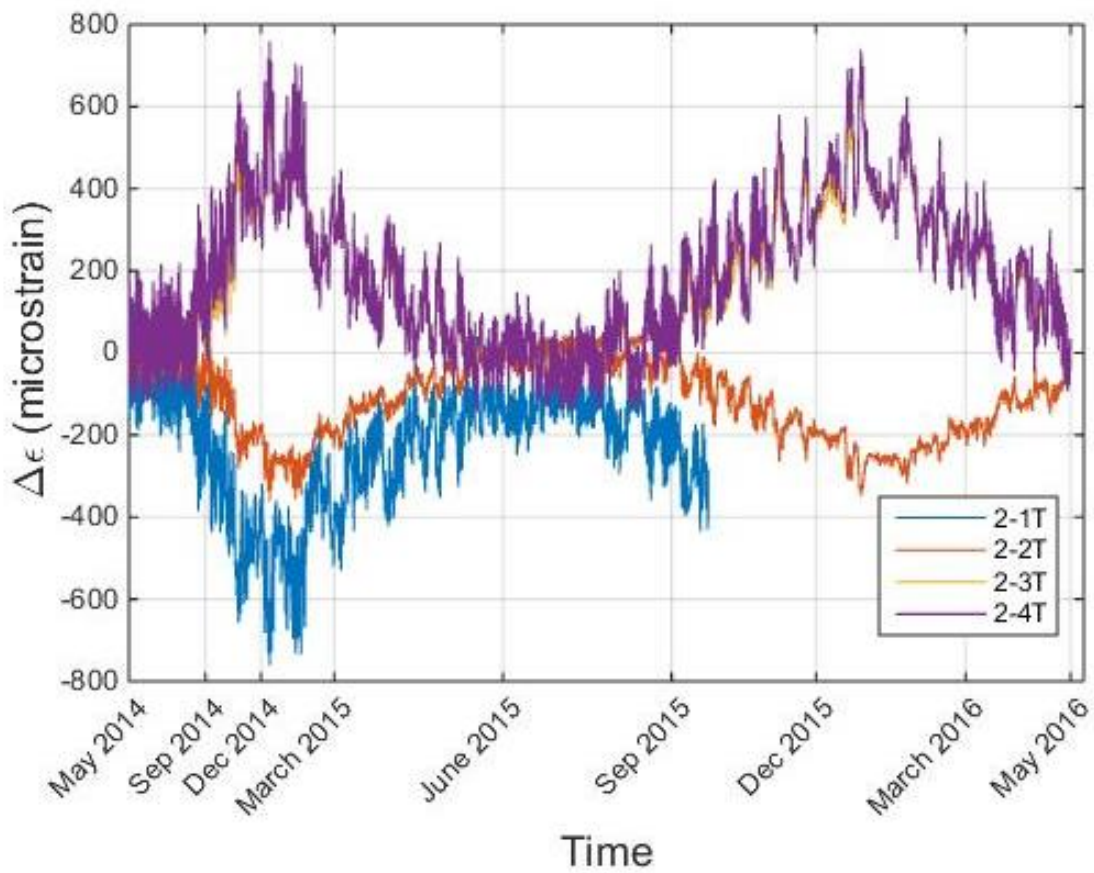


Figure 33. Kishwaukee acute pile strains over time.

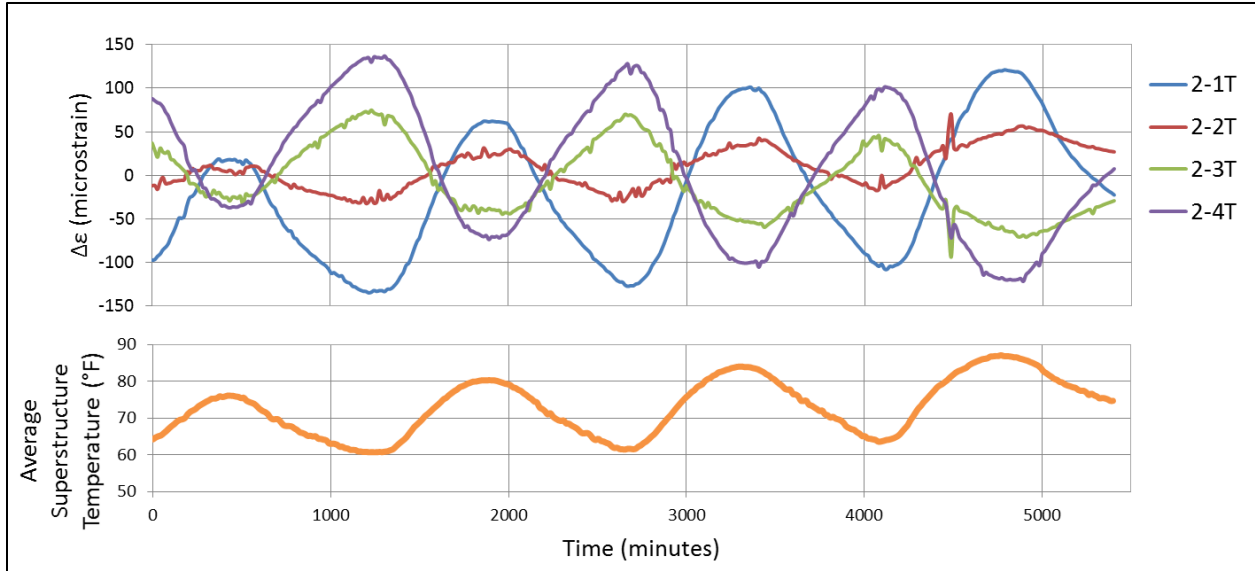


Figure 34. Kishwaukee acute pile strains from 10:00 a.m. on 5/28/2014 to 4:00 a.m. on 6/1/2014.

A strong linear trend between pile strain and change in superstructure temperature can be seen in the field data from both Kishwaukee and UPRR (see Figure 35 through Figure 42). The maximum strains reported at the gage locations are significantly lower than the yield strain of 1724 microstrain. The strain at the flange tip/extreme fiber was extrapolated utilizing the collected pile strains at the gage locations. Figure 43 shows the flange-tip pile strains at the acute pile (location of peak pile strains), which are all also lower than the pile yield strain. Therefore, the results seem to indicate that some additional remaining elastic pile-deformation capacity could still be available, especially at UPRR.

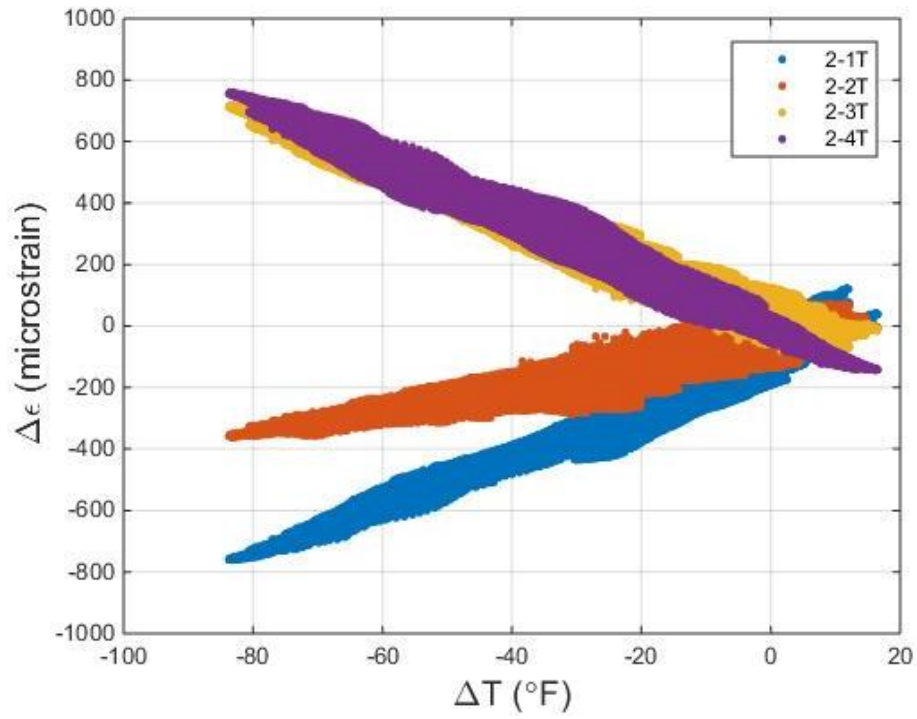


Figure 35. Kishwaukee acute (north) pile head strains.

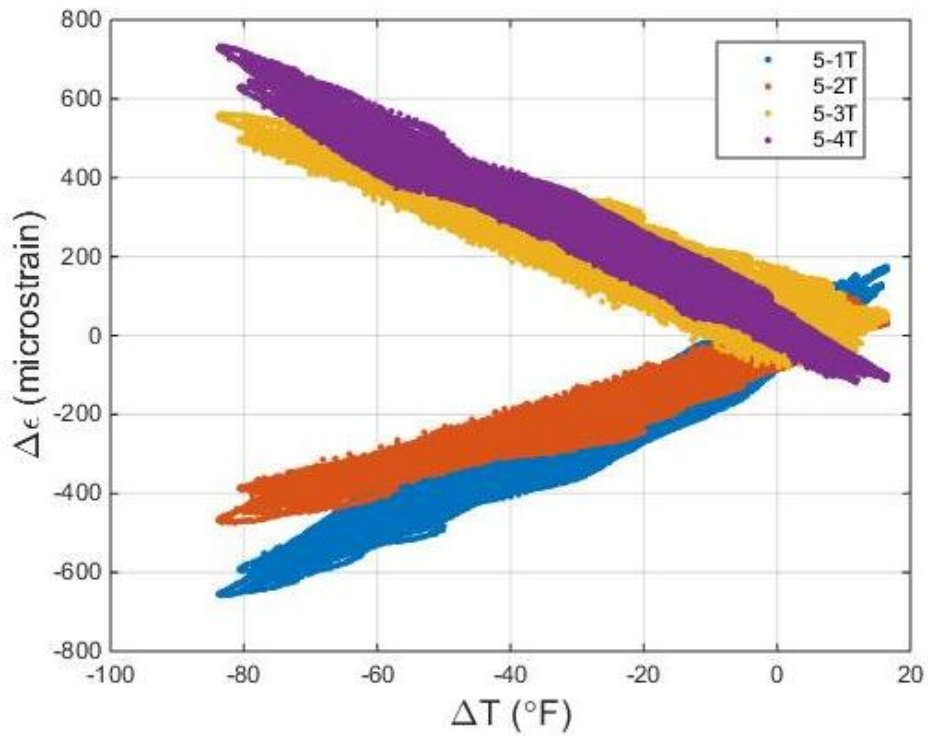


Figure 36. Kishwaukee middle-pile head strains.

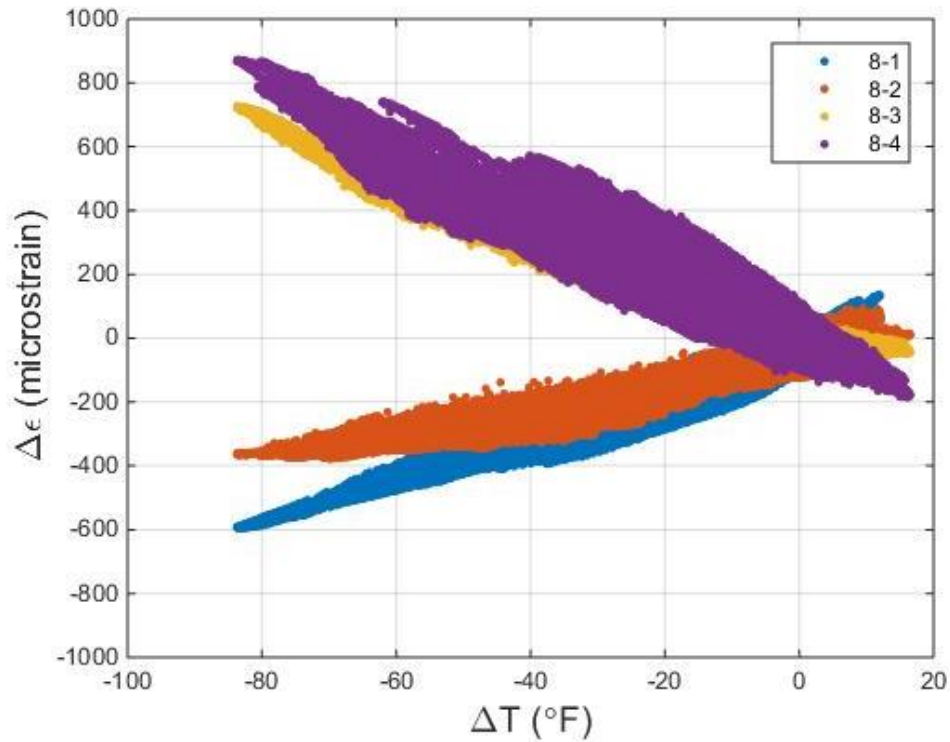


Figure 37. Kishwaukee obtuse (south) pile head strains.

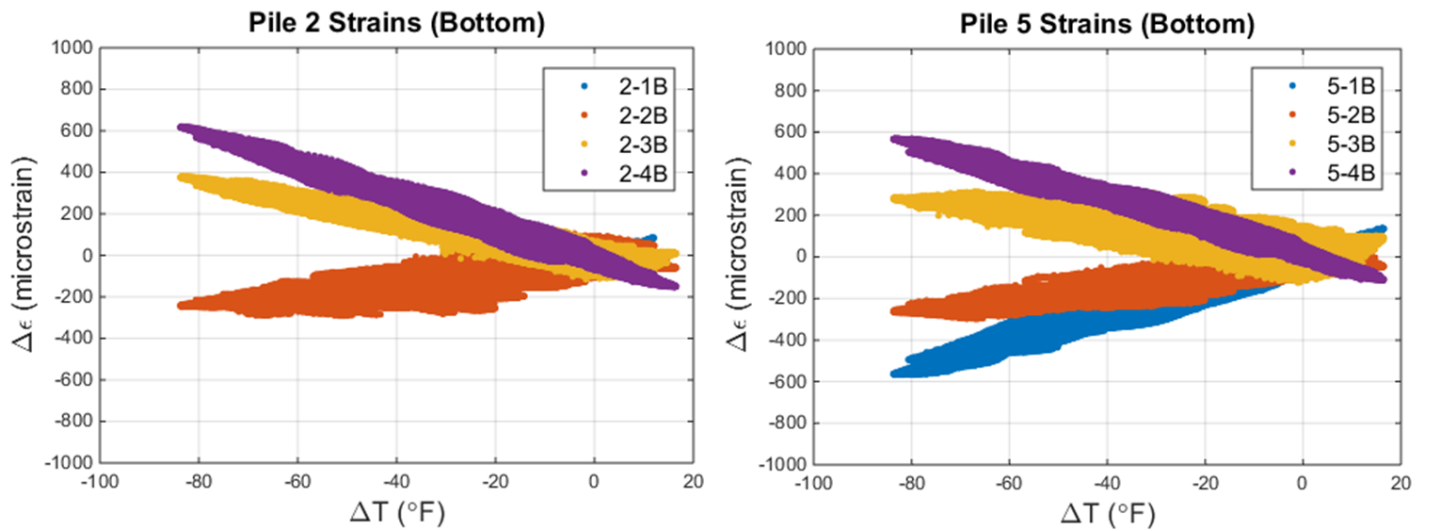


Figure 38. Kishwaukee acute (north) and middle-pile strains below the pile-cap boundary.

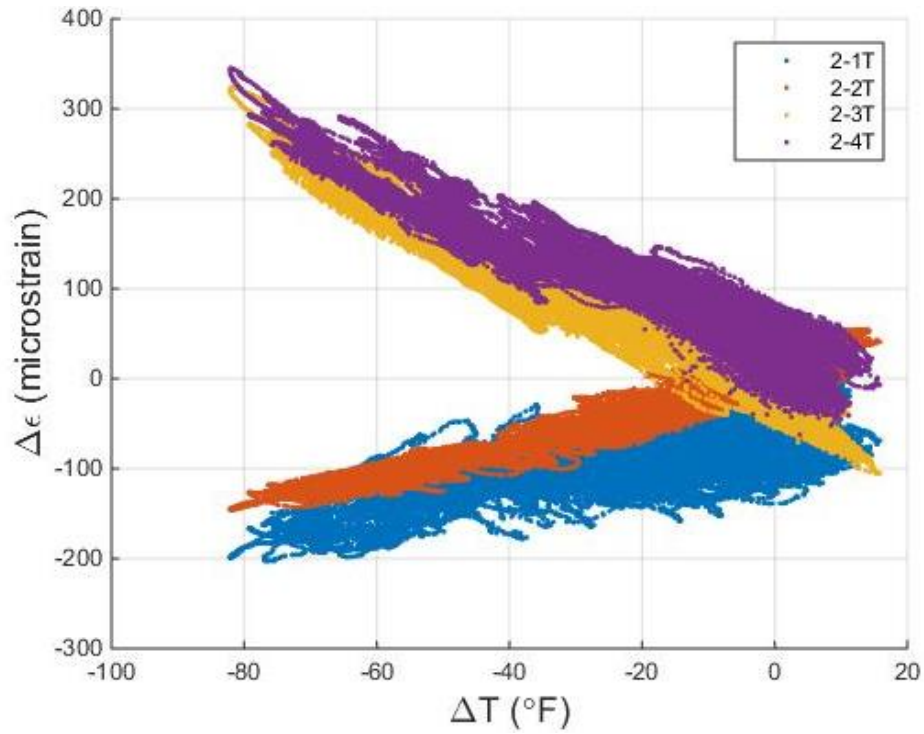


Figure 39. UPRR acute (north) pile head strains.

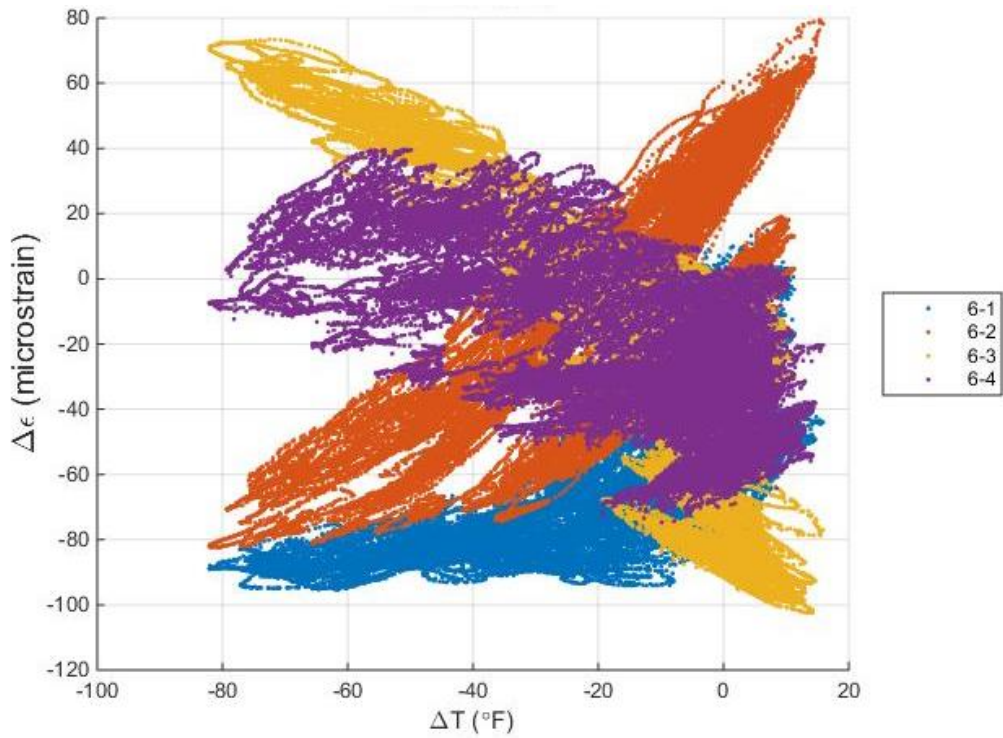


Figure 40. UPRR middle-pile head strains.

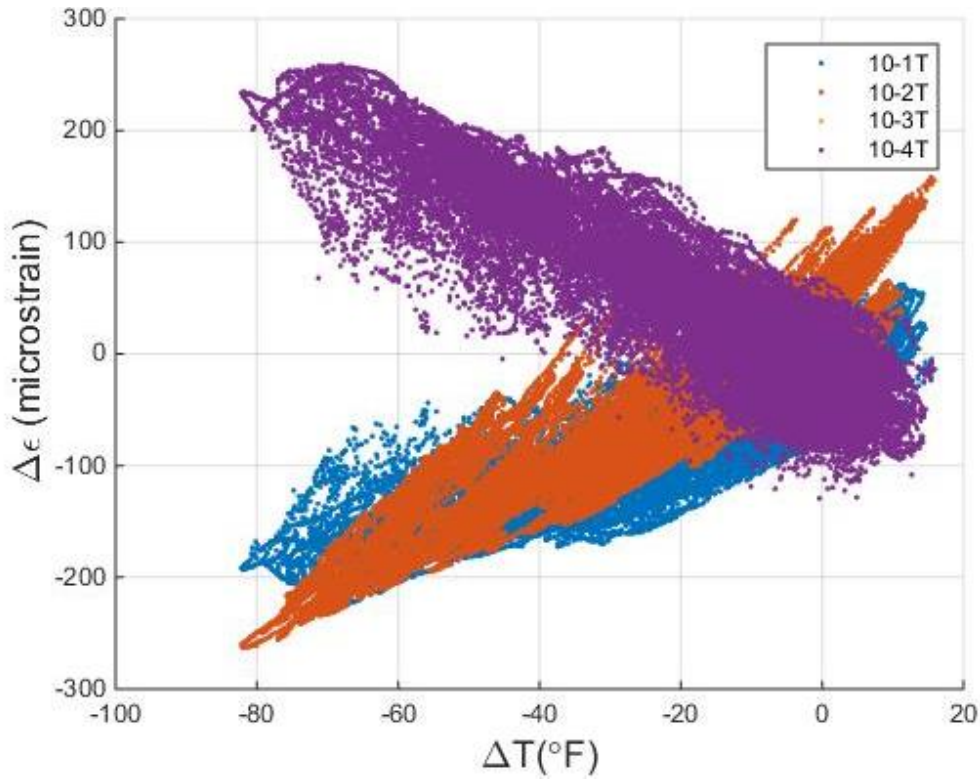


Figure 41. UPRR obtuse (south) pile head strains.

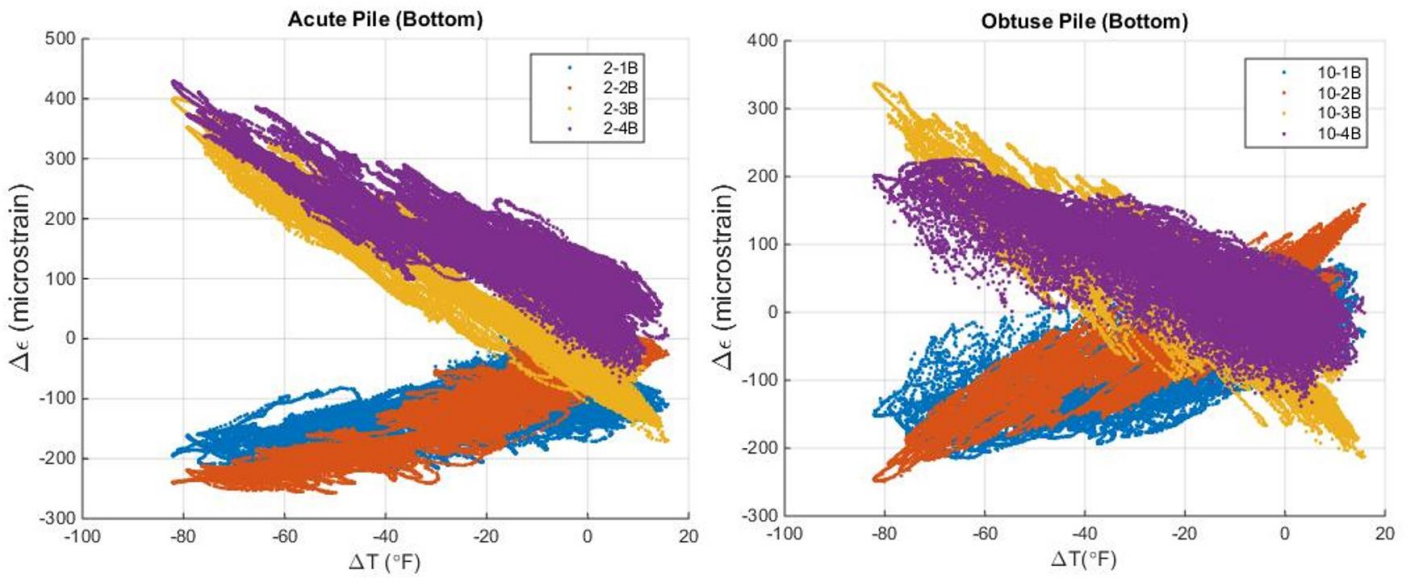


Figure 42. UPRR acute (north) and obtuse (south) pile strains below pile-cap boundary.

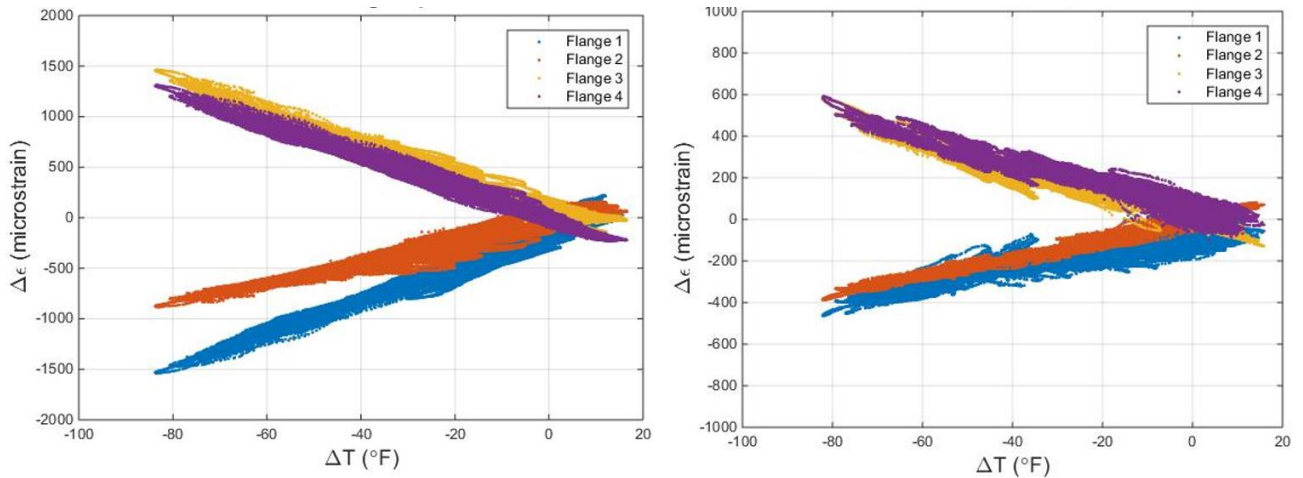


Figure 43. Kishwaukee (left) and UPRR (right) acute pile flange-tip strains.

After analyzing the pile strain gage data from the field, it was determined that the majority of recorded pile strain is due to weak-axis bending. Figure 44 through Figure 46 show the pile stresses at both bridges due to axial force, strong-axis moment, and weak-axis moment. The largest stress component for all of the piles is from weak-axis moment, as expected because the piles at both bridges are placed in weak-axis orientation. Stresses due to weak-axis moment and strong-axis moment are fairly consistent in magnitude between all the instrumented piles at each bridge. However, stresses due to axial force appear to be higher at the exterior piles. It is important to note that the middle pile (pile 6) at UPRR shows much lower magnitudes of total pile strain and stress components, most likely due to an error during construction that resulted in those pile gages being approximately 8 in. higher (i.e., partially embedded up into the pile cap) than the corresponding gages on the exterior piles.

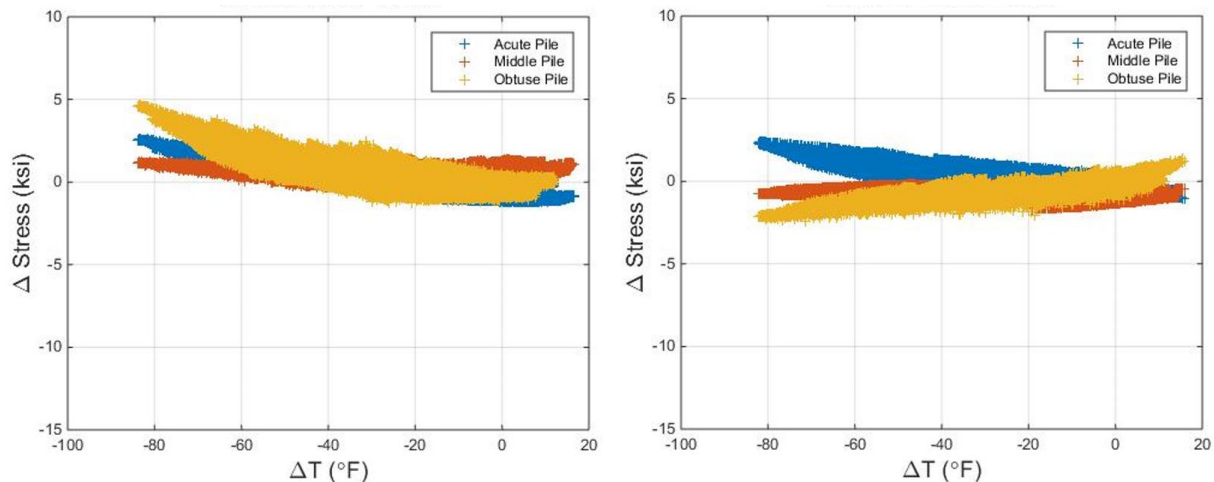


Figure 44. Pile stress due to axial force in the piles at Kishwaukee (left) and UPRR (right).

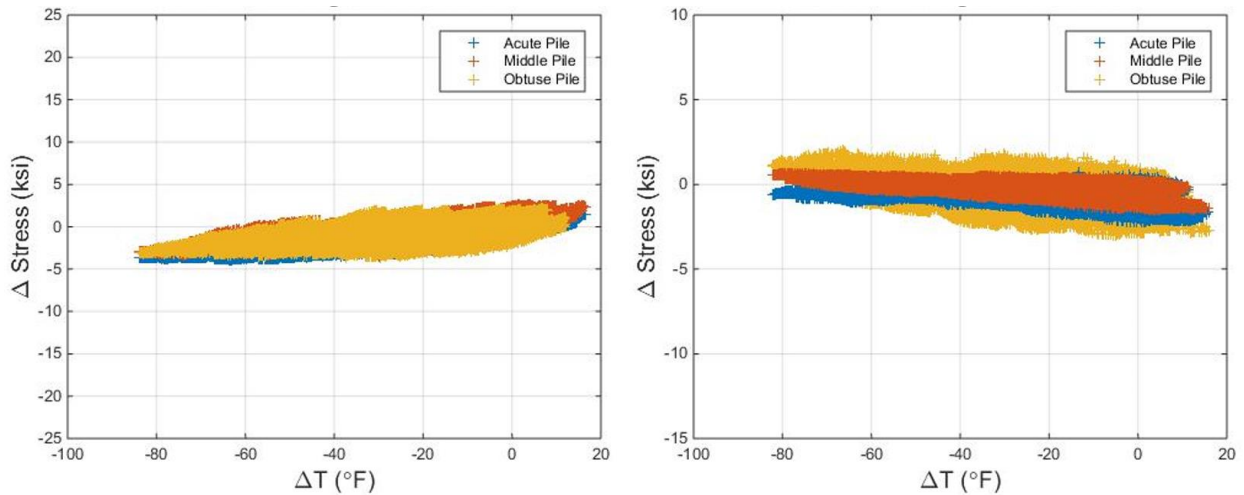


Figure 45. Pile stress due to strong-axis moment in the piles at Kishwaukee (left) and UPRR (right).

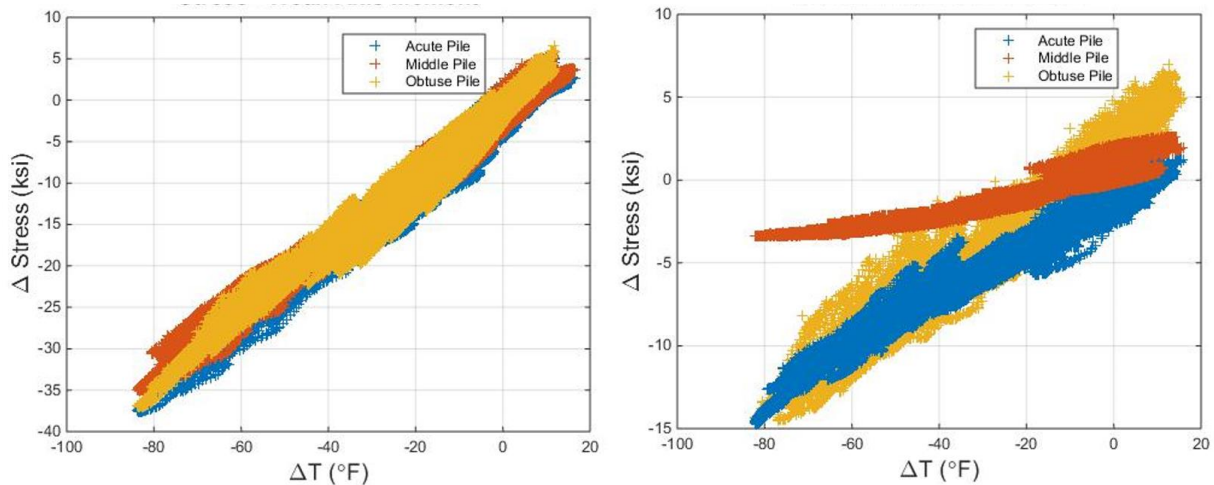


Figure 46. Pile stress due to weak-axis moment in the piles at Kishwaukee (left) and UPRR (right).

Looking even more closely at the data from Kishwaukee, one sees that a separation between compressive strain gage pairs (gages 1 and 2) and tensile strain gage pairs (gages 3 and 4) can be noted in some of the pile data, as seen back in Figure 37. This behavior is likely due to pile strong-axis bending, and it generally appears to increase in magnitude from the acute to the obtuse corner. The field data further show an upward shift in strain magnitude, away from the data being symmetric about zero strain, as also seen in Figure 37. This is likely due to pile axial force effects. This shift in strain magnitude also appears to increase from the acute to the obtuse pile. Additionally, strain values from the gages below the pile-cap boundary are lower in magnitude and show a larger separation between gage pairs, as can be seen in Figure 38.

At UPRR, some of the previously mentioned trends are not quite as apparent in the field data. The field data still show a small separation between gage pairs due to strong-axis bending.

However, this separation is much smaller, as compared to that at Kishwaukee; and it appears to be more uniform across all of the piles. UPRR pile strains also show a much smaller shift in magnitude due to axial force. Strains from the gages below the pile-cap boundary demonstrate a slightly larger separation between gage pairs; but unlike at Kishwaukee, the strain magnitudes are actually higher than those at the pile-cap boundary.

4.6 GIRDER DEMANDS

The strain gages on the girders have proven to be the most variable of all the gages in terms of their fluctuating and sometimes noisy data. Some of this variability can be attributed to the fact that the girder strain gages are the most exposed to the elements and have the greatest influence from live loads. In spite of this, clear trends over time and with temperature change can still be seen in the girder strain data. Low girder stresses were generally observed in the parametric study, so the girders at both bridges have been assumed to remain elastic; and thus for analysis, the strain gage data have simply been converted to stress by utilizing the elastic modulus. For reference, the instrumented girder cross sections are labeled in the format of <girder number>-<location number>, with the girder number encircled in black and the location number boxed in blue in Figure 47.

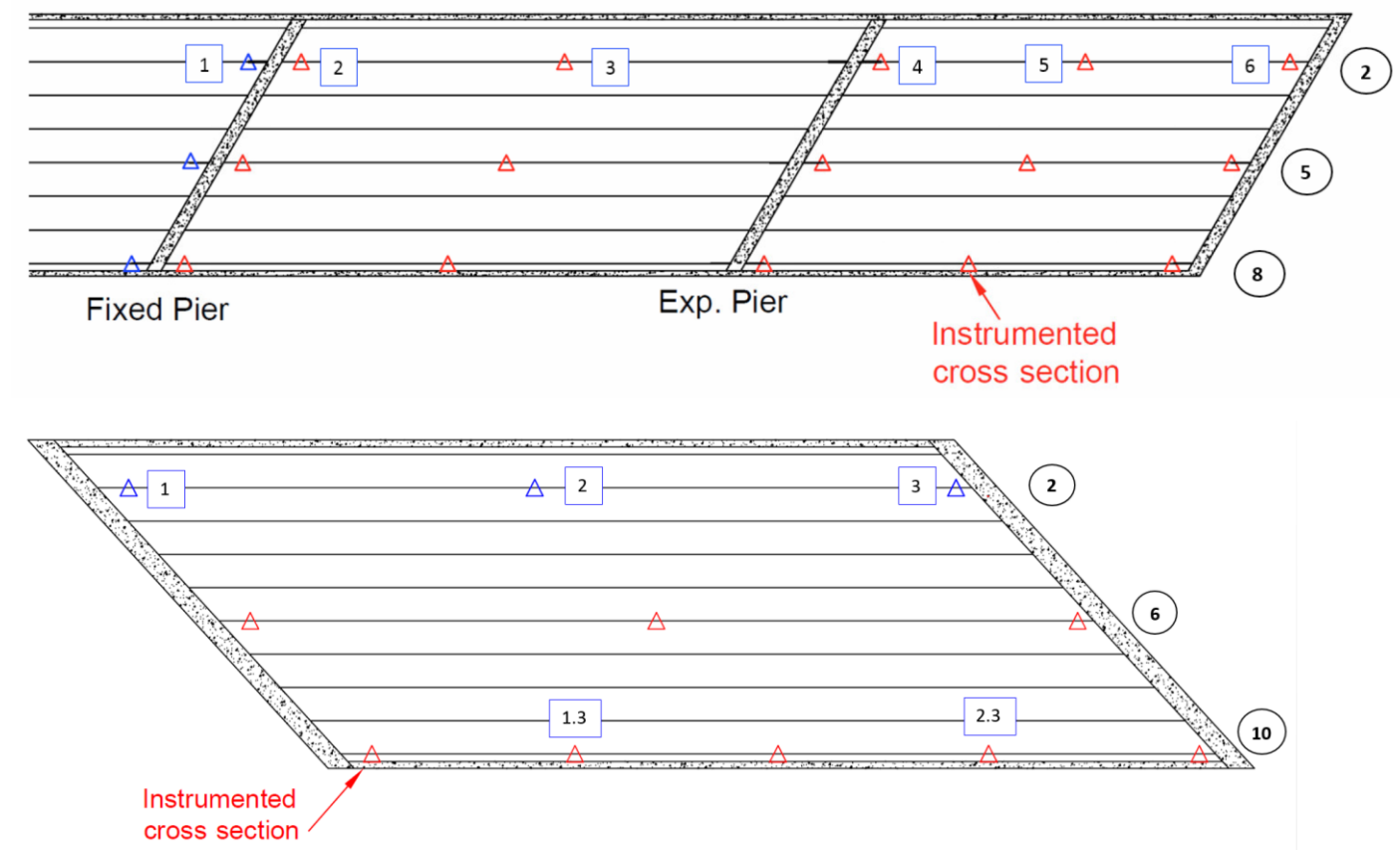


Figure 47. Girder cross-section labeling scheme for Kishwaukee (top) and UPRR (bottom).

As seen in the left plot of Figure 48, the girder stress data is somewhat noisy and thus clear trends are difficult to observe. In order to improve the data analysis, a daily running average was calculated. Utilizing a running average removed some of the noise seen in the data, which is likely due in part to live load conditions. The resulting plots utilizing the daily running average provide a more clear picture of overall girder stress trends, as can be seen in the right plot of Figure 48. All of the following girder plots in this section and in section 6.4 therefore depict the calculated daily running average girder stresses.

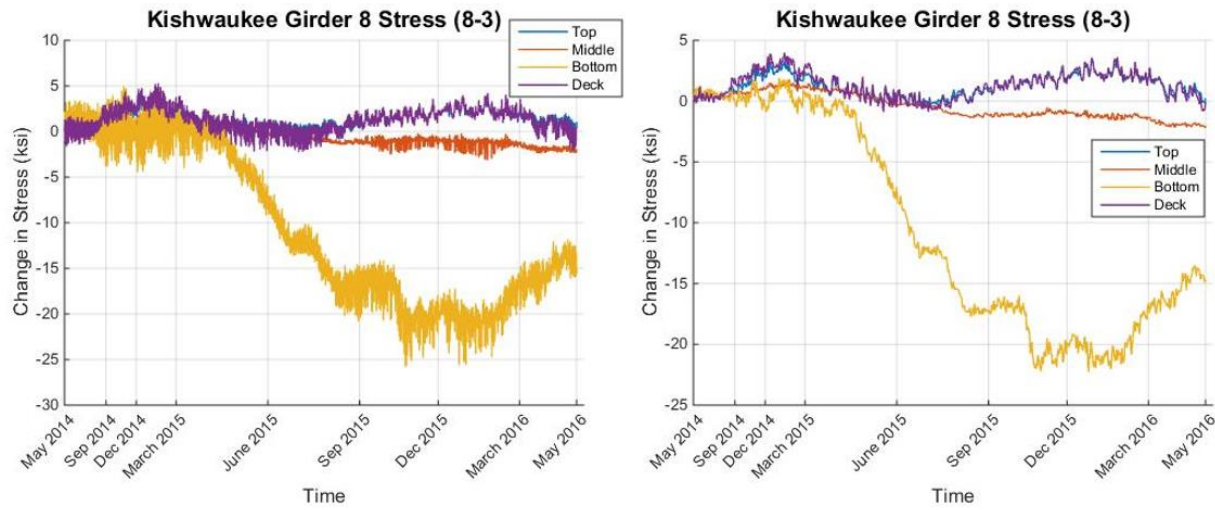


Figure 48. Original data (left) and daily running average data (right) for Kishwaukee girder 8 stresses at the mid-span of the interior span.

As expected from the parametric study, the steel-girder, bottom-flange field data display the highest magnitude of stresses. However, the bottom-flange data are also the most variable over time. Figure 49 displays the stresses from all the gages at one girder cross section for Kishwaukee and UPRR, respectively. The data show that the top girder, middle girder, and concrete-deck stresses exhibit clear trends over time due to temperature. The girder bottom-flange stresses follow this same trend for a period of time, but then they tend to deviate into further tension or compression (depending on location) after approximately the first year of data collection and typically do not return to their original state. This behavior is observed at approximately three-fourths of all the instrumented girder cross sections for both bridges; therefore, it does not appear to be an error from the gage readings but rather some sort of systematic behavior of the girder bottom flanges.

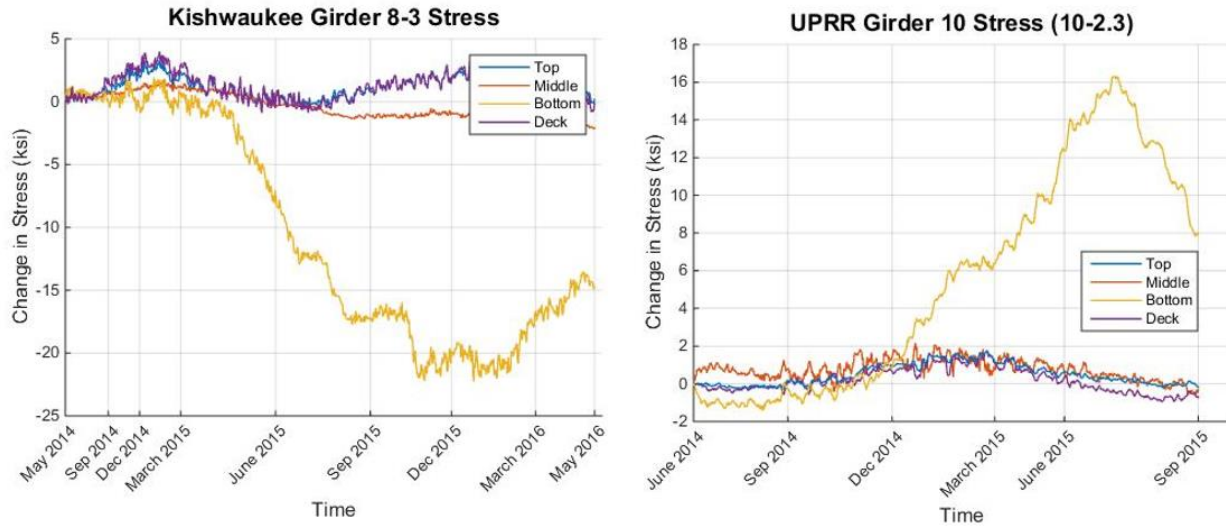


Figure 49. Kishwaukee girder 8 stresses at the mid-span of the interior span (left) and UPRR girder 10 stresses at the east quarter-span (right).

Figure 50 and Figure 51 show the same girder stresses as above, only now plotted versus change in temperature. The top, middle, and deck stresses all follow a clear linear trend with change in temperature. The bottom-flange stress also shows a clear linear trend for part of the data but then deviates into either more tension or more compression. This deviation seems to typically initiate after the temperature increases again and reaches a net change in temperature (ΔT) of around $-40\text{ }^{\circ}\text{F}$ or else at the initial temperature ($0\text{ } \Delta T$).

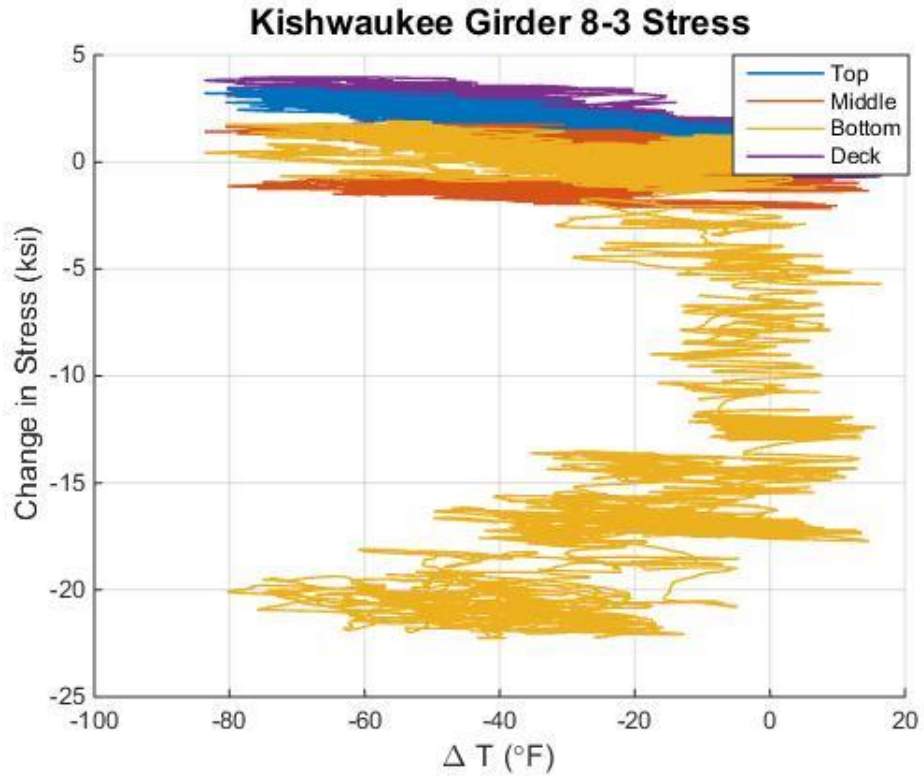


Figure 50. Kishwaukee girder 8 stresses at interior mid-span versus change in temperature.

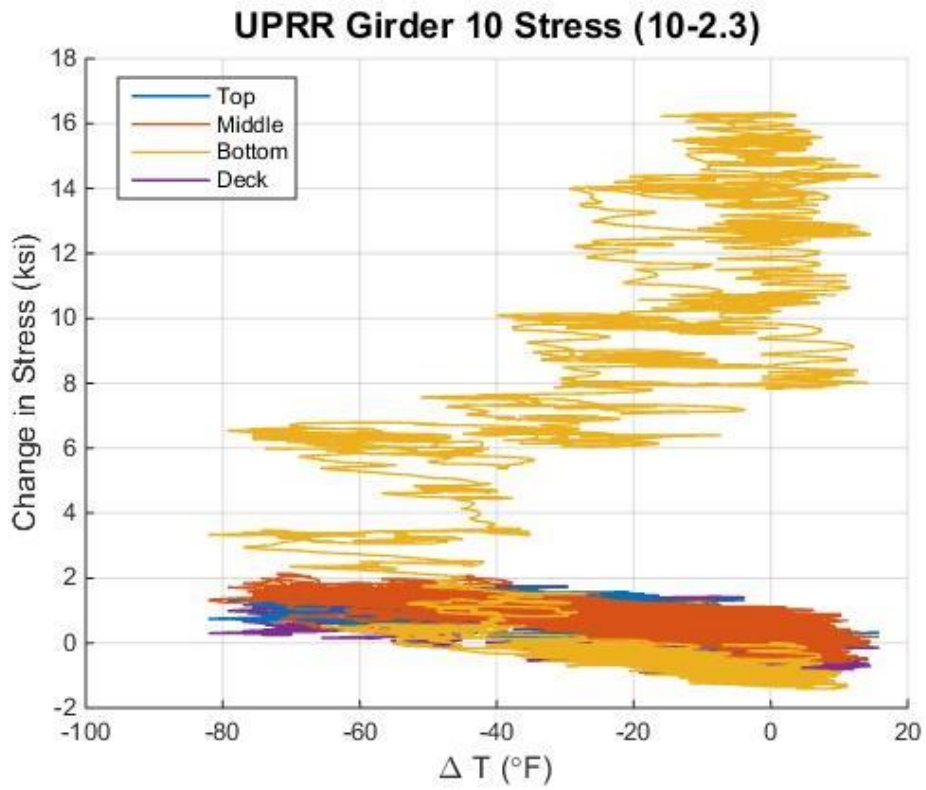


Figure 51. UPRR girder 10 stresses at the east quarter-span vs. change in temperature.

To further analyze what is happening along the length of each girder, specific representative “hot” and “cold” days were chosen for each year of data collection. At Kishwaukee, the representative hot days are July 22, 2014, and June 10, 2015, both of which correspond to a change in temperature of +10 °F. The representative cold days at Kishwaukee are January 7, 2015, and January 18, 2016, which correspond to a change in temperature of -80 °F. At UPRR, the representative hot days are August 24, 2014, and July 17, 2015, which correspond to a change in temperature of +10 °F. Because data collection at UPRR only lasted 16 months, there is only one representative cold day, November 17, 2014, which corresponds to a change in temperature of -60 °F.

Focusing first on the top flange, Figure 52 through Figure 55 show top-flange girder stress along a girder on the hot and cold days for Kishwaukee and UPRR. At Kishwaukee, the stresses near the pier and the abutment are typically the highest in magnitude. The data from both bridges also show that the top-flange stresses increase in magnitude slightly from the first to the second year, but the general trends along the girder remain similar. This small increase can likely be attributed to cyclic effects. It should be noted that the top flange along girder 2 at Kishwaukee demonstrates a switch from compression (negative) to tension (positive) from the first-year to second-year “hot” day, as seen in Figure 52. This finding could be indicative of some “relief” of girder axial force after a year of data collection, which could be related to the shift in approach–transition slab crackmeter displacement seen after the first year (Figure 18).

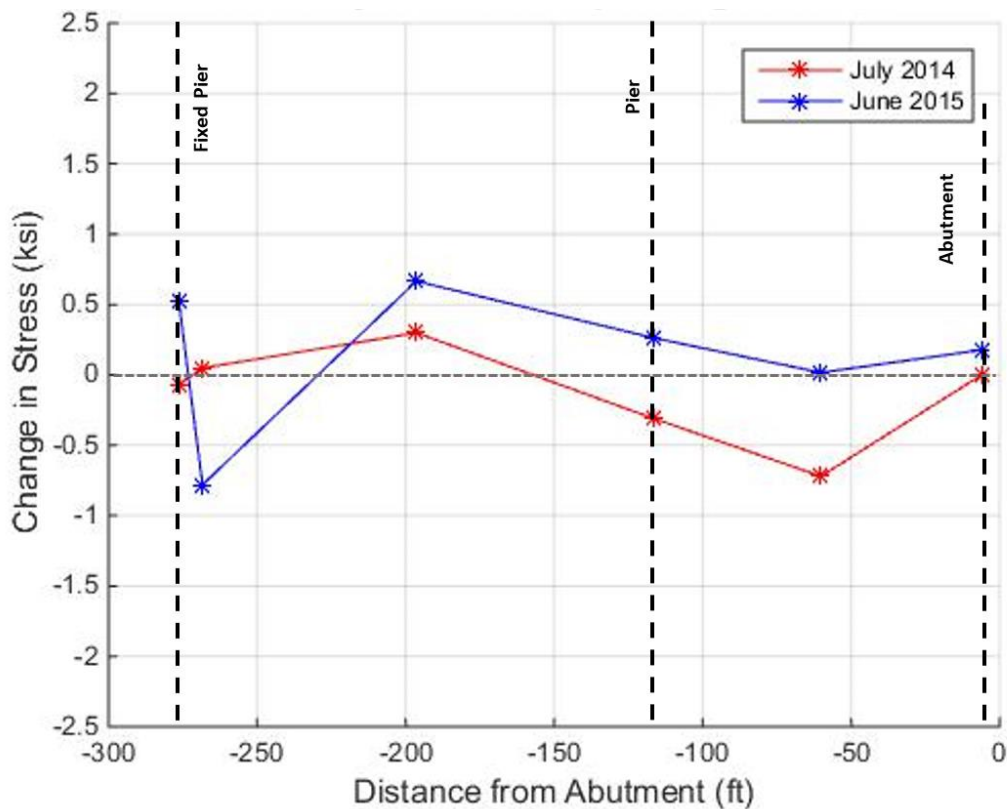


Figure 52. Kishwaukee top-flange stresses along girder 2 on “hot” days.

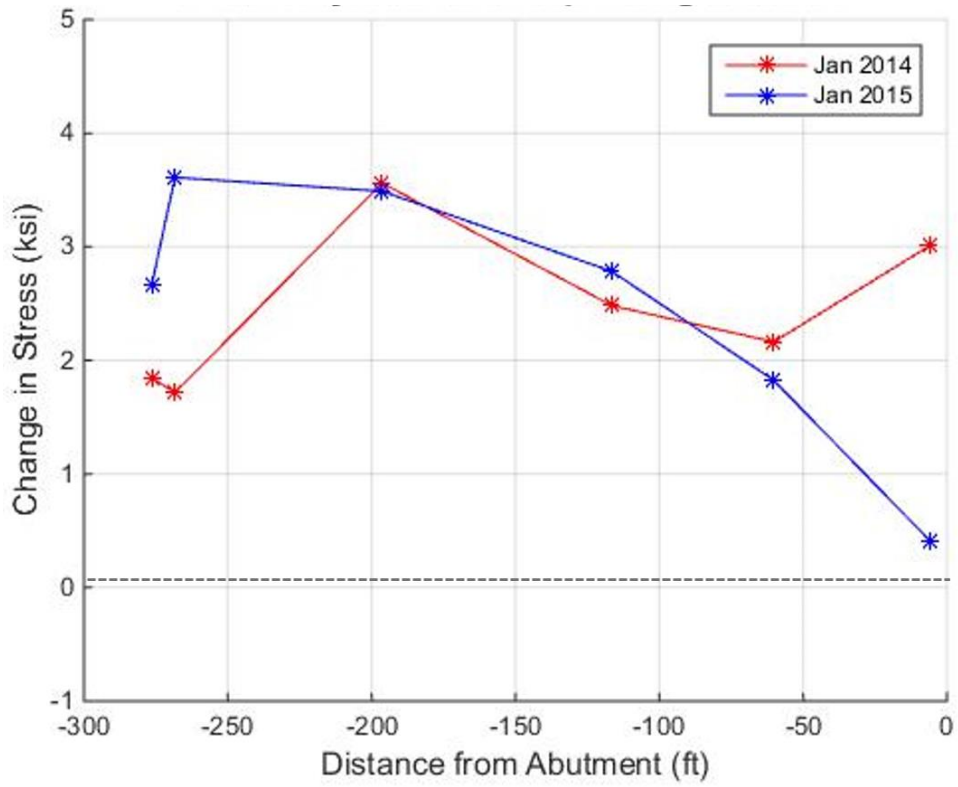


Figure 53. Kishwaukee top-flange stresses along girder 2 on "cold" days.

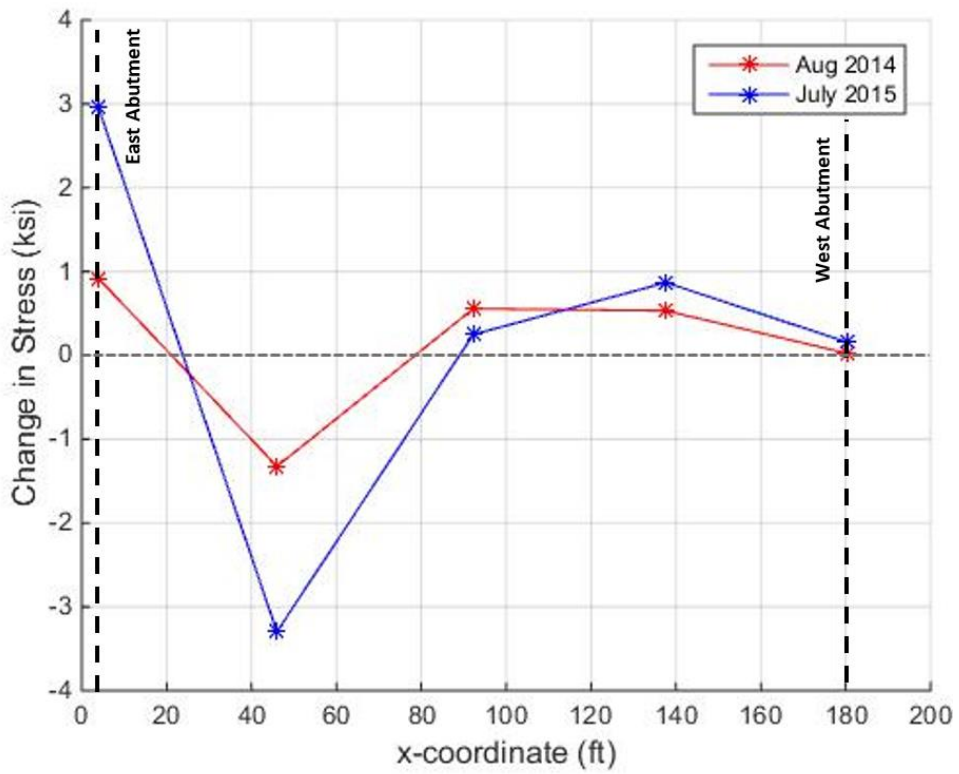


Figure 54. UPRR top-flange stresses along girder 10 on "hot" days.

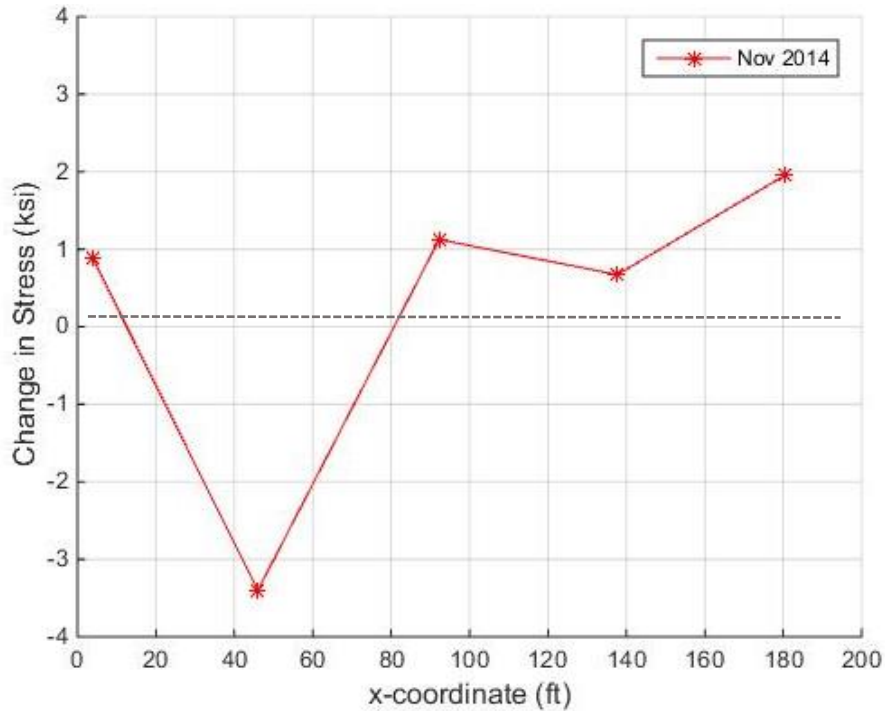


Figure 55. UPRR top-flange stresses along girder 10 on a “cold” day.

The bottom-flange stresses have been analyzed in the same fashion, as shown in Figure 56 through Figure 59. Focusing on the first year (2014) of collected data, the bottom-flange stresses are typically highest in magnitude at the abutment and/or fixed pier, as expected from the parametric study trends. And compared to the top-flange stresses, the bottom-flange stresses overall show a larger increase from the first to the second year. It should be noted that this increase is particularly large near the supports (including the abutments and the piers), and for UPRR also at the quarter-spans. For most mid-span locations at both bridges, the bottom-flange stresses tend to stay more consistent from year to year, with only small increases in stress.

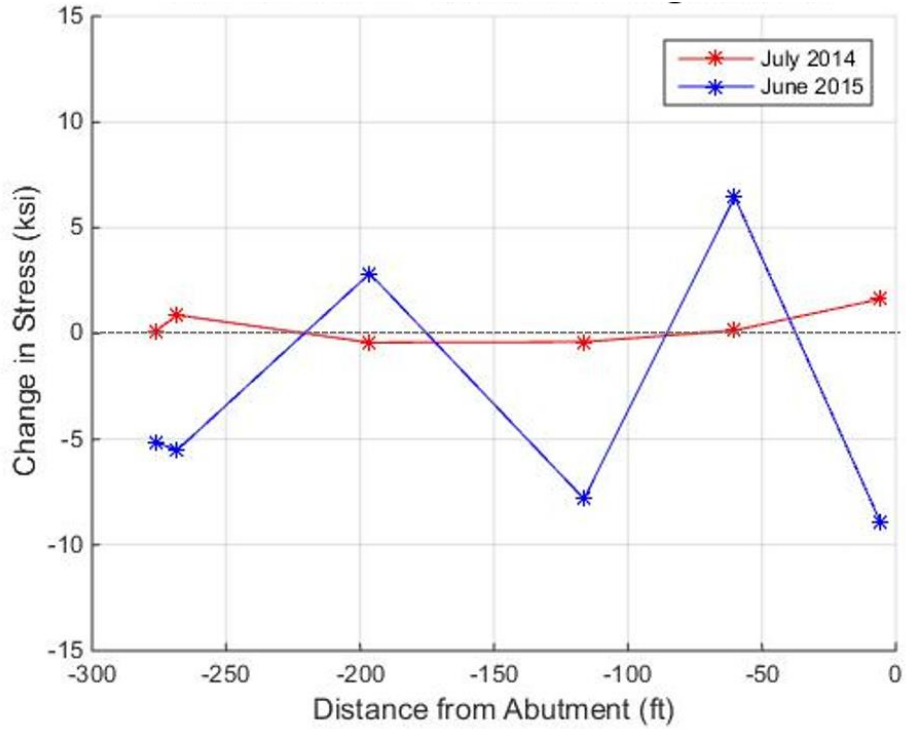


Figure 56. Kishwaukee bottom-flange stresses along girder 2 on “hot” days.

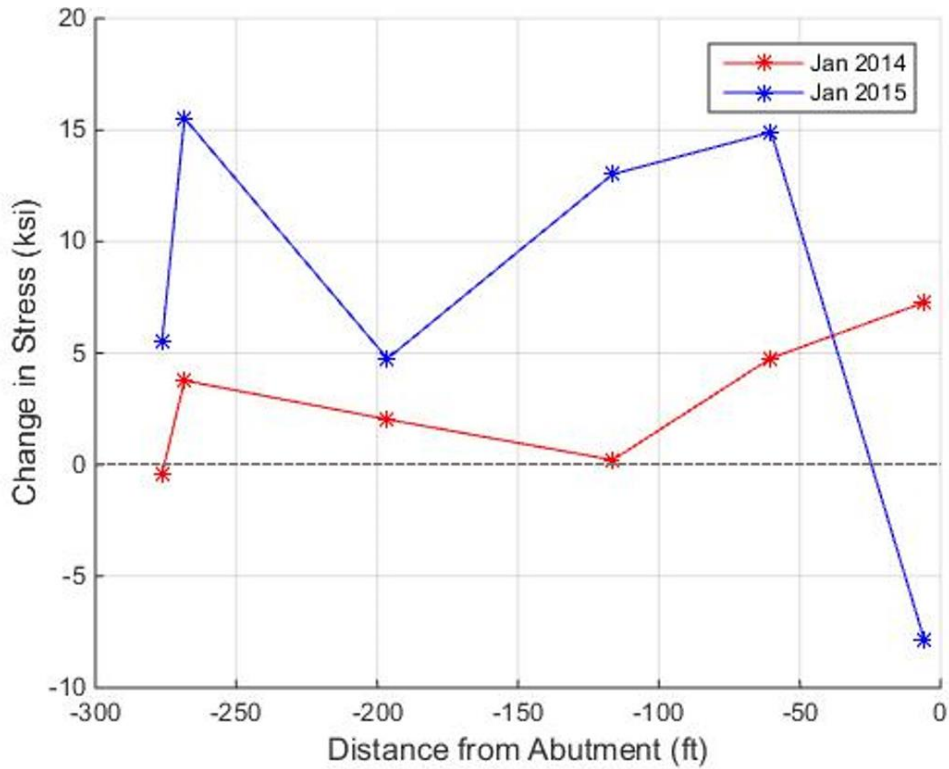


Figure 57. Kishwaukee bottom-flange stresses along girder 2 on “cold” days.

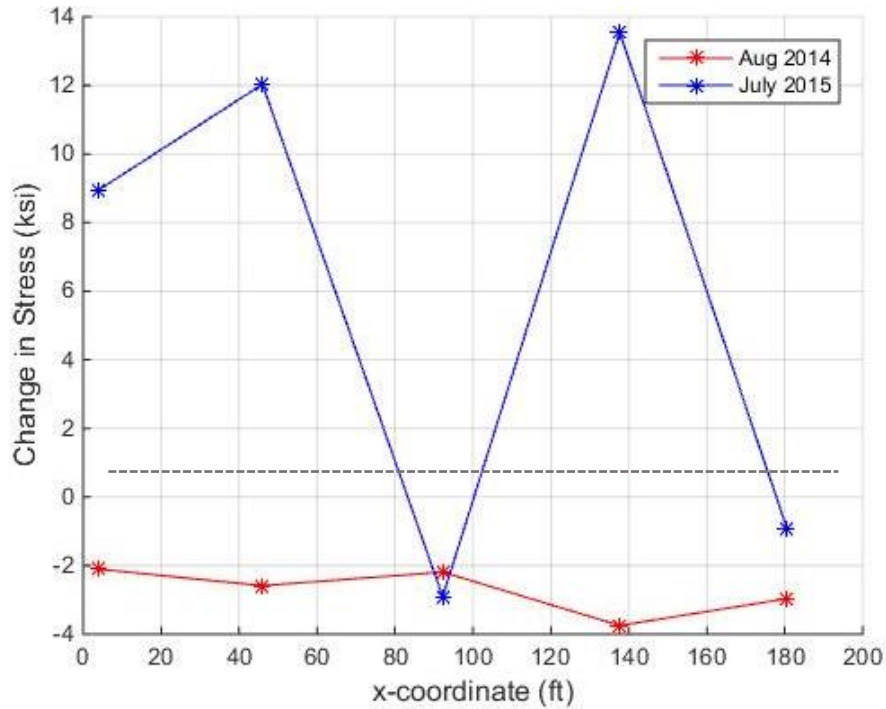


Figure 58. UPRR bottom-flange stresses along girder 10 on “hot” days.

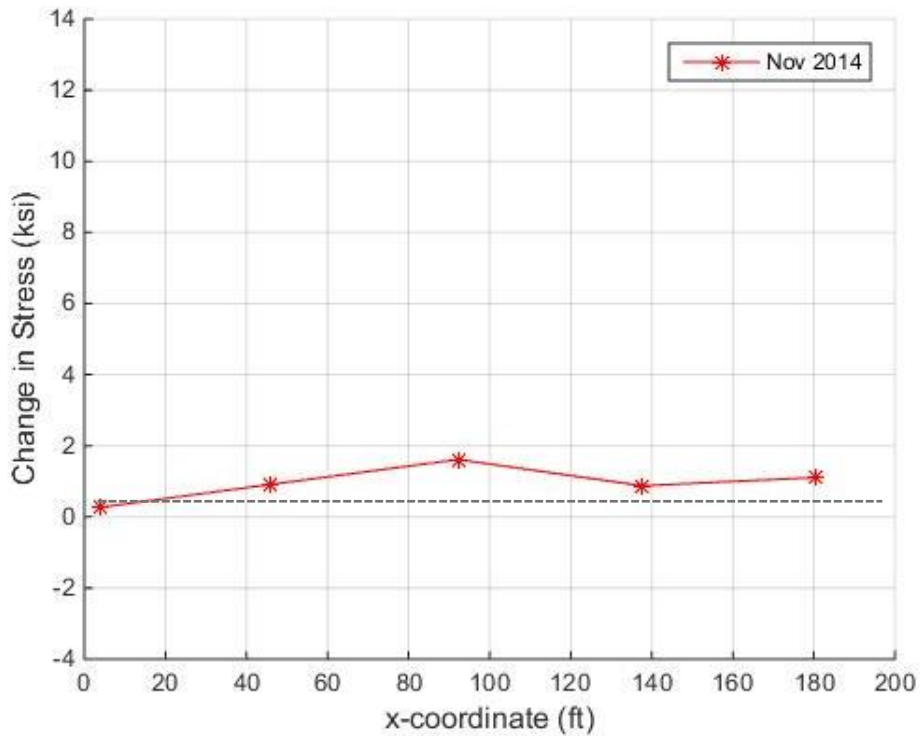


Figure 59. UPRR bottom-flange stresses along girder 10 on a “cold” day.

Overall, the girder-stress field data show a clear trend over time due to temperature. Further increases in stress are observed over time, most likely due to cyclic and time-dependent effects.

These effects appear to be much larger at the girder bottom flange. Compared to the top flange, the girder bottom flange is more prone to out-of-plane bending because the top-flange movement is locally restricted due to the girder being composite with the bridge deck. This out-of-plane bending could account for why higher increases in stress are seen at the bottom flanges, especially as the bottom flange is further from the composite section's neutral axis. It should also be noted that any relief or additional stresses imparted during construction or before monitoring cannot be accounted for due to the initialization scheme. Therefore, the absolute values of girder stress may actually be somewhat higher or lower in magnitude than what is represented by the field data. And finally, there were no clear trends observed in terms of any differences in girder stress between interior and exterior girders.

CHAPTER 5: FINITE-ELEMENT MODELING OF SITE BRIDGES

5.1 MODELING ASSUMPTIONS AND PROCEDURE

For each of the instrumented bridges, a finite-element (FE) model was created using the structural analysis software SAP2000 v14 (CSI 2009). These models were used in part to evaluate the results from the field monitoring investigation, as well as to expand more generally upon the understanding of IAB behavior. These bridge site models were built using the same modeling assumptions and procedure as were used in the parametric study models summarized in the preceding volume of this report (LaFave et al. 2016a). While the modeling assumptions and procedure will be summarized in the following section, further details can be found in that previous report from LaFave et al. (2016a).

The bridge structural components were modeled in SAP2000 using both frame and shell elements, as shown in Figure 60. The bridge deck and abutment were modeled using thin- and thick-shell elements, respectively. These elements were modeled as linear elastic without reinforcement, based on an assumption that minimal cracking was to occur under service loading. The bridge girders were modeled using frame elements and were made composite with the deck shell elements. The insertion-point method (CSI 2013) was utilized to create the composite section, as shown in Figure 61. The girder-to-abutment connection was assumed as rigid when modeling, due to the girder's embedment into the abutment. This fixed connection was created using a rigid link to attach the girder-frame elements to the corresponding abutment shell elements. Similarly, the abutment cold joint was also assumed to be a rigid connection.

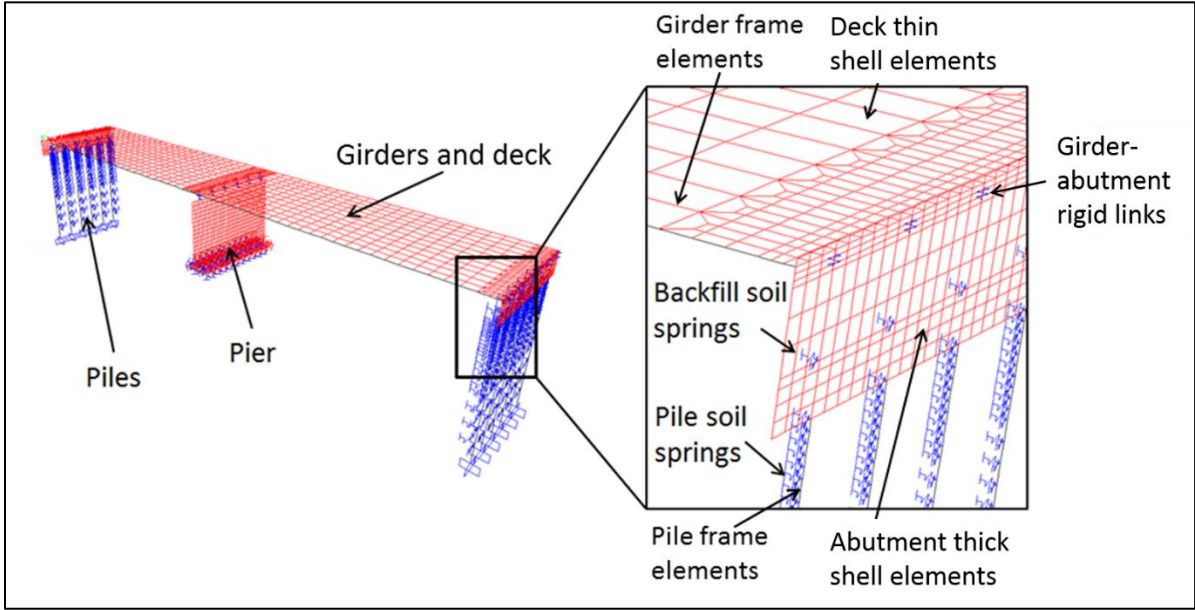


Figure 60. Typical finite-element model of an integral abutment bridge (IAB).

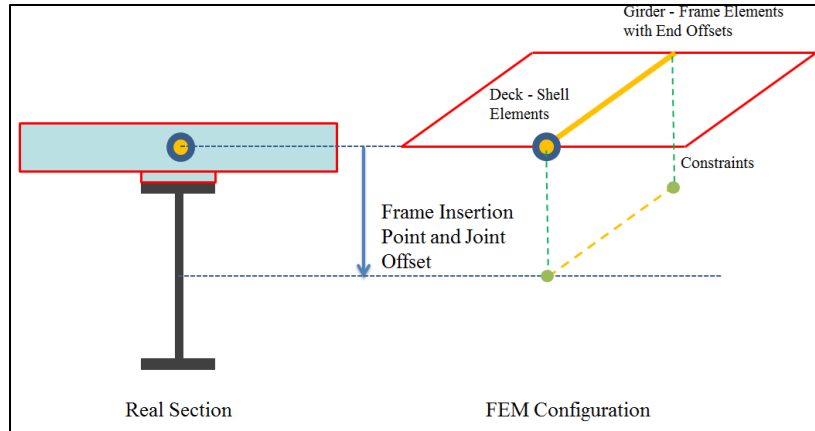


Figure 61. Composite section modeling and girder-end offset (adapted from CSI Technical Knowledge Base “Composite Section Tutorial”).

The bridge piles were modeled using frame elements with a series of 6-in.-long elements with fiber section hinges for the top 5 ft of the pile in order to account for nonlinear behavior in this critical region. To facilitate postprocessing, only one fiber hinge was assigned at the middle of each frame element and occupies the entire element length. This modeling approach allowed for the hinge behavior to be calculated automatically with MATLAB, by using the nodal displacements and forces. Similarly for the girders, the pile–abutment connection was modeled as being rigid, which was done by constraining the degrees of freedom of the section of the pile embedded in the abutment to those of the shell elements representing the bottom of the abutment.

At the Kishwaukee Bridge, the middle pier has fixed bearings, with expansion bearings elsewhere. At the middle pier, the wall pier was modeled using thick-shell elements. Below the wall pier footing (pile cap), the piles and associated soil are represented using a linear 6-DOF nodal spring. The spring stiffness was determined utilizing LPILE (Ensoft 2005), by applying a small deformation at the pile top with the appropriate boundary conditions in each degree of freedom. The fixed bearings that connect the pier to the superstructure were modeled as rigid links. The intermediate piers with expansion elastomeric bearings were simply modeled as rollers.

The abutment backfill for both bridges was modeled using single springs at the soil-pressure resultant locations across the width of the abutment. These links have two orthogonal components, aligned with the abutment axes. The component normal to the abutment surface represents soil pressure, while the other component represents soil friction parallel to the abutment surface. Normal resistance was determined by calculating the limiting passive pressure, while soil frictional resistance was determined based on the skin friction angle and normal passive pressure. The at-rest soil pressure before positive thermal loading and active soil pressure during negative thermal loading were both neglected to simplify the model. Even more details about the abutment backfill model and its verification, including with respect to the critical abutment displacement at which passive pressure is reached, may be found in LaFave et al. (2016b).

Soil surrounding the piles is represented with a series of nonlinear springs. Each spring has two orthogonal components, which are aligned with the bridge directions (and there is no vertical component modeling soil friction). The springs were placed every 6 in. for the top 5 ft, every 1 ft for the following 5 ft, every 2 ft for the subsequent 10 ft, and then every 20 ft for the remaining depth of the pile after that. The lateral load-displacement (P-y) curves for each of the springs were generated utilizing LPILE. The boring-log data for each site were used to determine the soil properties that were input into LPILE. For the Kishwaukee Bridge, the P-y curves obtained from LPILE were then modified to take into account pile relief due to the bentonite slurry surrounding the top 10 ft of the piles, as shown in Figure 62.

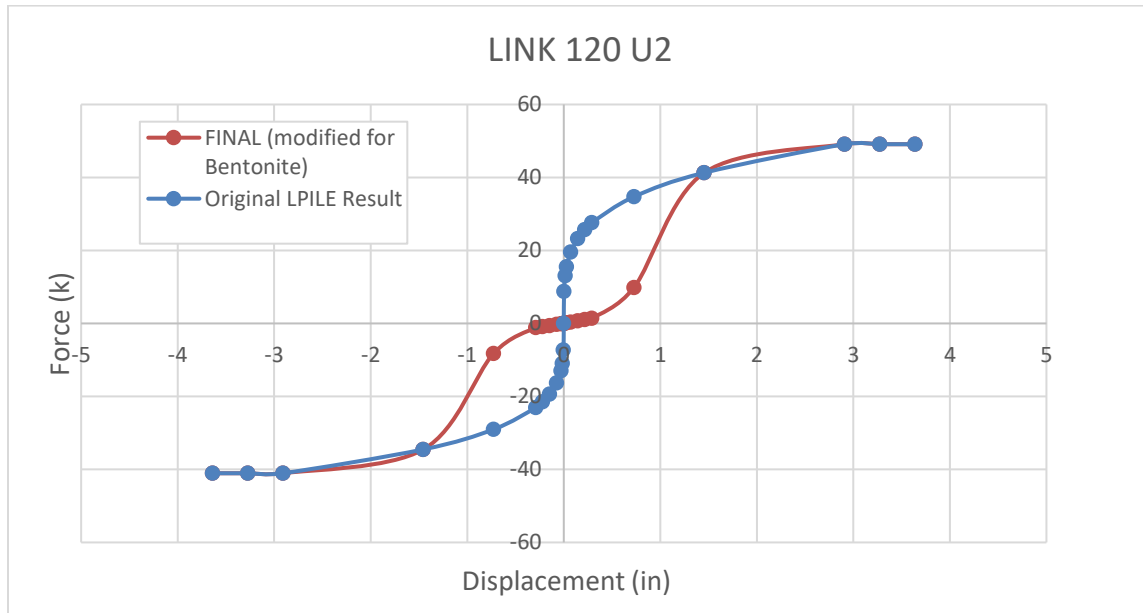


Figure 62. Kishwaukee P-y curve for soil spring in the longitudinal bridge direction at 10-ft depth.

At the UPRR Bridge, there is more uncertainty regarding soil modeling because the sandy soil and MSE wall effects are much more difficult to model accurately. An initial model of UPRR was created using the given boring-log data but with no consideration of the MSE wall. That model's pile results greatly overestimated the strains seen in the field measurements. Therefore, several different methods of modeling the site conditions were explored, with their results then compared to the measured field pile strains. The most promising results came from using a so-called "P-multiplier" to consider the effect of the MSE wall. As mentioned in Section 2.2, this P-multiplier has been explored by Han and found to be an appropriate method to consider MSE wall effects (2014). The P-multiplier modifies the soil stiffness to account for the fact that a pile closer to an MSE wall requires less force to create a certain displacement. This indirect pile "relief" is modeled utilizing a P-multiplier, which is determined based on the pile diameter and distance to the MSE wall. The corresponding P-multiplier of 0.42 for the UPRR piles was implemented to the top 20 ft of the longitudinal soil springs, only in the contraction direction, as shown in Figure 63. The resulting pile strains from implementing this existing method led to

better correlation between the field and model data. More details about the final changes to the UPRR model and other options explored can be found elsewhere (Brambila 2017).

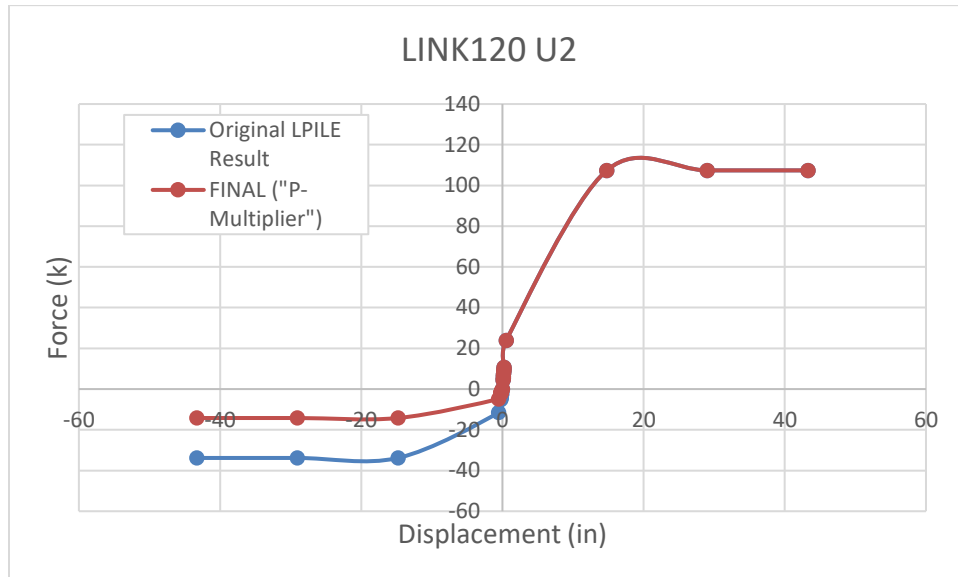


Figure 63. UPRR P-y curve for soil spring in the longitudinal bridge direction at 10-ft depth.

Several other modeling simplifications that were explored and implemented in the parametric study models were also implemented into these site bridge models. Wingwalls were excluded from the models based on previous research at Minnesota (Huang et al. 2004) and at Illinois (Olson et al. 2012), which concluded that wingwalls should only have a minor effect on IAB behavior. Approach slabs were also excluded from the models after analyzing results from parametric study models including approach slabs. Those models showed that bridge behavior was not affected by the approach slabs, and they were therefore excluded to simplify the models. Several parametric study models were also created taking into account girder camber. Girder forces, pile forces, and superstructure and abutment-pile displacement results from these models were very close to the corresponding models without girder camber. Therefore, girder camber was not explicitly included in the modeling process. The effect of including cross-frames was also explored with two bridge models, one with angle cross-frames and one with horizontal channel diaphragms. Bridge behavior was largely unaffected, and thus cross-frames were not considered in the models.

5.2 LOAD CASES AND ANALYSIS

The site bridge models were run for applied dead-load, thermal-load, and live-load conditions. The main objective of the project was to investigate relatively short-term bridge behavior under service conditions, so the applied loads were all unfactored and time-dependent effects were not incorporated. All of the load cases evaluated are listed in Table 3. Staged construction was modeled using a nonlinear staged construction analysis with three different stages. Both the thermal- and live-load cases were modeled using nonlinear static analysis. Positive and negative thermal-load cases with temperature changes of +80 and -80 °F were applied uniformly to the

girder frame elements and deck shell elements. Coefficients of thermal expansion of $5.5 \times 10^{-6}/^{\circ}\text{F}$ and $6.5 \times 10^{-6}/^{\circ}\text{F}$ were used for concrete and steel, respectively. For live loading, an HL-93 truck load was used. This truck loading was applied as a uniform load on the entire bridge to represent the design lane load, along with an additional equivalent uniform load placed at the center of one end-span. With the main focus of this project being to explore behavior under thermal loading, analysis of the model data was primarily focused on the pure positive thermal and pure negative thermal load cases. Therefore, the FE model data presented from this point forward is for the pure thermal positive and negative load cases, unless specifically noted otherwise.

Table 3. Load Cases

Method	Actual Loading	Shorthand
Analyzed in SAP2000	Dead: Staged Construction	Dead Staged
	Dead + HL-93 Live	HL-93
	Dead + Positive Thermal	Positive Thermal
	Dead + Negative Thermal	Negative Thermal
	Dead + Positive Thermal + HL-93 Live	HL-93 Positive Thermal
	Dead + Negative Thermal + HL-93 Live	HL-93 Negative Thermal
Computed from results	Dead + Positive Thermal—Dead Staged	Pure Positive Thermal
	Dead + Negative Thermal—Dead Staged	Pure Negative Thermal

CHAPTER 6: FE MODEL RESULTS VS. IAB FIELD DATA

6.1 GLOBAL BRIDGE MOVEMENT

As expected, the modeled global bridge movement is directly related to change in temperature due to the bridges' thermal expansion and contraction. As shown in Figure 64 and Figure 65, results from both the UPRR and Kishwaukee FE models exhibited longitudinal and transverse bridge movement at the abutments with change in temperature. This bi-directional movement is due to the fact that both UPRR and Kishwaukee are skewed bridges, with respective skews of 42.5° and 30°. These results are in line with the findings of the previous parametric study, which concluded that bridges with higher skew, of approximately 35° or greater, exhibit an increase in bridge transverse movement, causing unsymmetrical displacements of the acute and obtuse corners (LaFave et al. 2016a).

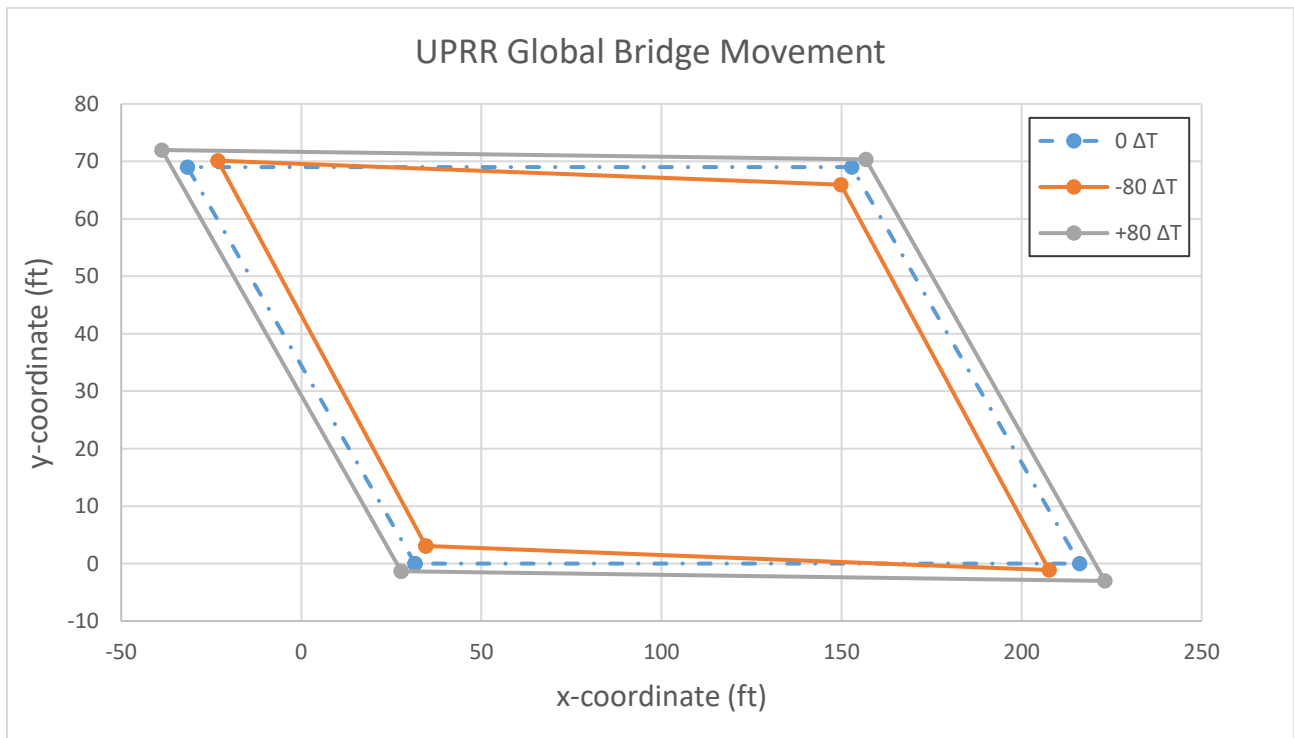


Figure 64. UPRR FE model global bridge movements due to change in temperature (125x scale; north is up).

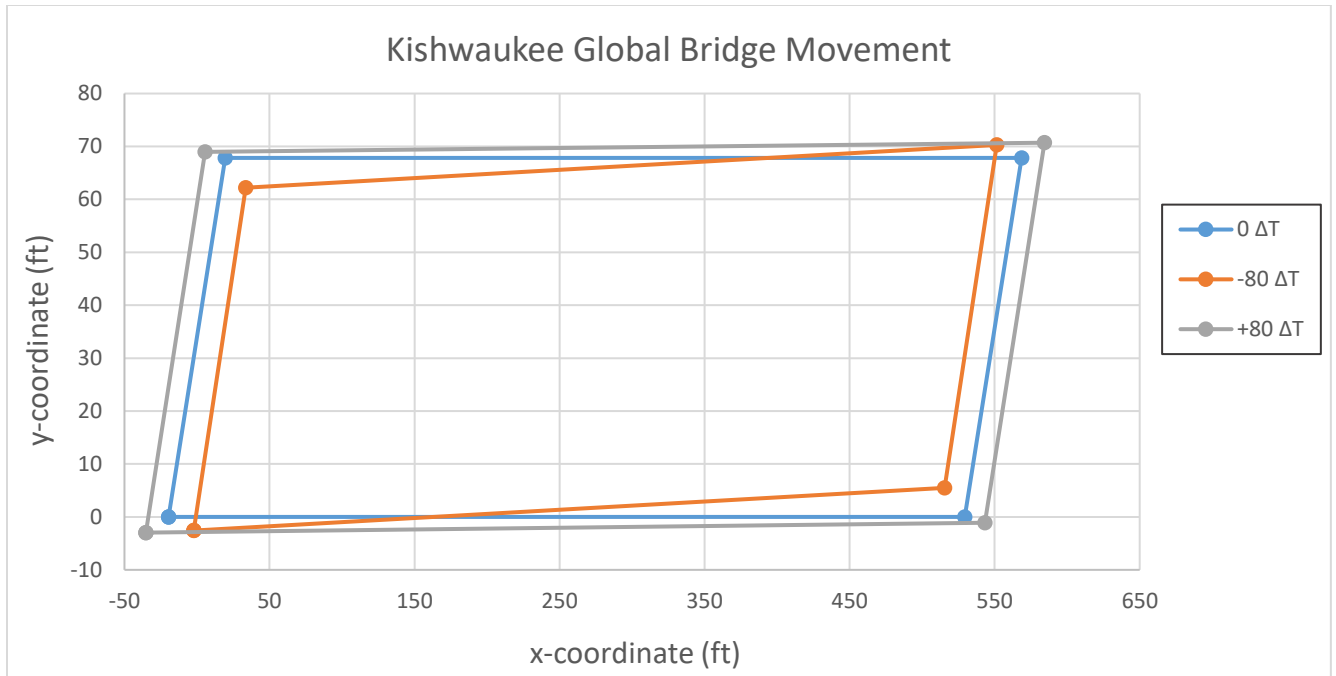


Figure 65. Kishwaukee FE model global bridge movements due to change in temperature (125x scale; north is up).

The crackmeters placed on the Kishwaukee Bridge measured only relative displacement, so it was not possible to determine the exact absolute global movement of the bridges in order to compare them with the model findings. However, using the crackmeter and approach-slab displacements allowed for calculation of an approximate longitudinal abutment displacement for Kishwaukee. Those calculated field abutment displacements (from section 4.3.3) are compared to the model results in Figure 66 and Figure 67. Despite the shift in displacement after the first year of data collection, the trends seen in the calculated field abutment displacements align well with the abutment displacements reported from the FE model, especially for the field data from the second year of monitoring. The displacements from the first year of field data are slightly more extreme than what is seen in the model, which could possibly be due to the data-initialization scheme.

Both model and field data at the north side of the abutment, near the bridge's acute corner, showed larger longitudinal displacement, as compared to the south side. This displacement differential supports findings from the parametric study, which found that more longitudinal movement is seen at the acute corners due to the unsymmetrical global bridge movement observed in higher-skew bridges.

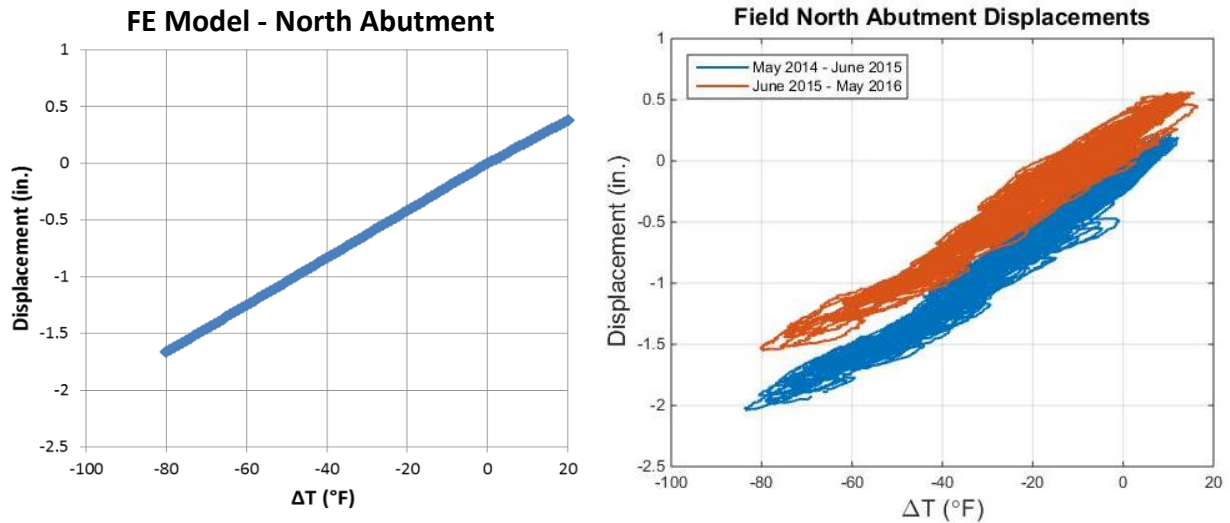


Figure 66. Comparison of Kishwaukee east-abutment north side longitudinal displacement.

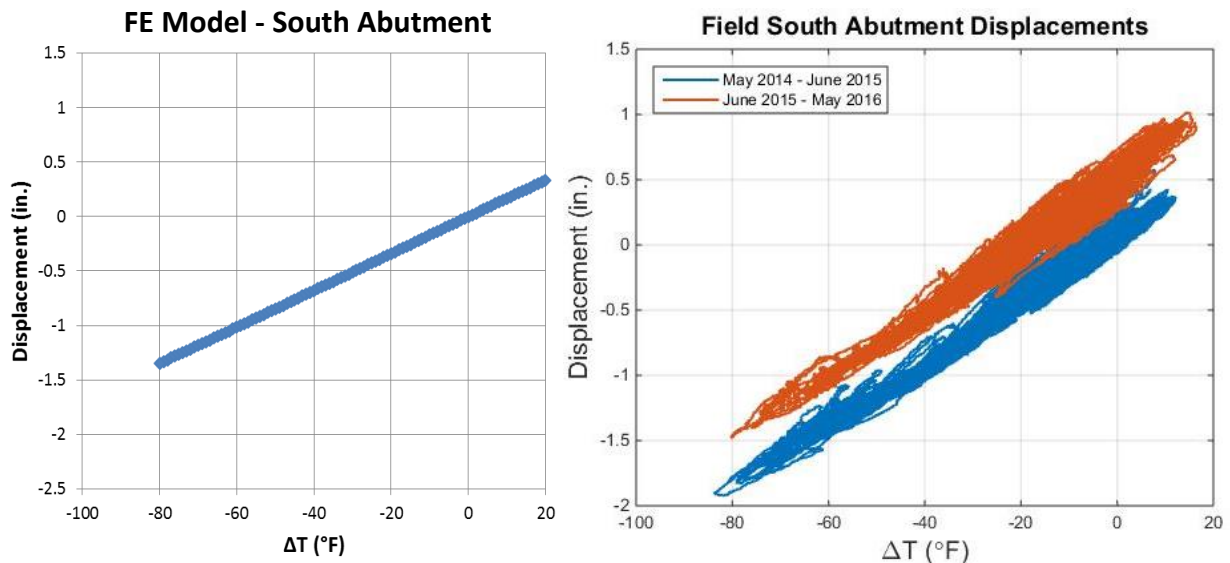


Figure 67. Comparison of Kishwaukee east-abutment south side longitudinal displacement.

6.2 ROTATIONS

Site bridge model abutment rotations were calculated utilizing the abutment top- and bottom-displacement data. As was seen in the field results, the FE model abutment rotations for both UPRR and Kishwaukee followed a clear linear trend with change in temperature. Figure 68 and Figure 69 demonstrate that the model abutment rotations underestimate the field rotations for both bridges, and the field and model data in the Kishwaukee Bridge displayed larger-magnitude abutment rotations than in the UPRR bridge. The fact that the FE models underestimated field abutment rotations could be interrelated with how the models slightly overestimated pile strains. This interdependence would occur because an increase in abutment

rotation would relieve the pile double curvature, thus reducing pile strains (Khodair and Hassiotis 2005, LaFave et al. 2016a). It should also be noted that, for the UPRR model results, the slight difference in slope of abutment rotation between the positive and negative change in temperature regions is due to the implementation of the MSE-wall, pile-relief effects, which only affects the contraction regime.

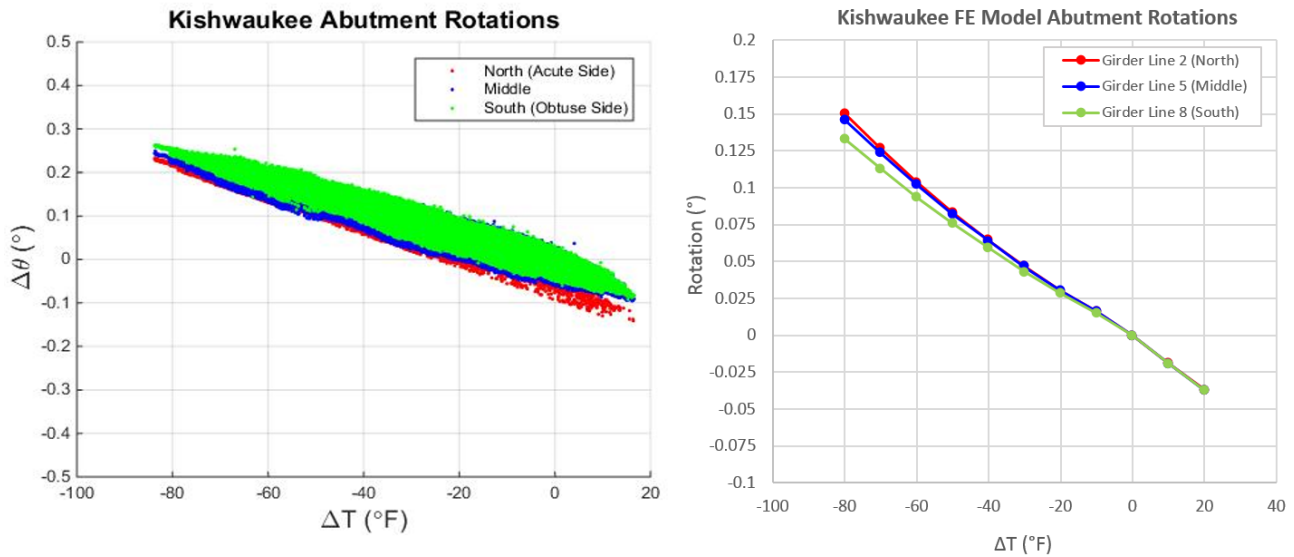


Figure 68. Kishwaukee field and FE model abutment-rotation measurements.

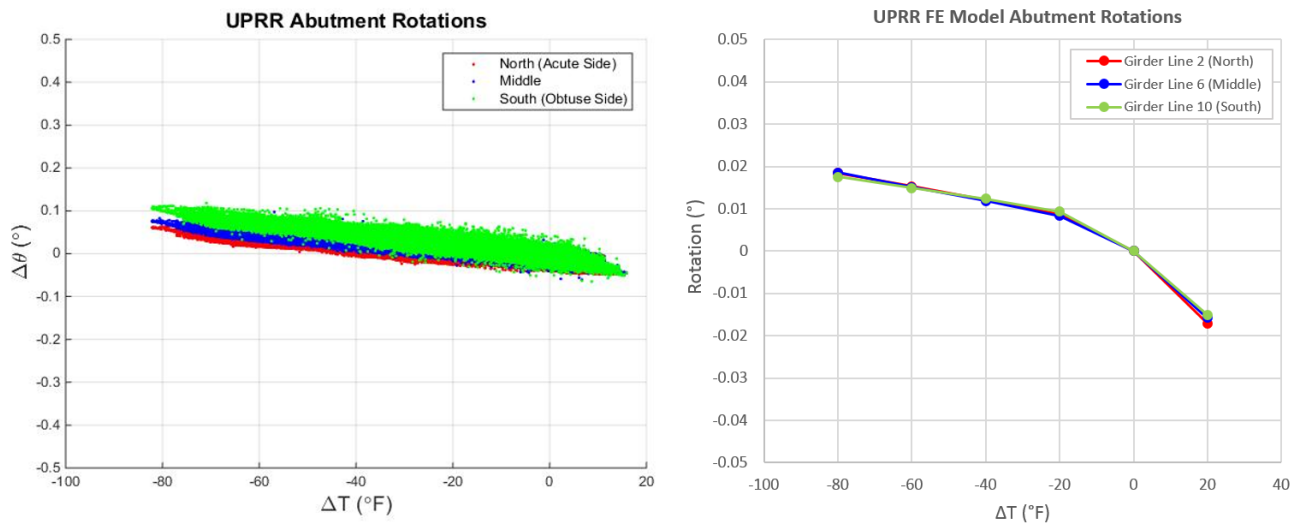


Figure 69. UPRR field and FE model abutment-rotation measurements.

One of the main purposes of the tiltmeter data was to compare the level of fixity at select interfaces of the abutment in the field to the rigid connection assumption utilized in modeling. Both the abutment cold-joint and girder–abutment connections were modeled as rigid for the parametric study of this project, and similarly for the site bridge models. In section 4.4, the presented field data demonstrated zero differential rotation between the upper diaphragm and lower abutment footing (pile cap), validating the modeling assumption of the cold joint as a

rigid connection. However, the girder–abutment connections at both bridges displayed a small amount of differential rotation, with maximums of 0.1° and 0.33° for UPRR and Kishwaukee, respectively. Therefore, the researchers conducted a limited sensitivity study to investigate the effects of using a rigid versus an only partially restrained girder–abutment connection in modeling. The Kishwaukee Bridge model was used as a basis for this study because it displayed the higher magnitude of measured field girder–abutment differential rotation.

Two new Kishwaukee Bridge models were created, one with a partially rigid girder–abutment connection and one with a nearly pinned girder–abutment connection. All other aspects remained the same as in the original Kishwaukee model. Both new models exhibited an increase in girder–abutment differential rotation, as compared to the original Kishwaukee model. These models further demonstrate that increased connection flexibility affects both superstructure and substructure demands. Girder stresses at the abutment (the location of highest girder stresses) decreased in magnitude as girder–abutment connection flexibility increased. Bottom-flange girder stresses along the length of the middle girder decreased overall, with only a small increase in magnitude seen at the expansion pier location. Similarly, the piles also exhibited a decrease in peak pile strains as girder–abutment connection flexibility increased. However, the pile strains did demonstrate increased combined flexure behavior. Results from this sensitivity study seem to indicate that implementing a rigid girder–abutment connection in the FE model is slightly conservative in cases where there is indeed some limited flexibility at the girder–abutment connection in the field. The actual level of fixity of the instrumented bridges cannot be determined exactly and may even be variable over time. Therefore, the girder–abutment connections of the final versions of the instrumented bridge models were not modified; and they simply utilized a rigid-connection assumption, as this provides slightly conservative and yet reliable results. Furthermore, the sensitivity study demonstrates that a fully continuous, moment-resisting connection assumption overall provides slightly conservative results, thus validating findings from the previous parametric study models.

6.3 PILE DEMANDS

Pile strain data from the site bridge FE models were collected at locations matching those of the pile strain gages in the field. Figure 70 and Figure 71 compare the Kishwaukee field pile strains with those from the model and show that the model slightly overestimates the field pile strains. The analytically determined peak pile strains can be viewed as slightly conservative in that they neglect possible beneficial softening effects of the pile soil system as a result of any gap that may have opened up between the top of the pile and surrounding soil (LaFave et al. 2016b). Pile strains from the UPRR model also overestimate the field strains, as seen in Figure 72 and Figure 73. Site conditions at UPRR, including the MSE wall and sandy soil, may not have been fully captured by the model, which likely accounts for a large part of the differences between the model and field data. Slight differences between the model and field data were to be expected anyway, though, as the bridge models do not include frictional forces acting on the piles; and the nature of loading differs somewhat from that in the field. In the field, the temperature goes through cyclic seasonal and daily changes, which are not fully captured with

the implemented monotonic loading. However, the overall similarity between the field and model data support that the use of monotonic loading is sufficient for most practical purposes.

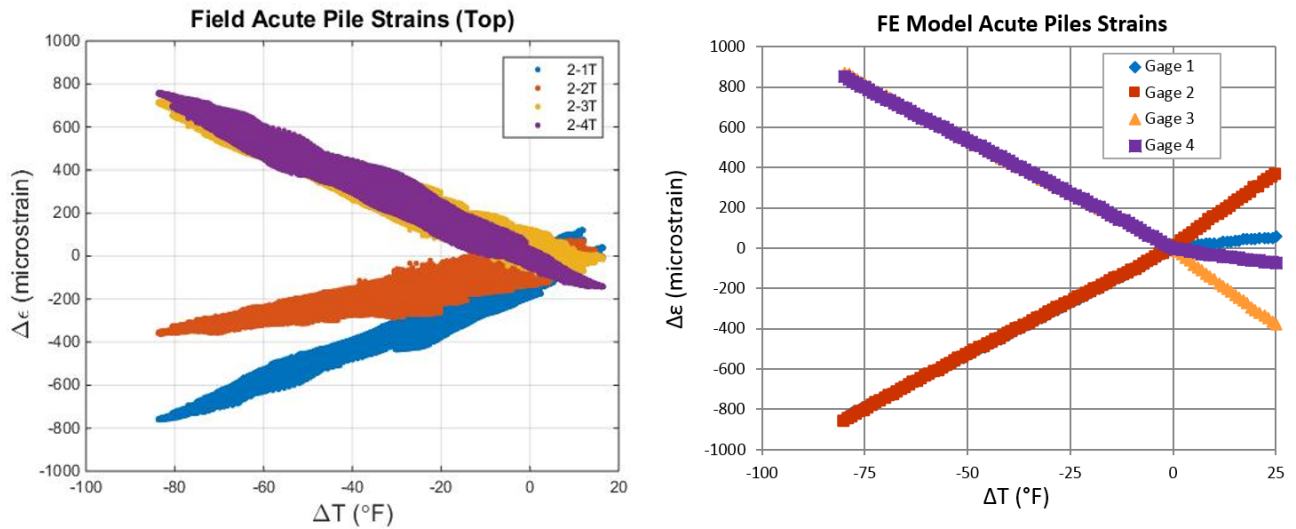


Figure 70. Comparison of Kishwaukee field-measured and FE-model acute pile strains at the pile-cap boundary.

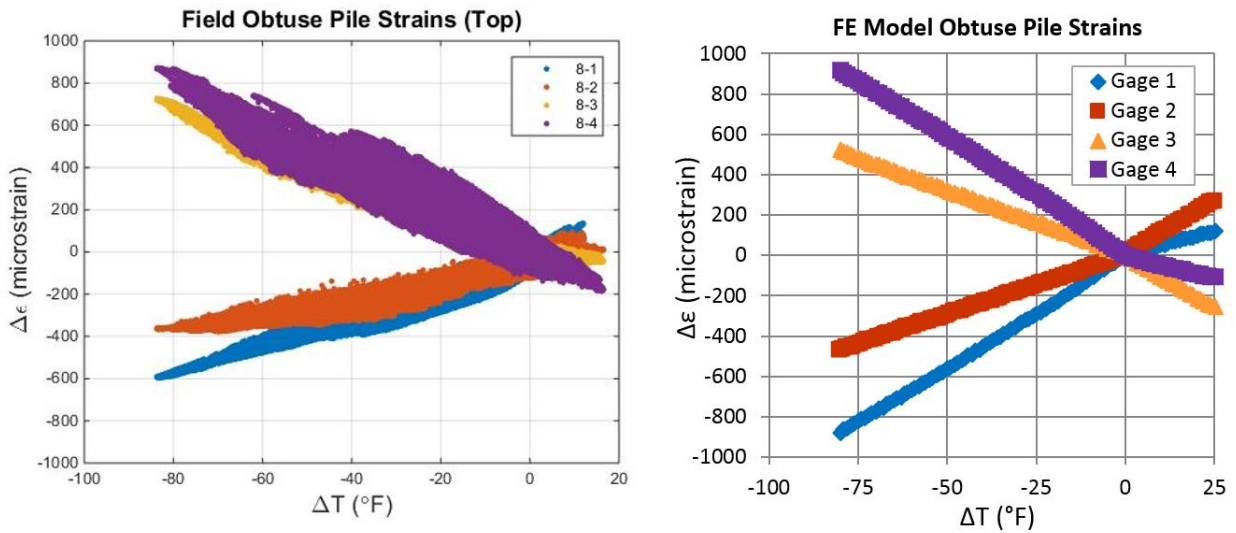


Figure 71. Comparison of Kishwaukee field-measured and FE-model obtuse pile strains at the pile cap boundary.

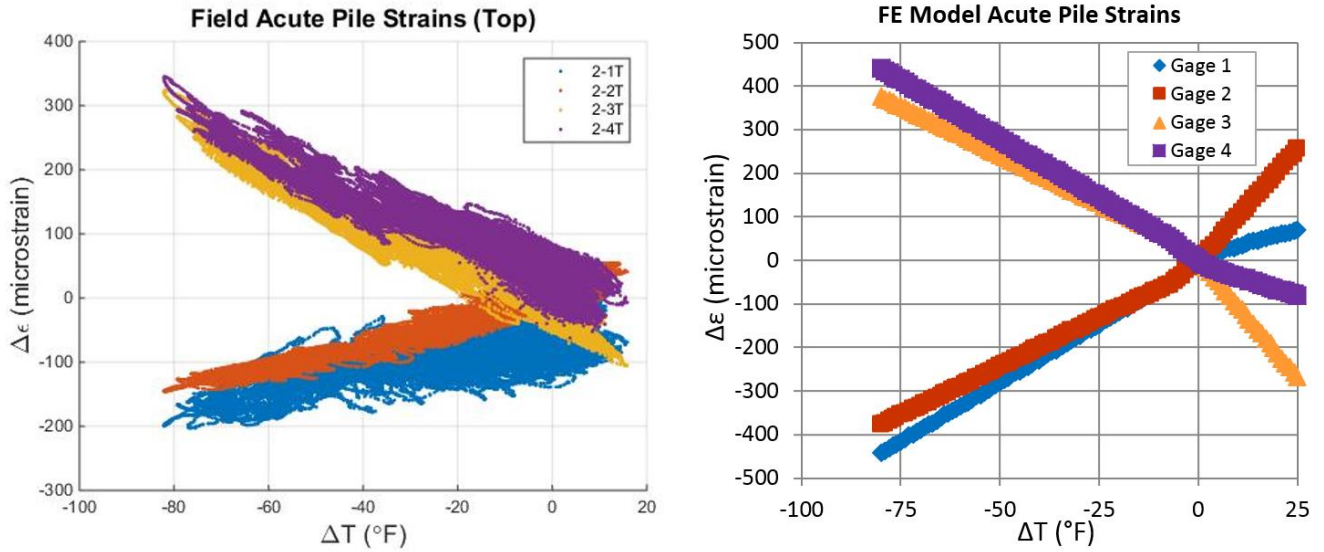


Figure 72. Comparison of UPRR field-measured and FE-model acute pile strains at gage locations at the pile-cap boundary.

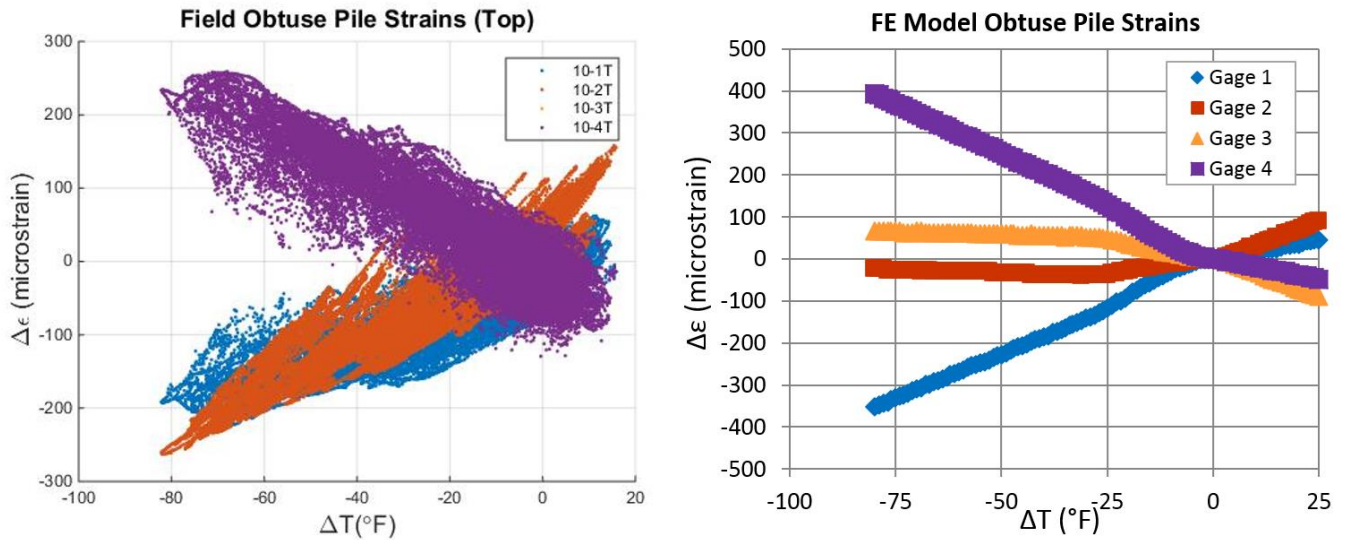


Figure 73. Comparison of UPRR field-measured and FE-model obtuse pile strains at gage locations at the pile-cap boundary.

The FE-model data also provides further insight into what behavior accounts for the majority of the resulting pile strain. Figure 74 through Figure 76 show the model pile strains due to axial force, strong-axis bending, and weak-axis bending contributions for both the acute (pile 2) and obtuse (pile 8) piles at Kishwaukee. When Gage 1 and Gage 3 data are not visible, they are identical to the data from Gages 2 and 4, respectively, and when Gage 1 and Gage 2 data cannot be seen, they are identical to the data from Gages 3 and 4, respectively. Similar trends are seen from the UPRR model strain components, only with overall lower strain magnitudes

(as expected). This breakdown shows that the majority of the pile strains come from weak-axis bending, as seen in the field data and as expected for an IAB with weak-axis-oriented piles such as Kishwaukee or UPRR. Focusing on the contraction regime, the FE-model axial and strong-axis contributions increased from acute to obtuse piles in the models. However, the axial force contribution from the field data was greater at both exterior piles (see Figure 44), with the strong-axis contribution being similar at all the piles (see Figure 45).

As mentioned previously, the strong-axis and axial force contributions would cause a separation between the gage pairs and a shift in magnitude from the data being symmetric about zero strain, respectively. Field pile strains at Kishwaukee exhibit trends related to both axial force and strong-axis bending effects; and both effects appear to increase from the acute to the obtuse corner, as seen in the model. However, the Kishwaukee obtuse pile data displayed a higher upward (tensile) shift in strain magnitude than the model and a lower magnitude of separation between gage pairs than the model data. When comparing the UPRR piles, the field results show only a small separation in gage-pair magnitudes. The model seems to allow a greater strong-axis bending contribution than in the field, especially at the obtuse pile.

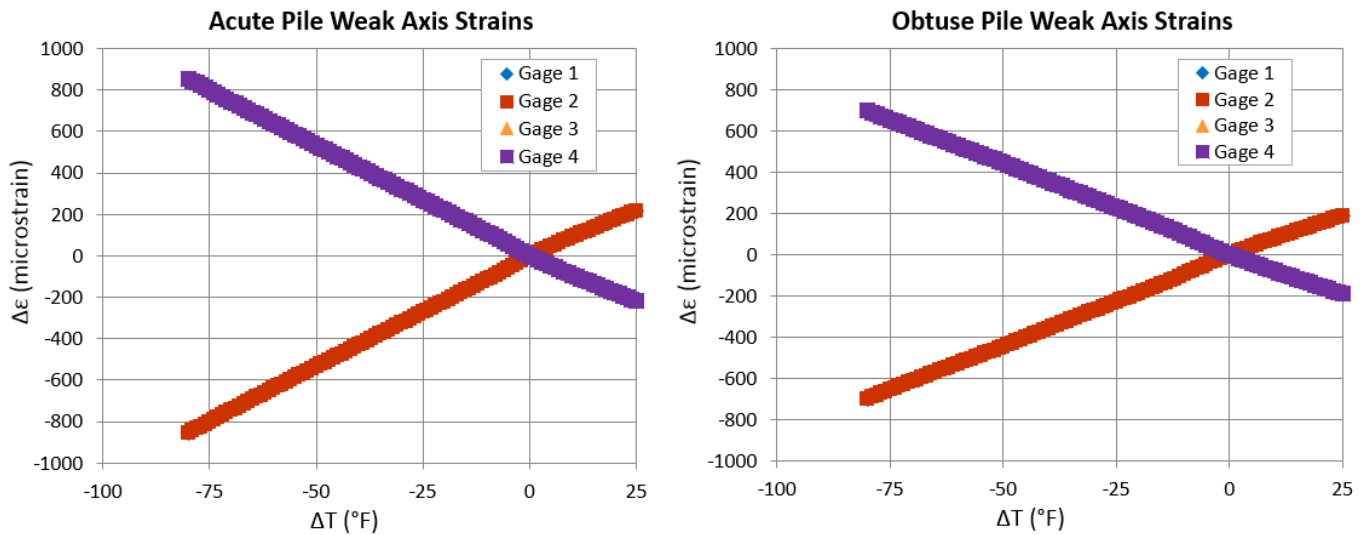


Figure 74. Kishwaukee FE-model pile strains due to weak-axis bending.

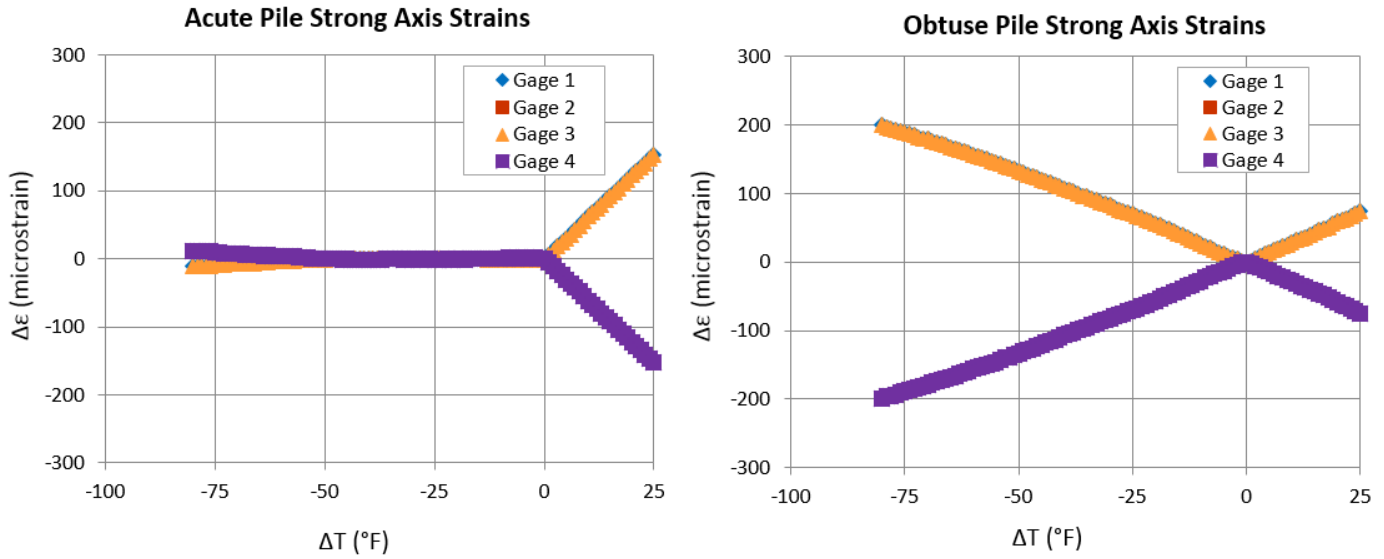


Figure 75. Kishwaukee FE-model pile strains due to strong-axis bending.

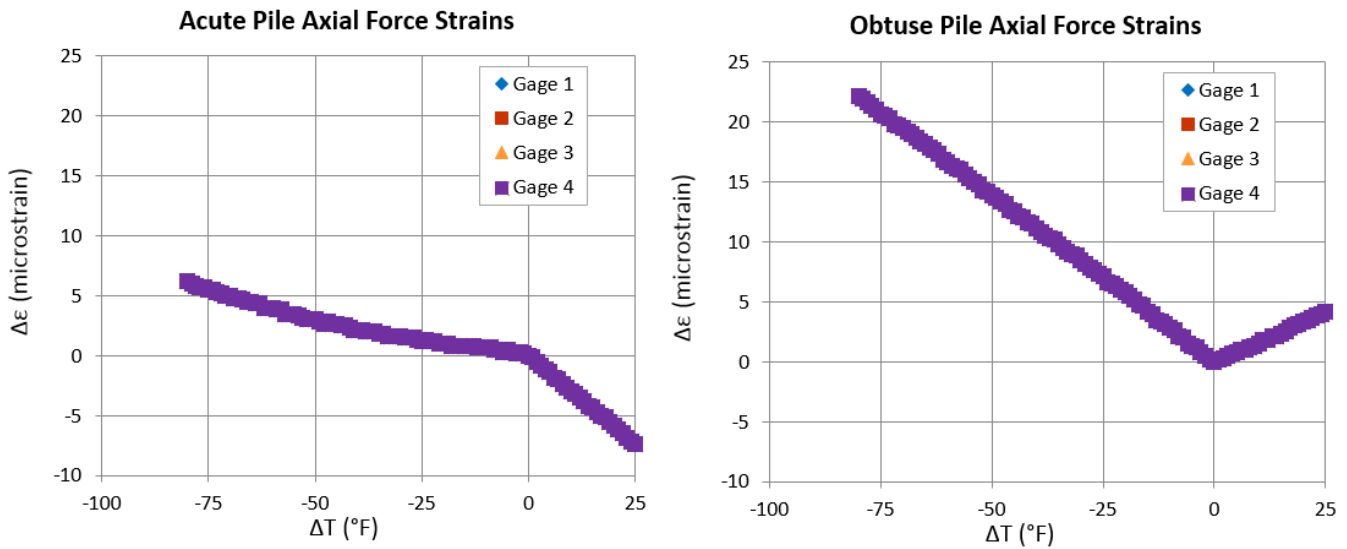


Figure 76. Kishwaukee FE-model pile strains due to axial force.

In spite of small differences, the field and model pile data exhibit a likeness that provides the opportunity to analyze maximum pile strain at the tips of the flanges through further analysis of the model and field pile data. Focusing on the acute pile, where maximum pile strains are typically found, Figure 77 and Figure 78 show the strains at the flange tips for piles along girder line 2 (near the acute corner) for both Kishwaukee and UPRR. FE-model maximum pile strains from the pure thermal loading cases were 852 microstrain and 1705 microstrain for UPRR and Kishwaukee, respectively, both of which are less than the 1724 microstrain required to reach yielding. These values are slightly higher than what was seen in the respective field data, which is assumed to represent only thermal loading. FE-model maximum pile strains from the dead-plus-pure-thermal-loading cases were 889 microstrain and 1864 microstrain for UPRR and

Kishwaukee, respectively. Therefore, both the slightly conservative FE models and the field data indicate some pile-deformation capacity is still available when limited pile yielding is allowed, especially at the UPRR Bridge.

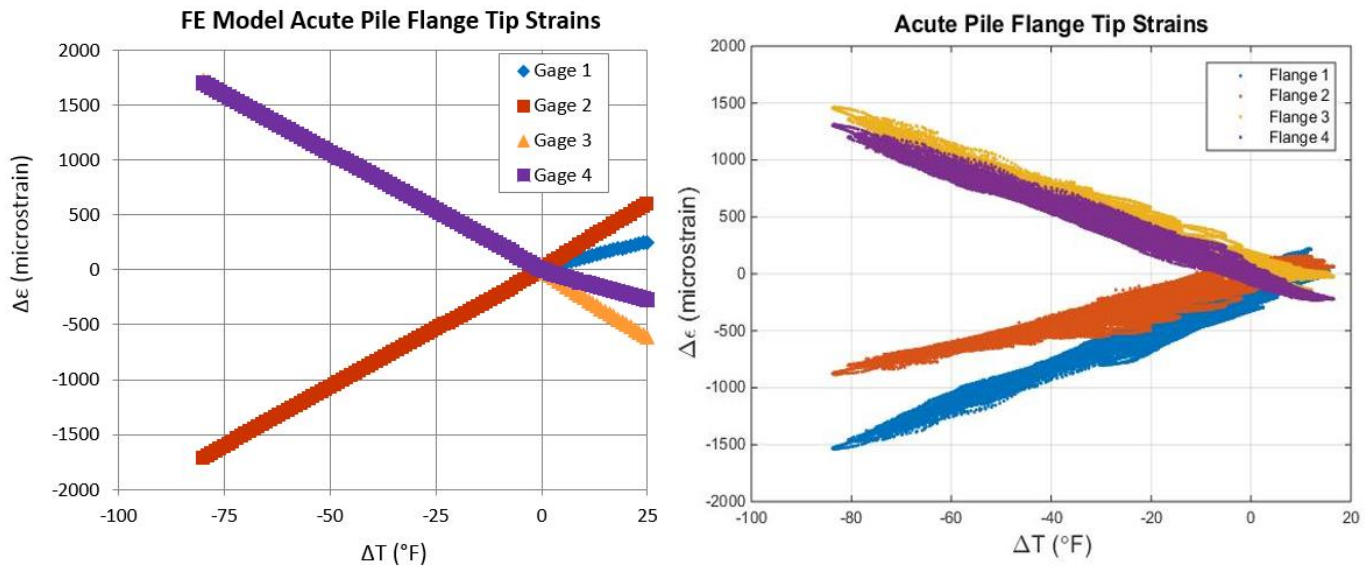


Figure 77. Kishwaukee FE model (pure thermal loading) vs. field-estimated pile strains at acute pile flange tips.

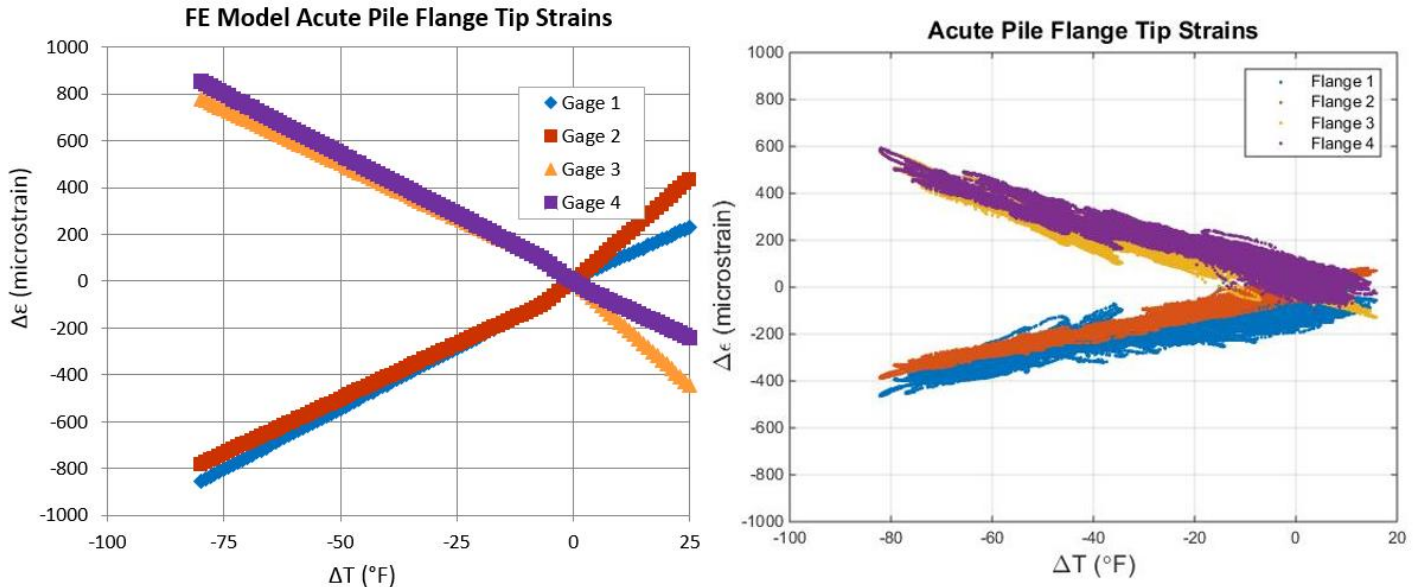


Figure 78. UPRR FE model (pure thermal loading) vs. field-estimated pile strains at acute pile flange tips.

Another aspect of interest regarding pile behavior is the pile–abutment connections. For both the Kishwaukee and UPRR bridges, each pile was embedded 2 ft into the abutment, essentially creating a rigid connection. The FE models for the two bridges assumed this connection to be

rigid due to pile embedment. However, it is possible that there could be some flexibility present in the connection, for instance due to any cracking of the concrete surrounding the piles. This flexibility could account for part of the difference in pile strain magnitudes observed between the field and model data. No tiltmeters were placed on the piles at either bridge, so the level of fixity of the pile–abutment connection could not be determined experimentally. However, to investigate the general effects of a rigid versus semi-rigid pile–abutment connection, a limited analytical sensitivity study was conducted.

The UPRR bridge model was utilized for this sensitivity study, and two new modified models were created—one with a semi-rigid connection and one with the extreme case of a completely released (or pinned) pile–abutment connection. Both cases showed a decrease in overall pile-strain magnitudes, with the extreme pinned case having an average 90% decrease in peak pile strains. Increased connection flexibility reduces pile demands as the imposed pile double curvature is relieved. Therefore, if the pile–abutment connections at the two bridges did indeed experience some limited flexibility, the use of a rigid connection in the model would account in part for why the models slightly overestimate the field pile strains.

6.4 GIRDER DEMANDS

To further analyze the field girder data, girder stresses from the site bridge FE models were calculated (at both the top and bottom flanges) using the strong-axis and weak-axis bending moments plus the axial force at the gage locations. Overall, the top-flange field data aligned well with the FE model results, as shown in Figure 79. At a couple locations, both bridge models slightly underestimate girder top-flange stresses, but overall the top-flange field data demonstrates the same linear trends as seen in the models.

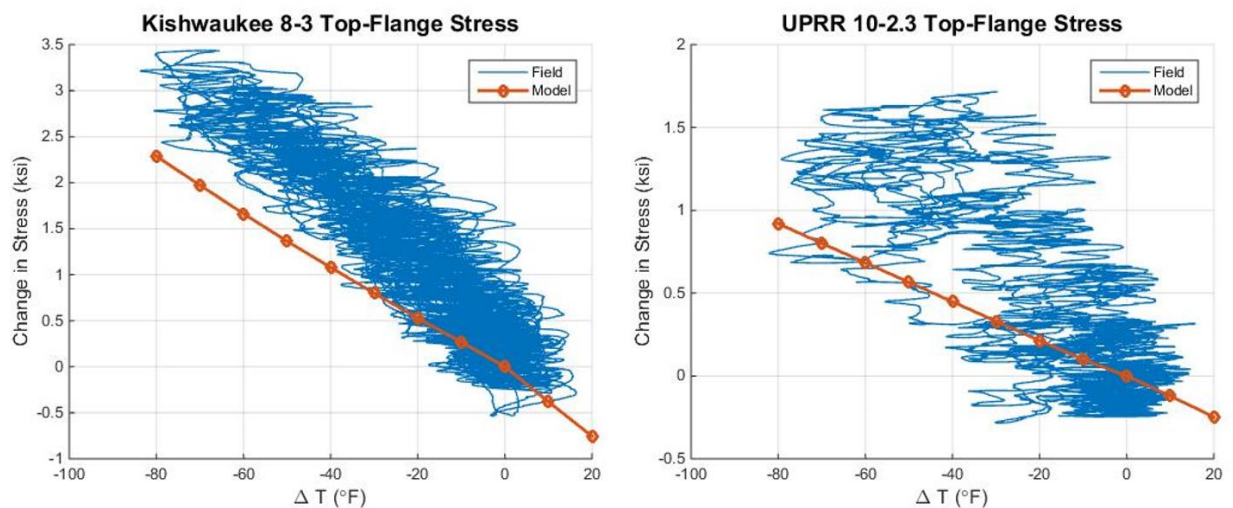


Figure 79. Top-flange stress comparison of field data to FE-model prediction for girder 8 interior mid-span at Kishwaukee and girder 10 east quarter-span at UPRR.

As seen in both the parametric study and the field data, the girder bottom flanges displayed the highest magnitude of stresses. Figure 80 shows there is fairly good correlation between the field data and FE-model girder bottom-flange stresses for part of the data. This period of time is indicated by the black line in Figure 81. This period represents the first few months of data collection during which the bottom-flange stresses tracked reasonably well with temperature. Focusing on this period of time, Figure 82 shows that the model matches the field data fairly well and follows a clear linear relationship. After this initial period, though, the girder bottom-flange field stresses tended to creep toward higher tension or compression values (depending on location) and deviate from the expected trends gathered from the model.

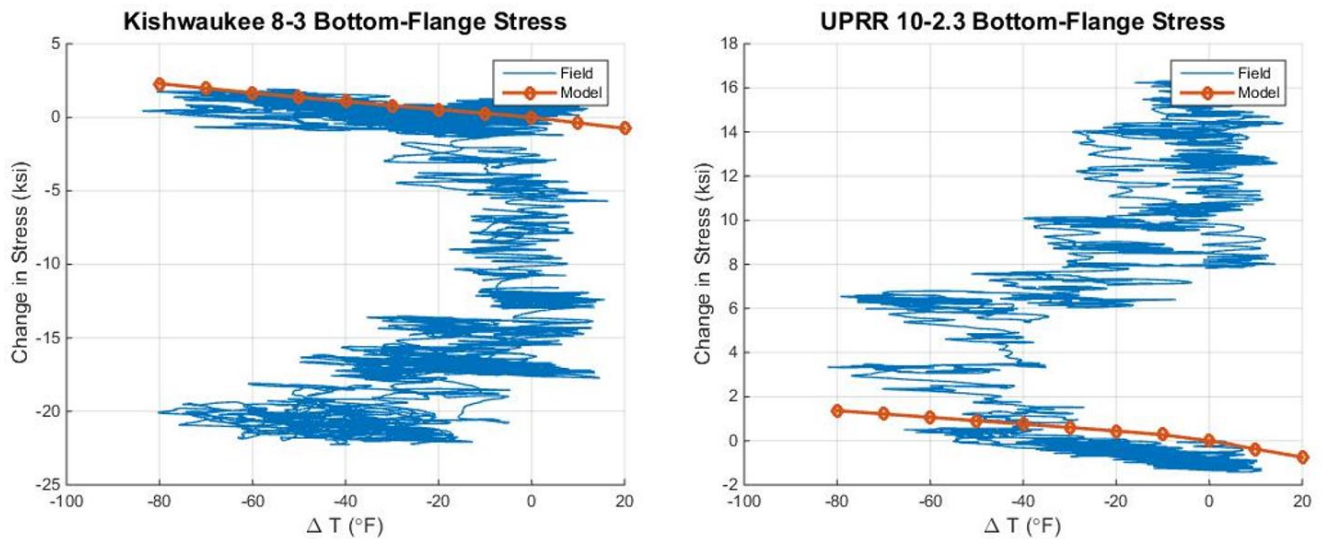


Figure 80. Bottom-flange stress comparison of field data to FE-model prediction for girder 8 interior mid-span at Kishwaukee and girder 10 east quarter-span at UPRR.

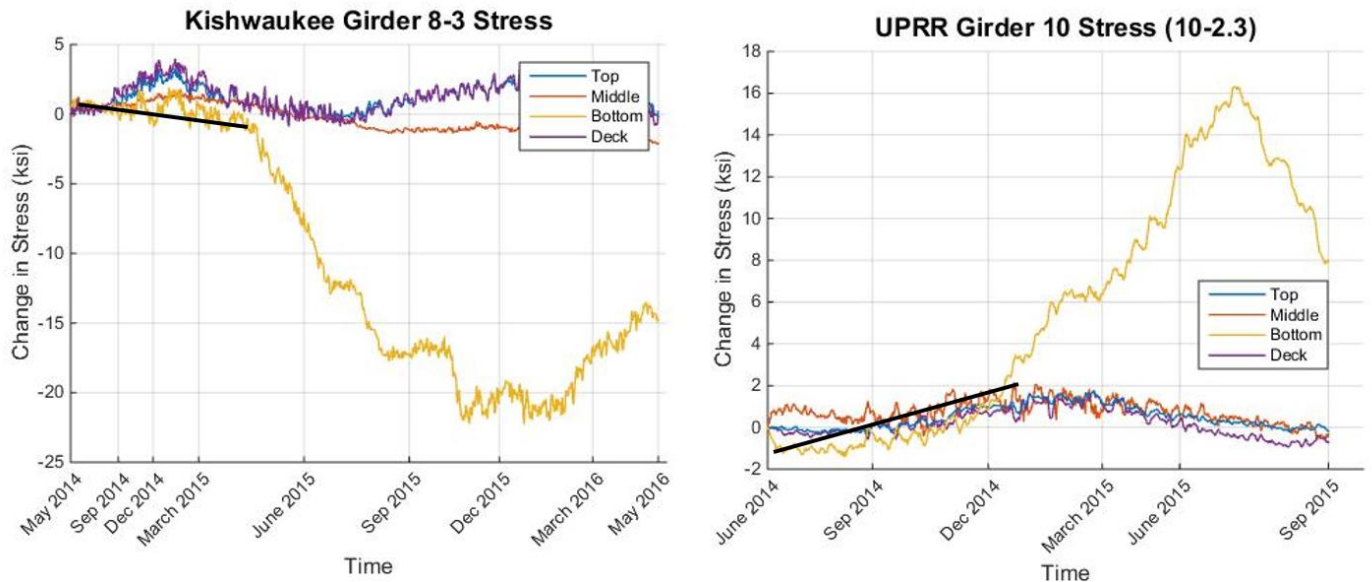


Figure 81. Girder stresses over time at Kishwaukee and UPRR.

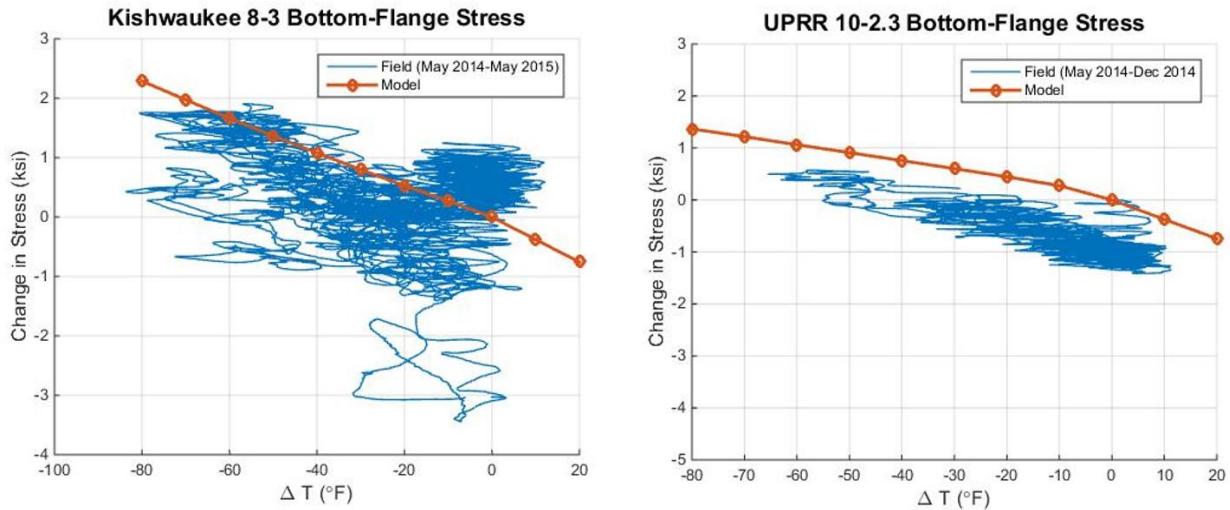


Figure 82. Bottom-flange girder stress for Kishwaukee 8-3 (May 2014–May 2015) and UPRR 10-2.3 (May 2014–Dec 2014).

Figure 83 and Figure 84 compare the field and model top- and bottom-flange stresses along a girder at Kishwaukee and UPRR, respectively, on representative hot and cold days (from section 4.6). At both bridges, the top-flange field stresses typically agree well with the model results during the entire period of data collection. At some locations, there were small deviations from the model results during the second year; but these typically varied only 1–2 ksi and were much smaller than those consistently seen from the bottom-flange field results. Field bottom-flange girder stresses from the hot and cold days of the first year were typically very similar to the predicted model results. However, results from the second year demonstrated a larger difference between the field and model data, which typically varied 5–15 ksi (and in only very select extreme cases reached a 35 ksi difference). Mid-span locations typically had the best correlation between girder bottom-flange field and model data, while the support locations (abutment and/or piers) typically displayed much larger differences. These large discrepancies seen in the bottom-flange data could possibly be a result of out-of-plane bending of the girder’s bottom flange. The cycles of bridge expansion and contraction could have caused this out-of-plane bending to result in localized yielding at some locations along the girder that were more restricted from movement, such as near the abutments and piers, which showed larger differences between the field and model data. Overall, the girder data does not provide a clear single explanation for this unexpected bottom-flange behavior; but it can be concluded that this is likely a real systematic behavior and not just an error in the gage performance.

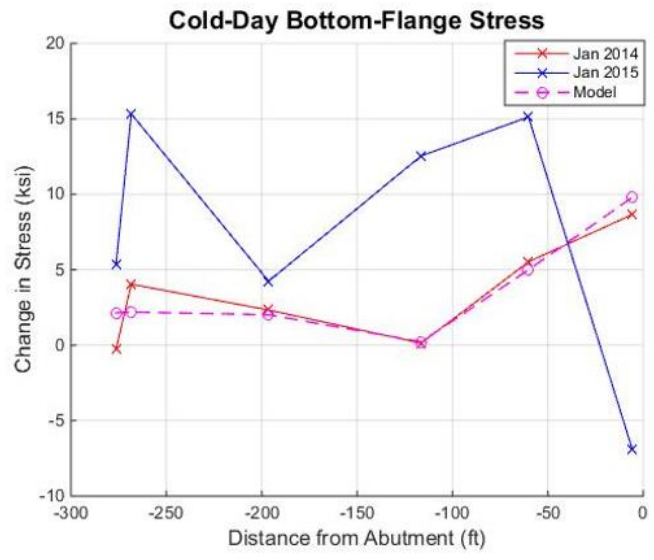
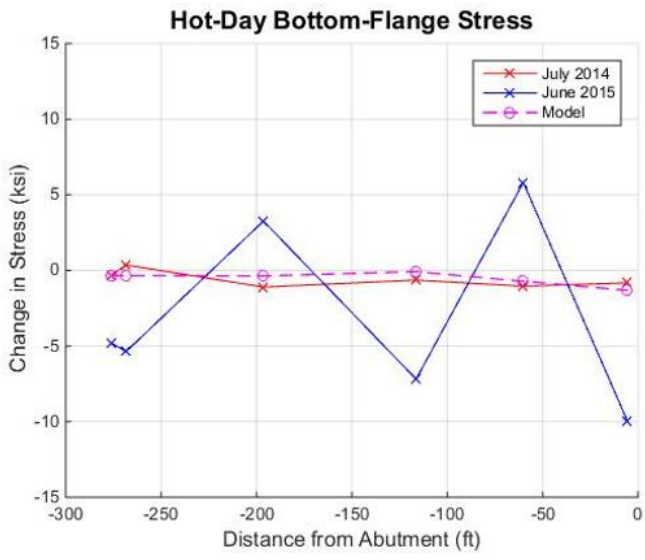
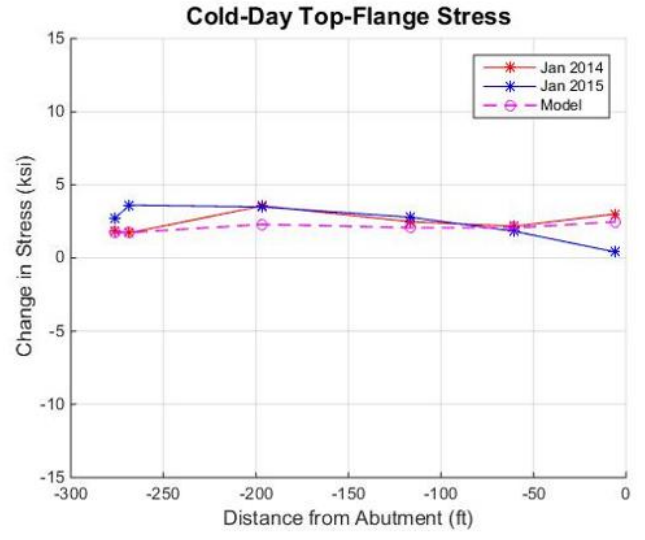
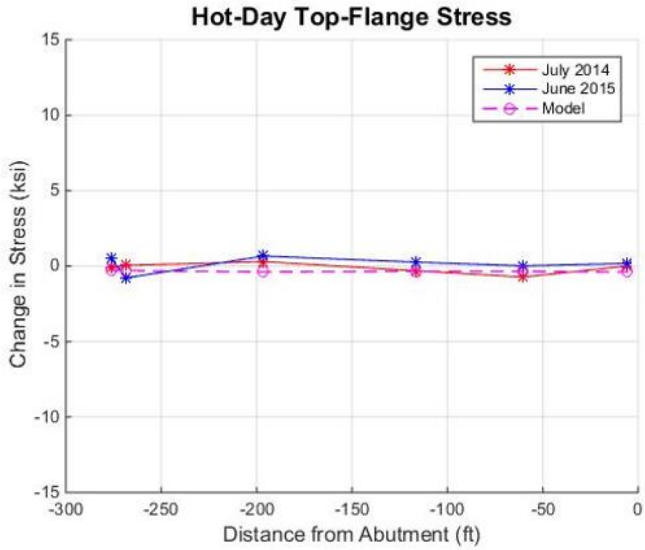


Figure 83. Hot- and cold-days field data and FE-model comparison of Kishwaukee girder 2 stresses.

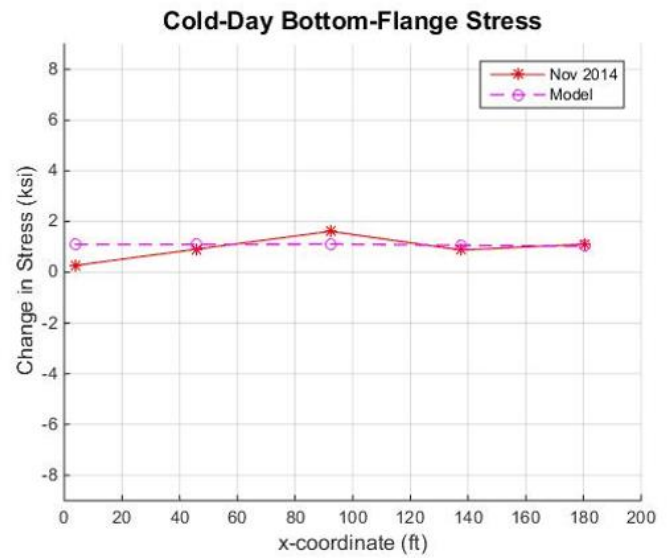
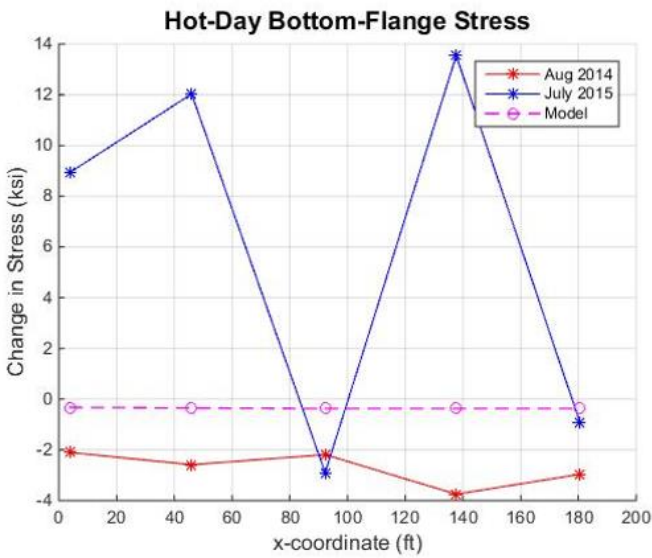
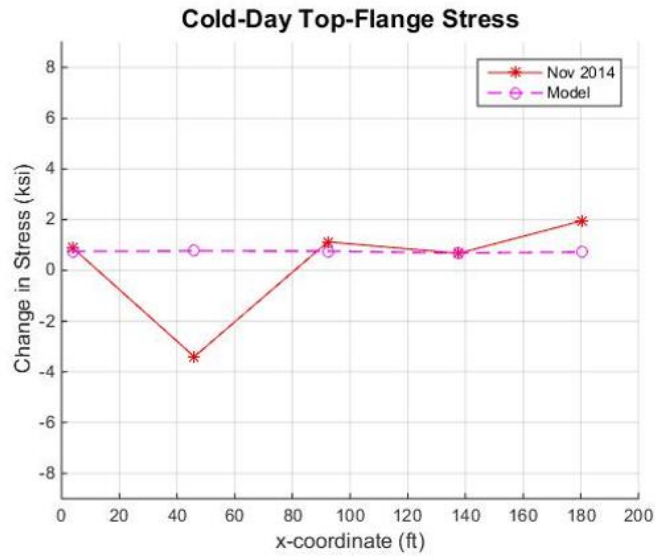
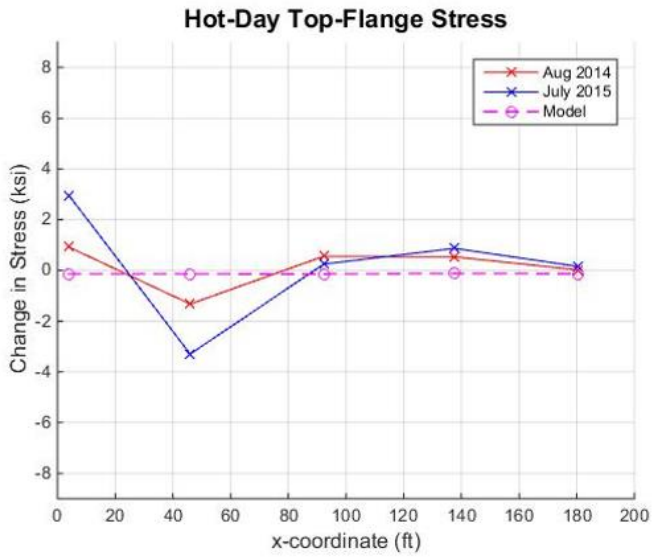


Figure 84. Hot- and cold-days field data and FE-model comparison of UPRR girder 10 stresses.

CHAPTER 7: CONCLUSIONS

7.1 BEST PRACTICES FOR FIELD MONITORING IMPLEMENTATION

Two Illinois IABs, the Kishwaukee River Bridge and Union Pacific Railroad (UPRR) Bridge, were selected for instrumentation and field monitoring to complement results of the parametric study phase of this project. The goal of the field monitoring program was to validate assumptions from previous numerical models associated with the project and provide further insight into IAB behavior. Because the project's main focus was on the behavior of IAB superstructures, that is where most of the instrumentation effort was aimed, with limited instrumentation on the substructure. Global movement, pile, girder, deck, and approach-slab strains were monitored to assess IAB behavior and any buildup of thermal stresses. Rotations at different interfaces of the abutment were also monitored to assess modeling and typical design assumptions. The instrumentation plans for the two bridges required extensive planning and coordination with several agencies. An abundant amount of time should be allotted for instrumentation planning as the gage installation, wiring, and data acquisition system are typically quite complex and highly interdependent on different factors. Despite a few setbacks and field complications, the University of Illinois research team successfully implemented the field monitoring system on both bridges and collected data for 16 months and 24 months at UPRR and Kishwaukee, respectively.

Spot-welded, arc-welded, and embedded vibrating-wire strain gages were utilized to instrument the girders, piles, and approach slab, respectively. All three types of gages provided high-quality data, with only very few gages that stopped functioning. One recommendation for future girder monitoring would be to utilize a schematic similar to that used on the piles, as shown in Figure 32, to allow for strong-axis moment, weak-axis moment, and axial force calculations. To measure movement of the different bridge joints, displacement transducers (crackmeters) were installed on all four corners of the approach slab. However, because the crackmeters provide only a measure of relative movement it could not be definitively concluded what component of the bridge was moving. In future monitoring projects, it would be recommended to include a measurement of absolute displacement utilizing a fixed reference point. Overall the implemented instrumentation scheme was successful and provided valuable insight into IAB behavior.

7.2 CONCLUSIONS FROM FIELD DATA

Field monitoring results from both the Kishwaukee and UPRR bridges demonstrated clear trends in regards to IAB superstructure and substructure behavior. All of the data exhibited clear trends with change in temperature. The calculated field abutment displacement was slightly less than the theoretical free expansion/contraction and showed unsymmetrical movement of the bridge acute and obtuse corners, corroborating findings from the parametric study. This global movement was one of the main driving factors influencing pile and girder behavior. Higher-magnitude pile strains were typically seen near the acute corner, which is shown to have greater longitudinal displacements. Pile strains correlated well with predictions

from the models and both the model and extrapolated field flange-tip pile strains showed some additional pile-deformation capacity is available. The most variable data resulted from the girders, particularly the bottom flange. Deck, girder top-flange, and girder web stresses all showed clear trends with temperature and matched well with model predictions. As seen in the parametric study, the bottom flange had the highest-magnitude stress, though the gages demonstrated a deviation into greater tension or compression (dependent on location) after the first 6 to 12 months of data collection. This behavior could be due to out-of-plane bending leading to localized yielding, or it could even be from live loading or other cyclic / time-dependent effects related to abutment fixity and/or deck cracking. However, one distinct cause for this behavior is not clear. Overall, the girders stresses showed clear trends with change in temperature that matched model predictions and are of significant magnitude that it is recommended they be considered in IAB design.

The field monitoring program also provided valuable data utilized to assess different modeling assumptions utilized in the parametric study models and instrumented-bridge models. Essentially no differential rotation was observed between the top diaphragm and lower footing (pile cap) of the abutment at either bridge, indicating that the abutment cold joint is virtually a rigid connection. The measured differential rotation between the abutment and girder was of slightly higher magnitude at both bridges. However, as compared to calculations for a pinned-girder scenario, the rotations are small enough to indicate a fixed-connection assumption is valid. Overall, results from the field monitoring program provided valuable insight into different aspects of IAB behavior and validated key modeling assumptions, demonstrating high potential for application of the parametric study and field monitoring results in IAB design.

7.3 MODELING CONCLUSIONS AND RECOMMENDATIONS

The finite-element models created for both instrumented bridges provided not only a basis of comparison for further analysis of the field data but also a method to validate and further investigate some of the modeling assumptions implemented. The models implemented the modeling assumptions and procedure from the parametric study. A unique modification implemented in the models of the instrumented bridges was the inclusion of pile-relief modeling. The soil springs were modified differently for each bridge to best represent the bentonite slurry at the Kishwaukee foundation and the MSE wall at the UPRR site. Results from the models implementing pile relief improved significantly and displayed better correlation with the field data, especially when comparing pile strains.

Other modeling assumptions were further investigated upon analysis of related field results. Tiltmeter results indicated a small amount of differential rotation at the girder–abutment connections of both bridges. A limited sensitivity study revealed that modeling the connection as rigid is slightly more conservative, thus validating the assumption and ensuing results. The bridge models also assumed the pile–abutment connection to be rigid. No field monitoring of this connection was employed, but a limited sensitivity study was implemented to assess the effects of this assumption. The sensitivity study showed that a rigid connection provides slightly conservative results, as compared to a semi-rigid connection. The results from the two

sensitivity studies validated the use of a rigid connection for modeling of the girder–abutment and pier–abutment connections for this project. The exclusion of approach slabs in the models was also further investigated through the field monitoring effort. Modeling investigation during the parametric study found that including the approach slab in the bridge models had no significant effect on the IAB behavior and thus excluded it from the models for simplicity. Field monitoring results show low-magnitude stresses in the approach slab, validating this assumption. Validation of the modeling methods further corroborates results from the models of the monitored bridges and the parametric study.

REFERENCES

- Arsoy, S., R. M. Barker, and J. M. Duncan. 1999. *The Behavior of Integral Abutment Bridges*. VTRC 00-CR3, Virginia Transportation Research Council, VA.
- Brambila, G. 2017. *Field Monitoring and Numerical Analysis of Two Illinois Integral Abutment Bridges*. MS thesis. University of Illinois at Urbana-Champaign, Urbana, IL.
- Burdette, E. G., E. E. Ingram, J. B. Tidwell, D. W. Goodpasture, J. H. Deatherage, and S. C. Howard. 2004. "Behavior of Integral Abutments Supported by Steel H-Piles." *Transportation Research Record: Journal of the Transportation Research Board* 1892:24–28.
- Computers and Structures, Inc. (CSI). 2009. SAP2000 Advanced 14.1.0 Structural Analysis Program, Berkeley, CA. <http://www.csiamerica.com/>
- _____. 2013. CSI Knowledge Base, <http://www.csiamerica.com/>.
- Dicleli, M. 2005. "Integral Abutment-Backfill Behavior on Sand Soil—Pushover Analysis Approach." *Journal of Bridge Engineering*, ASCE, 10(3):354–364.
- Dicleli, M., and S. M. Albhaisi. 2004. "Effect of Cyclic Thermal Loading on the Performance of Steel H-Piles in Integral Bridges with Stub-Abutments." *Journal of Constructional Steel Research* 60:161–182.
- Ensoft, Inc. 2005. LPILE Plus v.5.0 Geotechnical Analysis Program (Student Version), <http://www.ensoftinc.com/>.
- Frosch, R. J., and M. D. Lovell. 2011. "Long-Term Behavior of Integral Abutment Bridges." Publication FHWA/IN/JTRP-2011/16. Joint Transportation Research Program, Indiana Department of Transportation and Purdue University, West Lafayette, Indiana. doi: 10.5703/1288284314640.
- Han, Jarell. 2014. *Lateral Resistance of Piles near 15-Foot Vertical MSE Abutment Walls Reinforced with Ribbed Steel Strips*. MS thesis. Paper 5320. Department of Civil and Environmental Engineering, Brigham Young University, Provo, UT.
- Hassiotis, S., Y. Khodair, E. Roman, and Y. Dehne. 2006. *Evaluation of Integral Abutments*. Final Report, FHWA-NJ-2005-025, New Jersey Department of Transportation and Stevens Institute of Technology, Hoboken, NJ.
- Huang, J., French, C., and Shield, C. 2004. *Behavior of Concrete Integral Abutment Bridges*. Minnesota Local Road Research Board. Report no. Mn/DOT 2004-43. Center for Transportation Studies, University of Minnesota, Minneapolis, MN.
- "IDOT Memorandum: 2012 Integral Abutment Bridge Policies and Details." 2012. Illinois Department of Transportation Bureau of Bridges and Structures, 25 July 2012, <http://www.idot.illinois.gov/Assets/uploads/files/Doing-Business/Memorandums-&-Letters/Highways/Bridges/ABD-Memos/abd123.pdf>

- Ingram, E. E., E. G. Burdette, D. W. Goodpasture, J. H. Deatherage, and R. M. Bennett. 2004. "Behavior of Steel H-Piles Supporting Integral Abutments," pp. 219–225. In *Proceedings of the ASCE Structures Congress*. Nashville, TN.
- Khodair, Y. A., and S. Hassiotis. 2005. "Analysis of Soil-Pile Interaction in Integral Abutment." *Computers and Geotechnics* 32(3):201–209.
- _____. 2013. "Rigidity of Abutments in Integral Abutment Bridges." *Structure and Infrastructure Engineering* 9(2):151–160. DOI:10.1080/15732479.2010.541264.
- Kim, W., and J. A. Laman. 2010. "Numerical Analysis Method for Long-Term Behavior of Integral Abutment Bridges," *Engineering Structures* 32(8):2247–2257.
- _____. 2012. "Seven-year field monitoring of four integral abutment bridges." *Journal of Performance of Constructed Facilities*, ASCE, 26(1):54–64.
- LaFave, J. M., L. A. Fahnestock, B. A. Wright, J. K. Riddle, M. W. Jarrett, J. S. Svatora, H. An, and G. Brambila. 2016a. *Integral Abutment Bridges Under Thermal Loading: Numerical Simulations and Parametric Study*. A report of the findings of ICT-R27-115. Illinois Center for Transportation Series No. 16-015. Research Report No. FHWA-ICT-16-014. Illinois Center for Transportation, Rantoul, IL.
- LaFave, J. M., J. K. Riddle, M. W. Jarrett, B. A. Wright, J. S. Svatora, H. An, and L. A. Fahnestock. 2016b. "Numerical Simulations of Steel Integral Abutment Bridges under Thermal Loading," *ASCE Journal of Bridge Engineering*, 21(10), Article # 04016061 (17 pp.).
- Nelson, K. R. 2013. *Lateral Resistance of Piles near Vertical MSE Abutment Walls at Provo Center Street*. MS thesis, Department of Civil and Environmental Engineering, Brigham Young University, Provo, UT.
- Olson, S. M., K. P. Holloway, J. M. Buenker, J. H. Long, and J. M. LaFave. 2012. *Thermal Behavior of IDOT Integral Abutment Bridges and Proposed Design Modifications*. Illinois Center for Transportation Research Report, ICT-12-022, University of Illinois, Urbana, IL.
- Paul, M.D., J. A. Laman, and D. G. Linzell. 2005. "Thermally Induced Superstructure Stresses in Prestressed Girder Integral Abutment Bridges." *Transportation Research Record: Journal of the Transportation Research Board*, CD 11-S: 287–297. Transportation Research Board of the National Academies, Washington, D.C.
- Price, J. S. 2012. *Lateral Resistance of Piles near Vertical MSE Abutment Walls*. MS thesis, Department of Civil and Environmental Engineering, Brigham Young University, Provo, UT.
- Quinn, B. H., and S. A. Civjan. 2017. "Parametric Study on Effects of Pile Orientation in Integral Abutment Bridges." *Journal of Bridge Engineering*, ASCE, 22(4): Article # 04016132 (14 pp.).
- Shoukry, S. N., G. W. William, and M. Y. Riad. 2008. "Response of an Integral Abutment Bridge to Temperature Variations." In *Proceeding of Structures Congress*, Vancouver, British Columbia, Canada.

William, G. W., S. N. Shoukry, and M. Y. Riad, 2012. "Study of Thermal Stresses in Skewed Integral Abutment Steel Girder Bridges." *Structural Engineering International* 22(3):308–317.

Wright B., J. LaFave, L. Fahnestock, M. Jarrett, J. Riddle, and J. S. Svatora. 2015. "Field Monitoring of Skewed Integral Abutment Bridges." In *Proceeding of the joint 6th International Conference on Advances in Experimental Structural Engineering and 11th International Workshop on Advanced Smart Materials and Smart Structures Technology*, University of Illinois, Urbana–Champaign, United States, August 1–2, 2015.

